

7.0 Results of Large-Scale Tests

This section presents the results of the pressure-drop measurements made in the large-scale loop. The large-scale tests were conducted in four test phases: Series 1, Benchmark, Series 2, and Coatings Tests (refer to Section 5.1 for the description of the test matrixes). The test results are presented for the following five types of debris beds:

- Screen only with no debris added, Section 7.1
- NUKON only, Section 7.2
- CalSil only, Section 7.3
- Combinations of NUKON and CalSil (denoted NUKON/CalSil), Section 7.4
- Coatings material tests, Section 7.5.

Results from the benchtop loop are presented for comparative purposes where appropriate. The bulk of the results from the benchtop loop are presented in Sections 3 and 6.

The discussion of the different types of debris beds includes results from multiple test series. As discussed in Section 5.3, there were slight differences in the test procedures applied to the various test series. The most significant differences are summarized below.

- Approach velocity during debris bed formation. Four Series 1 tests used an initial debris bed formation velocity of 0.2 ft/sec (0.06 m/s). The pump speed was then left constant, and the velocity declined as the pressure drop across the accumulating debris bed increased. For the remainder of the test program, the bed formation velocity was maintained at 0.1 ft/sec (0.03 m/s) throughout the bed formation process. Faster approach velocities of up to 0.8 ft/sec (0.24 m/s) were used for the coating tests (see Section 7.5). The majority of the testing conducted in the benchtop loop used a screen approach velocity of 0.2 ft/sec (0.06 m/s).
- Velocity sequence. The velocity sequence to which debris beds were subjected during testing was changed from one test series to another. Debris beds generated during the Series 1 tests were subjected to velocities at least 3 times the maximum velocity tested during the Benchmark or Series 2 tests. The velocities tested during Series 1 produced pressure drops at the higher velocities in excess of 400 in. H₂O (app 14.4 psi [99.3 kPa]). Due to perceived NPSH margins of typical centrifugal pumps, obtaining pressure drops in excess of 1 atm (14.7 psi [101.3 kPa]) was subsequently determined not to be of interest. Following the Series 1 tests, perforated plate was used exclusively for the remaining tests because this material better represented configurations being proposed by utilities for the resolution of GSI-191. Therefore, the combination of the perforated plate and the perceived NPSH margins of typical pumps motivated alterations to the velocity sequence used for the Benchmark and Series 2 tests, resulting in a lower range of approach velocities. Section 6.5 discusses the effects of the debris bed flow history on measured pressure drops. Comparisons of pressure drop measurements for different debris beds at various approach velocities should consider the complete flow history to which the debris beds were subjected.
- Filtering following debris bed formation. A 10- μ m bag filter was included in the test loop to remove suspended debris material from the flow following debris bed formation. Because debris beds compress as the approach velocity increases, it was anticipated that the filtering efficiency of a

compressed debris bed would increase with increasing approach velocity. As a result, the debris bed mass could be a function of the approach velocity and flow history (velocity cycle). Filtering after the completion of debris bed formation was only applied to the Series 2 tests.

- The Series 1 tests were conducted to simulate as closely as possible the test conditions of the 2004 LANL test conditions (Shaffer et al. 2005). No filtering was used by LANL following debris-bed formation; therefore, no filtering was applied during the Series 1 tests.
 - The Benchmark tests were conducted to obtain measurements that could be compared with those from a test loop at ANL (Kasza et al. 2006). The ANL tests, and therefore the Benchmark tests, applied no filtering following debris bed formation.
 - During the Series 2 and Coatings tests, the test fluid was passed through the filter housing at the completion of the first ramp up in the screen approach velocity to reduce the amount of suspended material and attempt to maintain a fairly constant mass on the debris bed through the remainder of the test.
- Debris preparation. The debris preparation used for the Benchmark tests used the R4 metric to match the debris preparation performed by ANL. Therefore, the prepared NUKON may have been slightly coarser for the Benchmark tests than for the Series 1 and 2 tests (see Section 5.1.2).
 - Screen material. The Series 1 tests used the 5-mesh woven cloth and the Benchmark, Series 2, and Coatings tests used the 1/8-in.-hole perforated plate. (Section 2.2 describes these screen materials in detail.) Section 7.1 compares the pressure drop measured across the screen materials.

Two additional factors that should be considered when comparing tests or evaluating trends are:

- The ratio of the retained debris loading to the target debris loading
- The flow regime (laminar, transition, or turbulent) existing in the test section when the pressure drop measurements were made.

The target debris loading is the amount of debris material introduced into the test loop; the retrieved debris bed loading is the dried mass of the retrieved debris bed and represents the amount of material on the screen at the end of the test. During testing, the debris bed was allowed to form until a steady-state condition was obtained with respect to measured pressure drop (refer to Section 5.3). However, even with a steady-state condition, it is possible for debris material to be suspended in the flow and pass through the debris bed. With an increase or decrease in the approach velocity, the debris bed may contract or expand, resulting in debris material being retained or lost, respectively. When comparing debris beds of the same retrieved mass, the initial target mass needs to be considered. If two debris beds have similar retrieved masses but different initial target masses were used to generate them, the potential exists for the debris bed with the higher initial target mass to be coarser and have a higher void fraction.

Turbulent flow is characterized by mixing action that results from eddies throughout the flow field. Most naturally observed flows, such as rivers and wind, exhibit turbulent flow. Laminar flow is a very uniform stable flow consisting of layers (lamina) of fluid gliding by each other. The streamlines of the flow are parallel, and there is no intense mixing. Any disturbances to the flow are readily damped out. Laminar flow is observed when pouring honey. Transition flow defines conditions in which neither fully laminar nor turbulent flow exists. The flow will tend to be unsteady and intermittent. Turbulent slugs of flow will be followed by intervals of near-laminar flow.

For the same debris bed and fluid properties, different pressure drop measurements can be obtained under each of the three flow regimes. One way to accomplish this is to obtain measurements from test sections of different diameter. While measurements taken in laminar or turbulent flow conditions will be repeatable, measurements taken under conditions of transition flow may yield inconsistent results.

To evaluate which flow regime is present, the Reynolds number (Re) is used. The Re is a nondimensional number that provides a relative ratio of the inertial to viscous forces existing in the flow. Re is a function of the fluid velocity, U, dynamic viscosity, μ , density, ρ , and pipe diameter, D. For pipe flow, Re is defined as

$$Re = \frac{U\rho D}{\mu} \quad (7.1)$$

For pipe flow, a $Re \geq 4000$ will produce turbulent flow, and a $Re \leq 1500$ can be assumed to yield laminar flow. For the condition of $1500 \leq Re \leq 4000$, the potential exists for transition flow to be present.

During testing, the pressure drop was evaluated at nominal temperatures of 68°F (20°C), 129°F (54°C), and 180°F (82°C). The fluid density and viscosity are temperature dependent. The flow regime present should be considered when comparing pressure drop measurements taken at different temperatures or from different test loops. Table 7.1 contains the velocity range in which the large-scale test section may have contained transition flow conditions for each nominal temperature tested.

Table 7.1. Velocity Range in Which a Transition Flow Regime May Exist for Each Nominal Test Temperature

Flow Regime	Re Used to Determine Velocity Limit	Critical Velocities for 68°F (20°C) ft/sec (m/s)	Critical Velocities for 129°F (54°C) ft/sec (m/s)	Critical Velocities for 180°F (82°C) ft/sec (m/s)
Condition defining upper bound of laminar flow	1500	0.032 (0.0098)	0.017 (0.0051)	0.011 (0.0035)
Condition defining lower bound of turbulent flow	4000	0.085 (0.0260)	0.044 (0.0136)	0.030 (0.0093)

In Sections 7.1 through 7.5, tables are presented that list all of the large-scale tests conducted for a particular debris loading condition. The tables include the test case, test series, and test ID for each associated large-scale test conducted. The test series and test ID are presented in Section 5.1. The test ID is used to identify the associated Quick Look report in Appendixes G through K. The Quick Look reports tend to reference the target debris loadings when presenting the results. In this section, test case numbers are assigned, and the results are compared relative to the retrieved debris bed mass loading.

The tables for each test condition also indicate whether a complete debris bed was formed. The formation of debris beds was characterized as complete, channeling formed, or incomplete. A complete debris bed means that following debris bed formation the entire screen and all flow areas through the screen were completely and uniformly covered. The designation "channeling formed" indicates that, at the completion of debris bed formation a complete debris bed existed, but through execution of the velocity sequence, channels were formed in the debris bed. An incomplete debris bed refers to a test condition in which a complete debris bed was never observed at any point during the test.

During the experiments, the head loss across the debris beds was measured in units of in. of H₂O at 68°F (20°C). In this section, the term pressure drop is used interchangeably with the term head loss. To convert the experimental measurements of head loss in inches of H₂O at 68°F (20°C) to pressure drop in units of psi, use the following:

$$P = \gamma hC \quad (7.2)$$

where

- P = pressure in psi
- γ = 62.214 lbf/ft³ specific weight of water @ 68°F
- h = measured head loss in in. H₂O @ 68°F
- C = 1ft³/1728 in.³ conversion factor.

In presenting the test results, less emphasis is placed on the results for incomplete debris beds. Sections 7.1 through 7.5 present the test results for each type of debris bed. Each section evaluates the effects of debris loading on the pressure drop and debris-bed height. Data on the effect of fluid temperature on the measured pressure drop are also presented. The Quick Look reports in Appendixes G through J contain the specific test conditions, the measured head loss as a function of velocity, and the measured debris bed heights for each of the tests.

7.1 Large-Scale Results of Screen-Only Tests

Testing was conducted to obtain baseline measurements of the pressure drop across the 5-mesh screen and perforated plate (1/8-in.-diameter holes) with no debris material present. Tables 7.2 and 7.3 list the screen only (SO) and plate only (PO) test cases conducted.

Table 7.2. PNNL Large-Scale Screen-Only Tests Conducted

Test Case	Test Series	Test ID	Target Debris Bed NUKON Loading (g/m ²)	Target Debris Bed CalSil Loading (g/m ²)	CalSil to NUKON Ratio	Total Target Debris Bed Loading (g/m ²)	Nom. Temp (°F)	Screen or Plate	Debris Bed Formed
SO1	1	051114_SO_0000_L1	0	0	N/A	0	70	screen	N/A
SO2	1	051128_SO_0000_L1	0	0	N/A	0	70	screen	N/A

Table 7.3. PNNL Large-Scale Plate-Only Tests Conducted

Test Case	Test Series	Test ID	Target Debris Bed NUKON Loading (g/m ²)	Target Debris Bed CalSil Loading (g/m ²)	CalSil to NUKO N Ratio	Total Target Debris Bed Loading (g/m ²)	Nom. Temp. (°F)	Screen or Plate	Debris Bed Formed
PO1	2	060804_PO_0000_LP1	0	0	N/A	0	83	plate	N/A
PO2	2	060804_PO_0000_LP2	0	0	N/A	0	131	plate	N/A
PO3	2	060805_PO_0000_LP1	0	0	N/A	0	179	plate	N/A

Measurements of the pressure drop across the bare 5-mesh screen were first taken for SO1 using a 0-to-30-in.-H₂O DP transmitter at a nominal temperature of 20°C. The fluid temperature ranged from 63°F (17°C) to 75°F (24°C) during testing. The small values obtained (<2 in. H₂O) indicated a transmitter with a lower span should be used. Test Case SO2 was a repeat of SO1 using a 0-5 in.-H₂O DP transmitter. Similar measurements were taken during test case PO1 for the bare perforated plate. The results for the pressure drop as a function of velocity for test cases SO1, SO2, and PO1 are presented in Figure 7.1 without error bars. The data series are identified by the test case and the range of the DP transmitter used to acquire the readings. Error bars for the data are included in Figure 7.2.

Comparing the cases of SO2 and PO1, the perforated plate material appears more restrictive than the 5-mesh screen. The measurements taken for SO1 tend to yield the same conclusion. All of the SO1 measurements were less than 7% of the full-scale reading for the 0-to-30-in. DP transmitter, and the main conclusion obtained is that a lower range transmitter needed to be employed.

The recorded pressure drops for all of the velocities tested for the SO and PO cases are included in the Quick Look reports in Appendix G. For comparison, the values of the measured head loss at approach velocities common to all of the tests are presented in Table 7.4

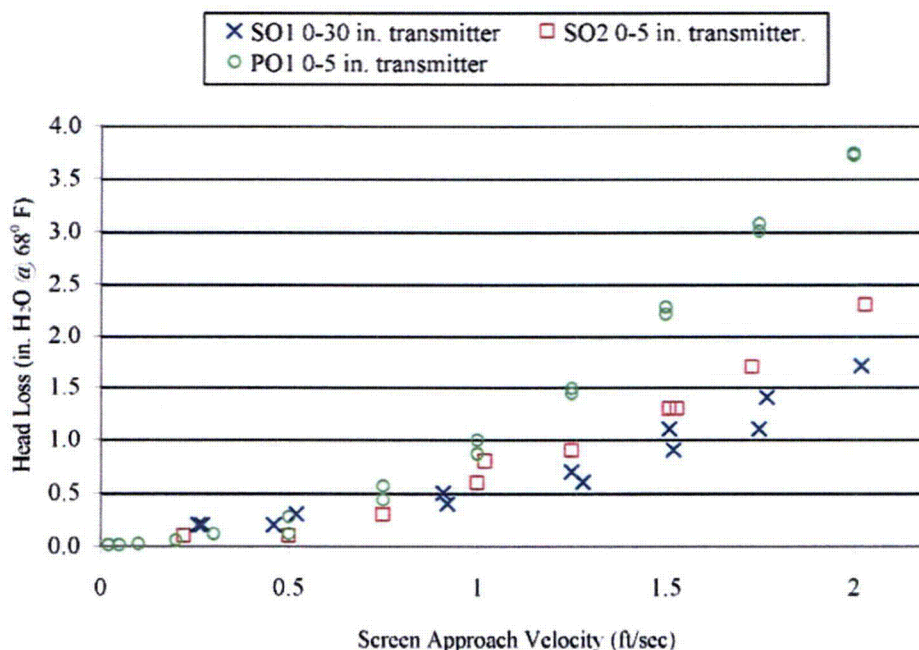


Figure 7.1. Pressure Drop as a Function of Screen Approach Velocity for the Bare Screen and Bare Perforated Plate Without Error Bars

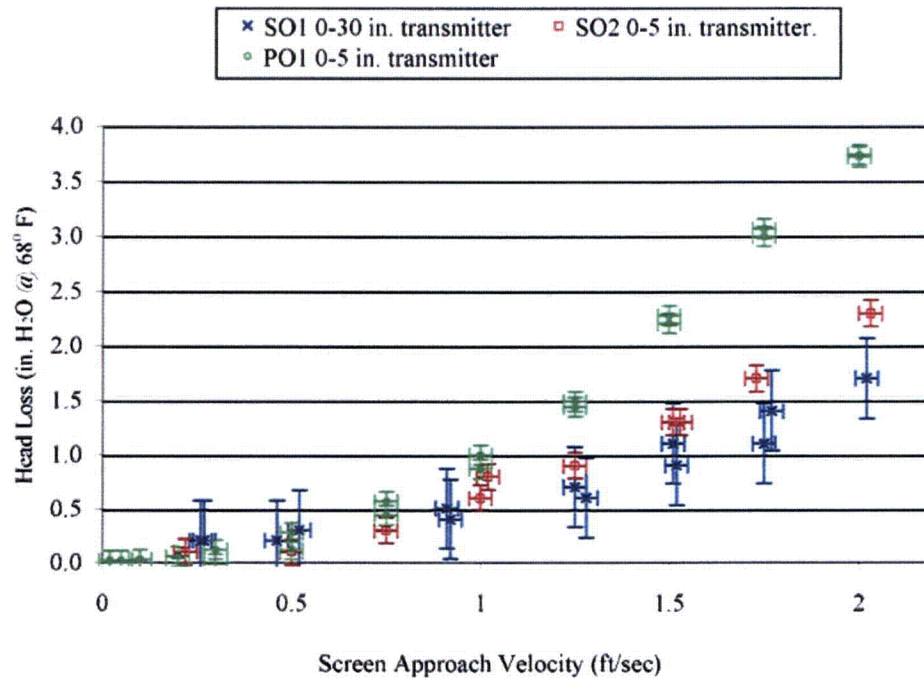


Figure 7.2. Pressure Drop as a Function of Approach Velocity for the Bare Screen and Bare Perforated Plate with Error Bars

Table 7.4. Comparison of Head Loss Measurements for Bare Screen and Bare Plate at Selected Screen Approach Velocities (temperature and zero offset corrections applied)

Screen Approach Velocity ±0.03 ft/sec	Test Cases		
	Pressure Drop Measurements for SO2 0.1 ± in. H ₂ O @ 68°F (psi)		Pressure Drop Measurements for PO1 ^(a) 0.1 ± in. H ₂ O @ 68°F (psi)
0.20–0.22	0.1 (0.00)		0.0 (0.00) 0.1 (0.00)
0.50	0.1 (0.00)		0.1 (0.00) 0.3 (0.01)
1.00	0.8 ^(a) (0.03)	0.6 ^(a) (0.02)	0.9 (0.03) 1.0 (0.04)
2.01–2.03	2.3 (0.08)		3.7 (0.13) 3.7 (0.13)

(a) Different head loss measurements were obtained for the same approach velocity. First measurements were obtained when incrementally ramping up the flow rate and the others when incrementally ramping down the flow rate.

7.1.1 Temperature Effects for Bare Perforated Plate

Because testing of debris beds generated on 5-mesh screens was not performed at elevated temperatures, no data were obtained for the bare screen at the elevated temperatures. Test cases PO2 and PO3 were performed at temperatures of 131°F (55°C) and 179°F (81°C), respectively, and are presented along with the results of PO1 in Figure 7.3 without error bars displayed. Figure 7.4 is a repeat of Figure 7.3 with the error bars included. The results have been corrected for the temperature difference between the DP manifold fluid and the test loop fluid. While lower head losses were expected at higher temperatures due to the reduced fluid viscosity and density, no significant differences were observed in the results measured for the different temperatures.

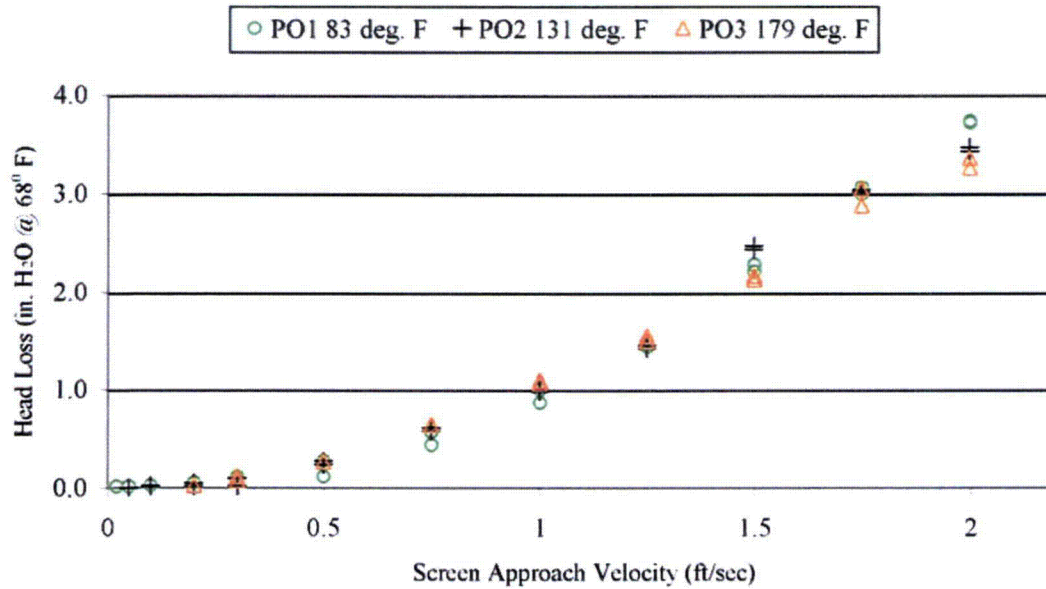


Figure 7.3. Comparison of Head Loss Across Bare Perforated Plate with 1/8-in. Holes as a Function of Screen Approach Velocity for Nominal Temperatures of 83°F (28°C), 131°F (55°C), and 179°F (81°C) Without Error Bars

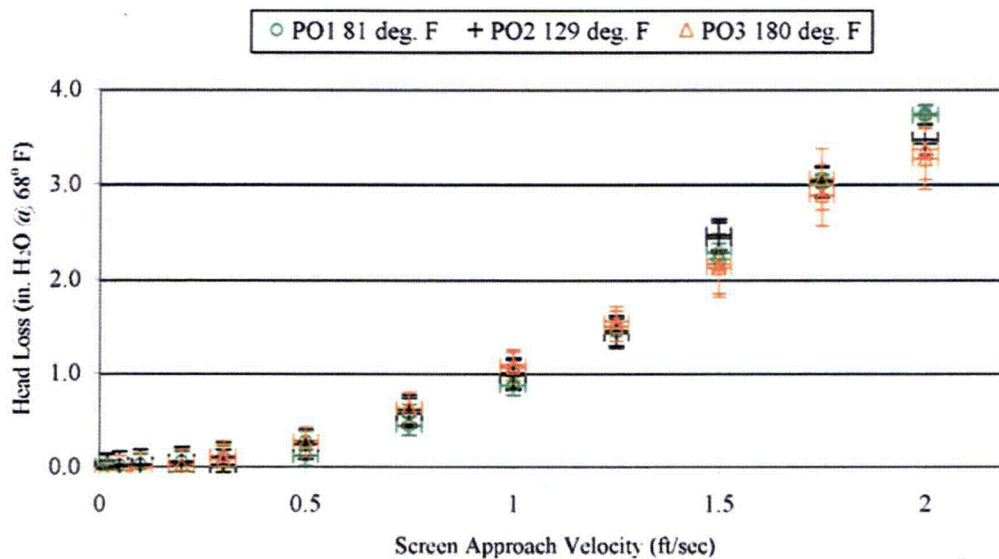


Figure 7.4. Comparison of Head Loss Across Bare Perforated Plate with 1/8-in. Holes as a Function of Screen Approach Velocity for Nominal Temperatures of 83°F (28°C), 131°F (55°C), and 179°F (81°C) with Error Bars

The recorded pressure drops for all velocities tested are included in Quick Look reports in Appendix G. For comparison, the values of the measured head loss at approach velocities common to all of the tests are

presented in Table 7.5. Due to the relatively low flow rate of the loop and the centralized location of the band heaters, the uncertainty of the loop temperature throughout the tests is $\pm 8^\circ\text{F}$ (4.4°C). The maximum uncertainty occurs at the low flow condition due to the cooling that occurs before fluid circulates back through the heaters. At 0.02 ft/sec (0.006 m/s), the loop circulation time was approximately 50 min.

Table 7.5. Comparison of Head Loss Measurements of Bare Plate at 83°F (28°C), 131°F (55°C), and 179°F (81°C) for Selected Screen Approach Velocities

Screen Approach Velocity ± 0.03 ft/sec	Test Case					
	Pressure Drop Measurements for PO1 ^(a) Fluid Temp = 83°F (28°C) ± 0.10 in. H ₂ O ^(b) (psi)		Pressure Drop Measurements for PO2 ^(a) Fluid Temp = 131°F (55°C) ± 0.16 in. H ₂ O ^(b) (psi)		Pressure Drop Measurements for PO3 ^(a) Fluid Temp = 179°F (81°C) ± 0.16 in. H ₂ O ^(b) (psi)	
0.20	0.00 (0.00)	0.06 (0.002)	0.02 (0.001)	0.05 (0.002)	0.00 (0.00)	0.03 (0.001)
0.50	0.12 (0.004)	0.28 (0.010)	0.24 (0.009)	0.27 (0.010)	0.27 (0.010)	0.27 (0.010)
1.00	0.87 (0.031)	1.00 (0.036)	0.98 (0.035)	1.00 (0.036)	1.06 (0.038)	1.09 (0.039)
2.00	3.72 (0.134)	3.74 (0.135)	3.47 (0.125)	3.43 (0.124)	3.36 ^(c) (0.121)	3.26 ^(c) (0.118)

(a) Different head loss measurements were obtained for the same approach velocity. First measurements were obtained when incrementally ramping up the flow rate and the others when incrementally ramping down the flow rate.
(b) Head loss measurements are referenced to H₂O at 68°F (20°C).
(c) Measurements have an uncertainty of ± 0.33 in. H₂O @ 68°F. Increased uncertainty is due to higher range instrument required to make measurements.

7.2 Large-Scale Results of NUKON Debris Beds

The NUKON-only cases provided the baseline conditions for evaluating debris bed pressure drop and the effects associated with debris loading, fluid temperature, and flow history. The single constituent debris bed condition reduced the complexity associated with debris bed formation resulting from multiple constituents (e.g., debris loading sequence).

Table 7.6 contains the test matrix of NUKON-only conditions completed during the test program. Cases NO4 and NO5 were conducted as part of the Series 1 tests and are repeat tests. For these cases, the initial bed formation velocity was set to 0.2 ft/sec (0.06 m/s) and the test-loop pump speed held constant. The screen approach velocity was then allowed to decrease with the increasing debris bed resistance throughout the course of bed formation.

Cases NO1, NO2, NO3a were all conducted in the same manner at ambient temperature. Cases NO3b and NO3c are a continuation of the test that generated the debris bed for case NO3a and were conducted at elevated temperatures of 129°F (54°C) and 180°F (82°C), respectively. For cases NO6a through NO7b, the debris bed was generated at elevated temperatures. The results of the cases conducted at elevated temperatures are discussed in Section 7.2.2. Bed height measurements of the debris beds are presented in Section 7.2.1. All of the mass loadings for NUKON-only debris beds tested in the large-scale loop formed complete debris beds.

As discussed in Section 5.3, the debris bed formation process was allowed to take place until a steady-state pressure drop was achieved. Following the formation of the debris bed, a velocity sequence was executed in which the screen approach velocity was incrementally ramped up and down with steady-state measurements of head loss taken at each pre-established velocity. As discussed in Section 6.5, the pressure drop was not only a function of the approach velocity but also the flow history to which the

debris bed had been subjected. For the NUKON-only tests, most repeat points for a given velocity resulted in an increase in the measured head loss. The results of Test Case NO4 provide an example of this phenomenon. Figure 7.5 is a plot of head loss as a function of screen approach velocity for the measurements obtained during the velocity ramp up phases of Test Case NO4. In examining the values obtained for velocities greater than 0.8 ft/sec, it is readily observed that the head loss increased with each consecutive ramp up of velocity.

The data provided in Figure 7.5 provide an example of the degree of repeatability that can be expected for head loss measurements obtained for the same debris bed formation conditions. The efforts put forth to control the debris preparation and debris introduction processes were made in an attempt to evaluate the variability of the debris bed formation process. Given the same debris prepared to a similar degree of fragmentation or disassociation and introduced to the screen at a similar concentration and rate, the question was whether the arrangement of the debris material on the screen would vary enough to create significant differences in the measured head loss.

Test Cases NO4 and NO5 were repeat tests performed in the large-scale loop, both with a target mass loading of 1645 g/m^2 . The retrieved mass loading for Test Case NO4 was approximately 4% higher than that for NO5. Figure 7.6 contains head loss measurements from test Cases NO4 and NO5 from bed formation through the second ramp down. Due to the velocities selected for NO5, no data points were collected for ramp down 2 (the peak velocity at the end of ramp up 2 was followed by the minimum velocity initiating ramp up 3). Head loss measurements obtained in the benchtop loop for two tests with similar debris loadings are compared with those of NO4 and NO5 in Figure 7.7.

The results presented in Figures 7.6 and 7.7 demonstrate that reasonable repeatability was obtained between debris beds of similar composition. The lowest head loss of NOBT1 corresponds to the debris bed with the lowest retrieved mass loading. Table 7.7 compares head loss measurements from Test Cases NO4, NO5, NOBT1, and NOBT2 for velocities common to the tests. The uncertainty of benchtop measurements is greater than that obtained from the large-scale loop due to different instrumentation.

Tests NO1, NO2, NO3a, NO4, and NO5 were all conducted at ambient temperature (approximately 70°F [21°C]) over a range of debris loadings. Figure 7.8 is a plot of the head loss versus ramp up 2 screen approach velocity for the varying NUKON-only debris loadings up to a screen approach velocity of 1 ft/sec (0.3 m/s). Only the Series 1 tests exceeded screen approach velocities of 0.2 ft/sec (0.06 m/s); therefore, Figure 7.9 presents the data from Figure 7.8 between 0 and 0.3 ft/sec. Values of head loss for screen approach velocities of 0.02, 0.1, and 0.2 ft/sec are presented in Table 7.8. The transition flow regime for ambient temperature is predicted to exist between 0.03 ft/sec (0.01 m/s) and 0.08 ft/sec (0.02 m/s), and no measurements in this range were taken for data presented in Figures 7.8 and 7.9.

The majority of the results presented in Figures 7.8 and 7.9 and Table 7.8 indicate that the head loss correlates well with increases in debris mass loading. An inconsistency in the trend is observed for the case of NO3 at a screen approach velocity of 0.2 ft/sec (0.6 m/s). The head loss obtained for NO3a at an approach velocity of 0.2 ft/sec (0.6 m/s) appears to follow the trend when compared to the results of NO1 and NO2; however, it appears high when compared to the data from NO4 and NO5. Measurements of 59 and 60 in. H_2O at 0.2 ft/sec were obtained during ramp up 1 and ramp up 3 of test NO3a; the uncertainties associated with the head loss measurements are too small to account for similar measurements being obtained for NO3a, NO4, and NO5.

Table 7.6. Target Test Matrix for Large-Scale NUKON-Only Debris Bed Tests

Test Case	Test Series	Test ID	Target Debris Bed NUKON Loading (g/m ²)	Target Debris Bed CalSil Loading (g/m ²)	CalSil to NUKON Ratio	Total Target Debris Bed Loading (g/m ²)	Total Retrieved Debris Bed Loading (±8 g/m ²)	Nom. Temp. (°C)	Screen or Plate	Complete Debris Bed Formed
NO1	BM	060321_NO_0405_LP1	217	0	0.00	217	171	21	plate	yes
NO2	BM	060313_NO_1349_LP1	724	0	0.00	724	576	21	plate	yes
NO3a	2	060425_NO_2703_LP1	1450	0	0.00	1450	1244	21	plate	yes
NO3b	2	060425_NO_2703_LP2	1450	0	0.00	1450	1244	54	plate	yes
NO3c	2	060425_NO_2703_LP3	1450	0	0.00	1450	1244	82	plate	yes
NO4 ^(a)	1	051108_NO_3067_L1	1645 ^(d)	0	0.00	1645	1788	21	screen	yes
NO5 ^(a)	1	060125_NO_3067_L1	1645 ^(d)	0	0.00	1645	1719	21	screen	yes
NO6a ^(b)	2	060731_NO_2703_LP1	1450	0	0.00	1450	1250	54	plate	yes
NO6b ^(b)	2	060731_NO_2703_LP2	1450	0	0.00	1450	1250	27	plate	yes
NO7a ^(b)	2	060802_NO_2703_LP1	1450	0	0.00	1450	1190	82	plate	yes
NO7b ^(b)	2	060802_NO_2703_LP2	1450	0	0.00	1450	1190	55	plate	yes
NOBT1 ^(c)	N/A	080305_NO_1363_1	1681	0	0.00	1681	1665	26	screen	yes
NOBT2 ^(c)	N/A	081505_NO_1363_1	1681	0	0.00	1681	1702	33	screen	yes

(a) Initial screen approach velocity during debris-bed formation = 0.2 ft/sec as opposed to a constant 0.1 ft/sec.
 (b) Debris bed formation took place at elevated temperature.
 (c) Tests conducted in the benchtop loop.
 (d) Target mass loading was intended to be the same as for Test Condition 1a, 1681 g/m². However, a value of 6 in. instead of 6.065 in. was used for the test section diameter in calculating the required mass of NUKON needed for the test.

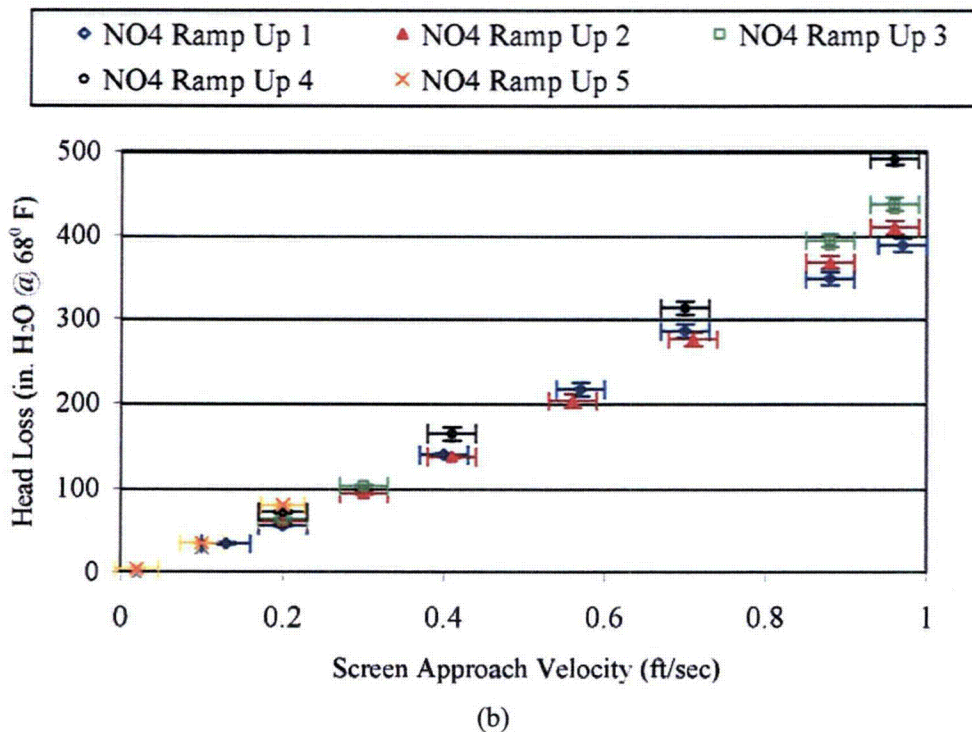
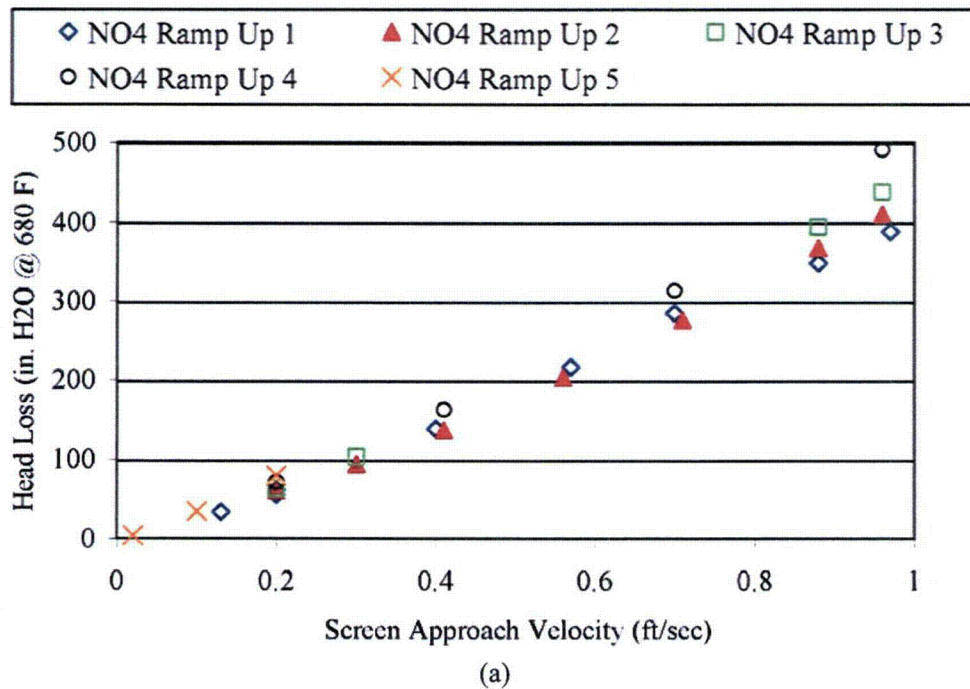


Figure 7.5. Head Loss Across Debris Bed as a Function of Screen Approach Velocity for Test Case NO4. The NUKON-only debris bed has a retrieved debris loading of 1788 g/m². The plot contains only head loss measurements obtained during the ramp up portions of the velocity sequence at ambient temperature (a and b are the same plot with and without error bars, respectively).

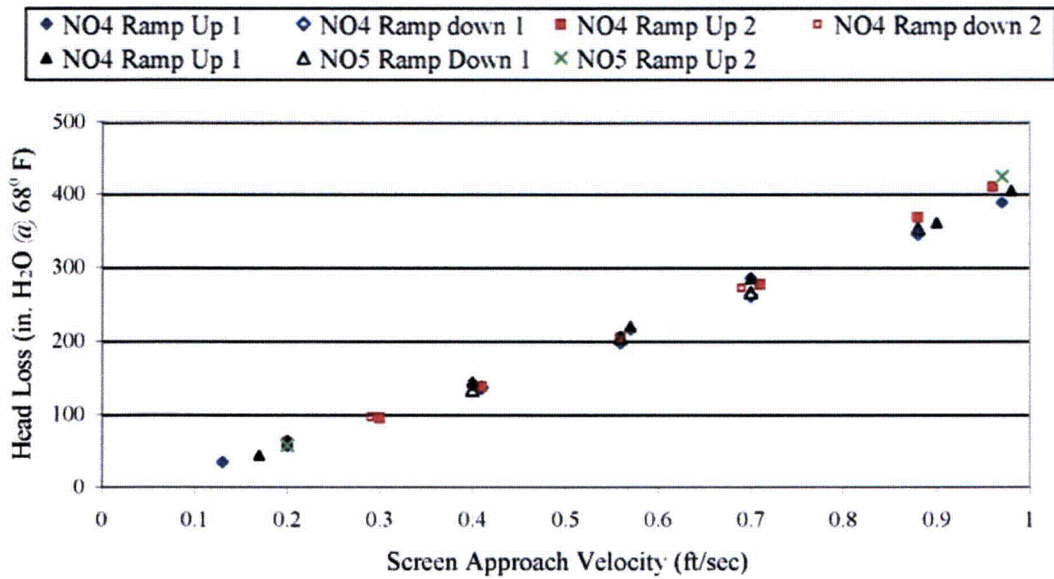


Figure 7.6. Comparison of Head Loss as a Function of Screen Approach Velocity for Repeat Test Cases NO4 and NO5. The retrieved mass loadings for NO4 and NO5 were 1788 and 1719 g/m², respectively. The data presented are from the first two velocity cycles for each test.

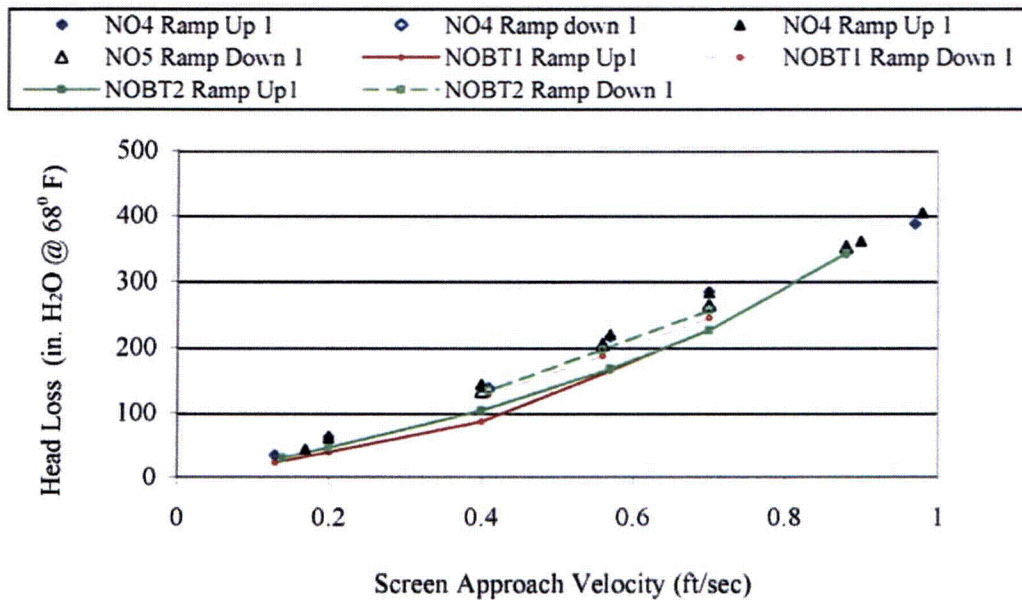


Figure 7.7. Comparison of Large-Scale and Benchtop Loop Results for NUKON-Only Test Condition 1a. The retrieved mass loadings for Test Cases NO4, NO5, NOBT1, and NOBT2 were 1788, 1729, 1665, and 1702 g/m², respectively. Data are from the first ramp up and ramp down of each velocity sequence.

Table 7.7. Comparison of Measured Head Loss at Selected Velocities for Test Condition 1a Debris Beds Generated in Both the Large-Scale and Benchtop Loops at Ambient Temperature

Screen Approach Velocity (ft/sec)	Test Case and Phase of Velocity Sequence							
	NO4 ^(a) Ramp up 1 (±1.6 in. H ₂ O) ^(c)	NO4 ^(a) Ramp down 1 (±1.6 in. H ₂ O) ^(c)	NO5 ^(a) Ramp up 1 (±1.6 in. H ₂ O) ^(c)	NO5 ^(a) Ramp down 1 (±1.6 in. H ₂ O) ^(c)	NOBT1 ^(b) Ramp up 1 (±11 in. H ₂ O) ^(c)	NOBT1 ^(b) Ramp down 1 (±11 in. H ₂ O) ^(c)	NOBT1 ^(b) Ramp up 1 (±11 in. H ₂ O) ^(c)	NOBT2 ^(b) Ramp down 1 (±11 in. H ₂ O) ^(c)
0.20	62	--	63	--	--	--	--	--
0.25	--	--	--	--	55	65	62	84
0.40-0.41	139	136	143	133	106	128	114	147
0.70	285	261	284	265	--	--	--	--
0.96-0.98	388	--	404	--	--	--	--	--
Retrieved mass loading (±8 g/m ²)	1788	1788	1729	1729	1665	1665	1702	1702
(a) Tests conducted in the large-scale test loop.								
(b) Tests conducted in the benchtop test loop.								
(c) Head loss measurements are referenced to H ₂ O at 68°F (20°C).								

The percent of the target mass retained on the screen also does not explain the higher than anticipated head loss measured for the case of NO3a. Slightly less than 80% of the target mass was retained for NO1 and NO2 compared with 86% for NO3a. It should be noted that after the head loss measurements were made at ambient temperature, two additional complete velocity sequences were run for loop temperatures of 129°F (54°C) and 180°F (82°C) prior to the retrieval of the NO3a debris bed. In comparison, the debris beds for NO4 and NO5 were slightly above 100% target mass retained due to small amounts of additional debris.¹

A major difference between the debris beds of NO1, NO2, and NO3a and those from NO4 and NO5 is the bed formation velocity. A constant screen approach velocity of 0.1 ft/sec (0.03 m/s) was maintained throughout the bed formation process of tests NO1, NO2, and NO3a. For the debris beds of NO4 and NO5, as well as those from NOBT1 and NOBT2, the screen approach velocity was initially set to 0.2 ft/sec (0.06 m/s) and allowed to decrease as the resistance of the debris bed increased during the buildup of debris.

It is plausible that starting with a screen approach velocity of 0.1 ft/sec (0.03 m/s) allowed debris material to settle within the loop or be transported at a slower rate. The settling of debris segregates debris material by size. This in turn results in the initial debris bed being generated with material of a different size distribution than what was initially introduced into the loop. Following the initial bed formation process, the screen approach velocity was increased, allowing settled material to be resuspended and deposited on the debris bed. During inspection of the test loop between NUKON-only tests, no deposits of NUKON material were observed.

The term “initial debris bed” describes the debris bed formed when steady-state conditions were reached at the end of the debris bed formation process. The potential exists for both suspended and settled

¹ During the Series 1 tests, process water from the lab was used as opposed to DI water. The test loop also contained a temporary fitting due to the back ordering of a malfunctioned component. The temporary component and process water resulted in small amounts of contaminants such as rust being retained on the debris bed.

material to be added to the debris bed during ramp up 1. As the approach velocity is increased, the debris bed compresses and becomes more efficient at retaining fine debris that may be suspended in the flow when steady-state conditions are achieved for the initial debris bed. The increased velocity within the loop also allows settled debris to be resuspended and to become deposited on the top of the debris bed. Visual observations made during testing tend to indicate this phenomenon occurred. For the Series 2 tests, filtration was performed at the peak velocity of ramp up 1 to reduce the amount of debris that could be added to the debris bed afterward.

The tests conducted with an initial screen approach velocity of 0.2 ft/sec (0.06 m/s) would have experienced less material settling and thus less segregation of the debris than a debris bed generated at a constant approach velocity of 0.1 ft/sec (0.03 m/s). Therefore, the difference in the debris bed formation velocity could influence the structure of the bed and its corresponding flow resistance. In developing a debris preparation process, it was demonstrated that changing the size distribution of the debris (i.e., changing the R4 value for the material) would affect the measured head loss (refer to Section 3.2). It has also been demonstrated that changing the sequence at which material arrives or is retained on the screen can affect the resulting head loss.

Therefore, it is suggested that the difference in debris bed formation velocity might explain the inconsistency observed in comparing the results of test NO3a with those from NO4 and NO5. Based on this explanation, it is possible that the NO1, NO2, and NO3a beds may have all generated lower head losses had they been created with a faster screen approach velocity. This is only a suggested explanation. Additional testing would be necessary to validate the impact of changing the velocity at which the debris bed is formed.

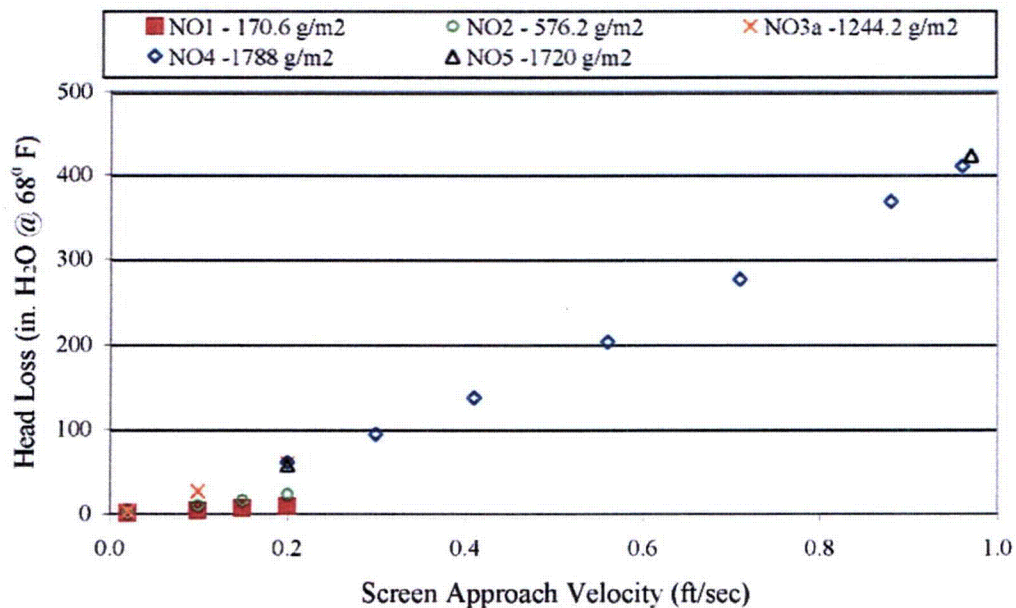


Figure 7.8. Head Loss Across the NUKON-Only Debris Beds as a Function of Screen Approach Velocity During the Ramp up 2 Portion of Each Velocity Sequence. The tests were all conducted at ambient temperature.

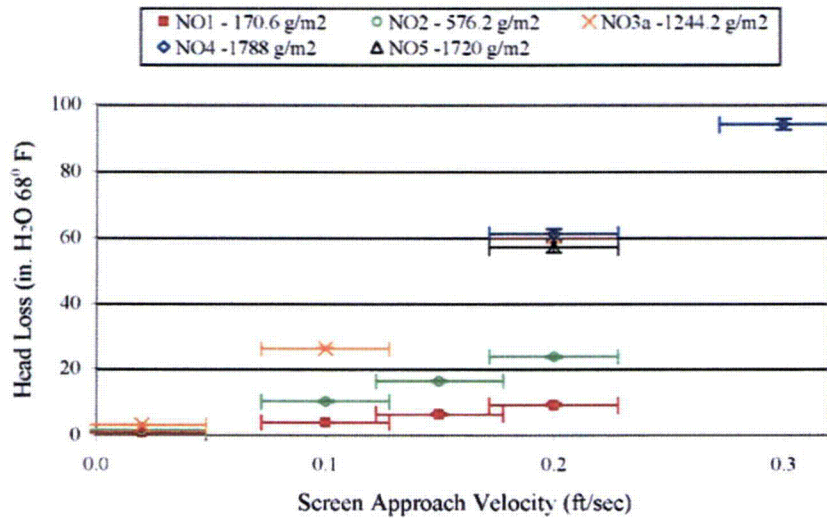


Figure 7.9. Head Loss Across the NUKON-Only Debris Beds as a Function of Screen Approach Velocity During the Ramp up 2 Portion of Each Velocity Sequence. Error bars for head loss are smaller than the symbols used. The tests were all conducted at ambient temperature.

Table 7.8. Comparison of Measured Head Loss at Selected Velocities for NUKON-Only Debris Beds Generated and Evaluated at Ambient Temperature

Screen Approach Velocity (ft/sec)	Test Case				
	NO1 Ramp up 2 (in. H ₂ O) ^(a)	NO2 Ramp up 2 (in. H ₂ O) ^(a)	NO3a Ramp up 2 (in. H ₂ O) ^(a)	NO4 ^(a) Ramp up 2 (±1.6 in. H ₂ O) ^(a)	NO5 ^(b) Ramp up 2 (±1.6 in. H ₂ O) ^(a)
0.02	0.6 ^(c)	1.4 ^(c)	3.0 ^(c)	--	--
0.1	3.9 ^(c)	10.0 ^(d)	26.0 ^(d)	--	--
0.2	8.9 ^(d)	23.5 ^(d)	60.1 ^(e)	60.9	57.0
Retrieved mass loading (±8 g/m ²)	171	576	1244	1788	1720

(a) Head loss measurements are referenced to H₂O at 68°F (20°C).
 (b) Initial screen approach velocity during debris-bed formation = 0.2 ft/sec as opposed to a constant 0.1 ft/sec.
 (c) (±0.12 in. H₂O).
 (d) (±0.34 in. H₂O).
 (e) (±1.6 in. H₂O).

7.2.1 Debris Bed Height Measurements from NUKON-Only Tests

As discussed in Section 5, three types of debris bed height measurements were taken during the test program. For all of the debris beds that were successfully retrieved, manual post-test debris bed measurements were taken. These measurements were taken after the test loop had been drained and while the debris bed was still in the test section. This method provided fairly accurate (± 0.03 in. [± 0.7 mm]) dimensions. However, the bed had been drained, and no correlation could be drawn between debris bed height under flow and the post-test dimensions of the drained debris bed. These measurements for the

NUKON-only debris beds are compared in this section. For those debris beds that were successfully retrieved, the actual measurements are included in the individual Quick Look reports (Appendix H).

In situ manual debris bed height measurements were taken during testing by an operator observing the surface of the debris bed through the TTS wall and comparing the elevation of the bed to a scale taped to the side of the TTS. For the bulk of the test, this method provided repeat measurements of the elevation of the annular rim of the debris bed at the wall of the test section. However, the outer rim of the debris bed was higher than the surface of the main body of the debris bed and precluded direct sighting of the bed surface when viewing in a horizontal plane. Attempts were made to obtain the elevation of the main body of the debris bed through the rim using back lighting. By back lighting, the surface of the debris bed was indicated by the line above which the back lighting showed through and below which the back lighting was absent. Due to the configuration and location of the mating seam for the top and bottom halves of the TTS, it was difficult to make bed height measurements of even the rim that were less than approximately 0.3 in. (8 mm) in height. For measuring the debris bed surface, this method was considered unreliable because multiple operators often reported varying results. The manual in situ measurements of debris bed height are reported in the individual Quick Look reports (Appendix H) but are not discussed in this section. Parameters affecting these measurements include the operator taking the measurements and the characteristics of the debris bed associated with the attenuation and reflection of light.

In situ debris bed height measurements were also taken via the optical triangulation method. Photographs of the debris beds were taken at each steady-state condition of the velocity sequence for post-test analysis. Due to the time and effort associated with analyzing the digital pictures, only a limited set of selected pictures was analyzed for each test. Additional pictures could be evaluated at a later date. Depending on the extent of the photo analysis, the elevation of specific points can be obtained or the entire topography of the debris bed surface can be mapped. In some instances, the optical triangulation pictures were not in focus due to opaqueness of the flow or a temporary change in lighting. Only pictures that are completely in focus can be analyzed. The optical triangulation system was not fully functional for the Series 1 tests except for Test NO5. The examination of the optical triangulation measurements will be the main focus of this section.

From measurements of debris bed height and dry retrieved bed mass, the bulk density of the debris in the bed can be calculated. Table 7.8 contains all the bed height measurements obtained with optical triangulation from the NUKON-only test cases. Table 7.8 also contains the calculated bulk dry density of the debris beds for all of the test conditions in which the photo imaging analysis was performed. The values of bulk dry debris bed density reported in Table 7.8 were obtained by calculating the debris bed volume using the product of the cross-sectional area of the test section and the average body height obtained from the optical triangulation measurements.

As expected, the height of debris beds tended to increase with retained mass loading on the screen. Figure 7.10 presents the debris bed height as a function of the screen approach velocity for the photos analyzed from Tests NO1, NO2, and NO3a. Based on the plot, for a given approach velocity, the debris bed height is relatively proportional to the debris mass loadings. A slight decrease in the bed height with increasing approach velocity is also observed.

A change in the bed formation velocity, as in the previous section, affected the observed trends in the data. The bed height measurements obtained from Test NO5 are plotted in Figure 7.11 along with the data from Figure 7.10. The results again indicate that the bed formation velocity impacts the structure of

Table 7.9. In Situ Debris Bed Height Measurements and Calculated Density Obtained from Optical Triangulation Measurements

Test Case	Retrieved Debris Bed Mass Loading ($\pm 4 \text{ g/m}^2$)	Screen Approach Velocity ($\pm 0.3 \text{ ft/sec}$)	Test Phase	Rim Ht ($\pm 0.03 \text{ in.}$)	Body Center Ht ($\pm 0.03 \text{ in.}$)	Average Body Ht ($\pm 0.03 \text{ in.}$)	Body Diameter ($\pm 0.03 \text{ in.}$)	Vol of Body (in.^3)	Bulk Dry Debris Bed Density ($\pm 0.02 \text{ g/mL}$)
NO1	170.6	0.10	RD1	0.18	0.12	0.08	5.55	1.94	0.084
		0.02	RD1	0.20	0.15	0.12	5.59	2.95	0.056
		0.20	RU2	0.20	0.12	0.10	5.60	2.46	0.067
		0.10	RU4	0.18	0.11	0.10	5.54	2.41	0.067
NO2	576.2	0.10	RD1	0.63	0.31	0.30	4.48	4.72	0.076
		0.02	RD1	0.60	0.33	0.32	4.47	5.03	0.071
		0.20	RU2	0.48	0.20	0.17	4.11	2.26	0.133
		0.20	RU3	0.45	0.18	0.17	4.29	2.46	0.133
		0.02	RD4	0.57	0.22	0.20	4.17	2.74	0.113
		0.10	RU4	0.46	0.18	0.17	4.10	2.25	0.133
NO3a	1244.2	0.10	RU1	0.72	0.40	0.38	4.44	5.88	0.129
		0.20	RU1	0.66	0.35	0.33	4.54	5.34	0.148
		0.02	RD2	0.71	0.43	0.41	4.72	7.17	0.119
		0.10	RU3	0.64	0.37	0.35	4.72	6.13	0.140
		0.20	RU3	0.61	0.31	0.29	4.72	5.07	0.169
		0.10	RD3	0.61	0.35	0.33	4.98	6.42	0.148
		0.02	RD3	0.67	0.40	0.38	4.86	7.05	0.129
		0.10	RU4	0.62	0.34	0.32	4.88	5.99	0.153
NO3c	1244.2	0.20	RU1	0.57	0.34	0.32	4.96	6.19	0.153
		0.02	RD1	0.66	0.42	0.40	4.84	7.37	0.122
		0.02	RD3	0.64	0.42	0.40	4.89	7.52	0.122
NO5 ¹	1719.5	0.96	RU4	0.36	0.26	0.27	5.24	5.82	0.251
		0.98	RU1	0.44	0.32	0.32	5.10	6.54	0.212
		0.05	RD4	0.44	0.32	0.32	5.28	6.99	0.212
		0.18	BF	0.62	0.42	0.42	4.45	6.52	0.161
NO6a	1250.1	0.10	RU1	0.64	0.50	0.48	5.24	10.37	0.103
		0.20	RU1	0.49	0.31	0.29	5.11	5.95	0.170
		0.20	RU3	0.50	0.31	0.29	5.09	5.91	0.170
		0.02	RD3	0.50	0.40	0.38	5.30	8.39	0.130
		0.10	RU4	0.50	0.33	0.31	5.14	6.42	0.159
NO6b	1250.1	0.20	RU1	0.20	0.49	0.23	0.21	5.08	0.214
		0.10	RU2	0.10	0.48	0.28	0.26	5.18	0.176

Table 7.9. (contd)

Test Case	Retrieved Debris Bed Mass Loading ($\pm 4 \text{ g/m}^2$)	Screen Approach Velocity ($\pm 0.3 \text{ ft/sec}$)	Test Phase	Rim Ht ($\pm 0.03 \text{ in.}$)	Body Center Ht ($\pm 0.03 \text{ in.}$)	Average Body Ht ($\pm 0.03 \text{ in.}$)	Body Diameter ($\pm 0.03 \text{ in.}$)	Vol of Body (in.^3)	Bulk Dry Debris Bed Density ($\pm 0.02 \text{ g/mL}$)
NO7a	1190.5	0.10	RU1	0.71	0.63	0.61	5.50	14.50	0.077
		0.20	RU1	0.65	0.52	0.50	5.52	11.95	0.094
		0.20	RU3	0.57	0.46	0.44	5.38	10.02	0.107
		0.10	RD3	0.57	0.46	0.44	5.49	10.42	0.107
		0.02	RD3	0.58	0.56	0.54	5.70	13.80	0.087
NO7b	1190.5	0.20	RU1	0.50	0.32	0.30	5.24	6.46	0.156
		0.10	RU2	0.50	0.33	0.31	5.18	6.53	0.151

¹ Debris bed formed with an initial screen approach velocity of 0.2 ft/sec as opposed to a constant 0.1 ft/sec

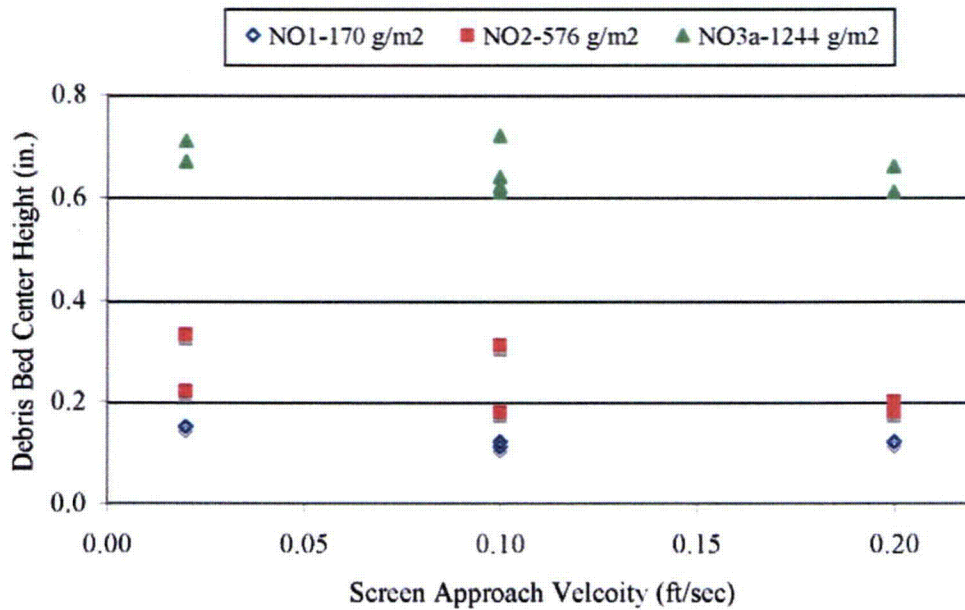


Figure 7.10. Center Height of Debris Beds from Tests NO1, NO2, and NO3a as a Function of Screen Approach Velocity. Tests NO1, NO2, and NO3a were all formed at a constant screen approach velocity of 0.1 ft/sec.

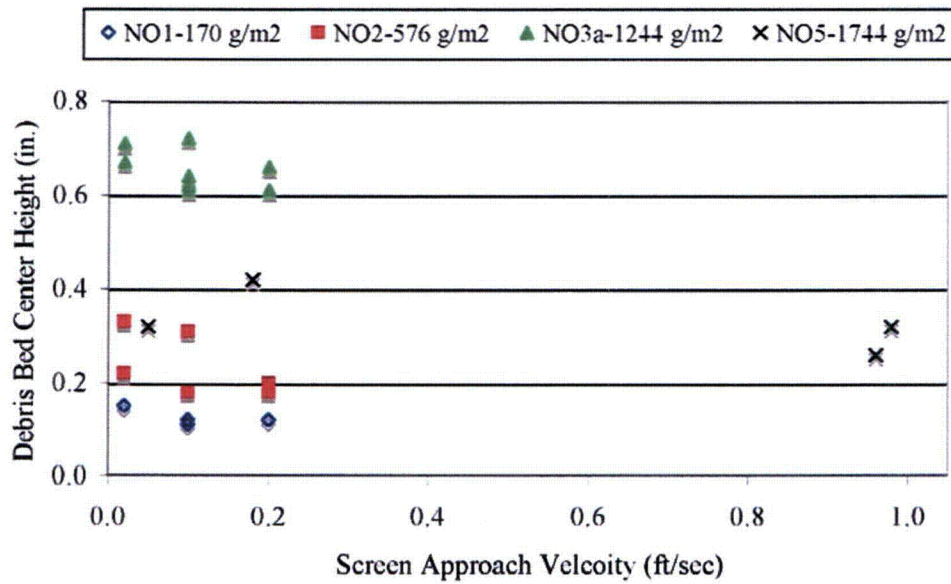


Figure 7.11. Center Height of Debris Beds from Tests NO1, NO2, NO3a, and NO5 as a Function of Screen Approach Velocity. Tests NO1, NO2, and NO3a were all formed at a constant screen approach velocity of 0.1 ft/sec and test NO5 at an initial velocity of 0.2 ft/sec.

the debris bed. Comparing the calculated bulk dry debris bed densities, from Table 7.8 for the tests plotted in Figures 7.10 and 7.11, the density of the debris bed from Test NO5 is seen to be approximately 1.2 to 4.5 times greater than that calculated for NO1, NO2, or NO3a. Considering the retrieved mass loadings for debris beds NO3a and NO5 along with the head loss data plotted in Figure 7.9, the higher-density cases did not correspond to the cases of highest head loss.

Figure 7.12 is a plot of the dry bulk density as a function of the retrieved debris bed mass loading for constant screen approach velocities. All of the data plotted is from debris beds generated with a screen approach velocity of 0.1 ft/sec (0.03 m/s). The relative bulk density of the debris beds is largest at the highest retrieved mass loadings. However, for the limited number of retrieved mass loadings obtained, no definitive relationship between the bulk density and the retrieved mass loading is observed.

The head loss across the debris bed is plotted as a function of the calculated bulk dry debris bed density for constant screen approach velocities in Figure 7.13. For all cases plotted the bed formation velocity was 0.1 ft/sec. The observed trends indicate that the bulk density increases with the screen approach velocity, and the head loss increases with the relative bulk density. Again it is noted that this trend is observed only for test cases having the same bed formation velocity (0.1 ft/sec).

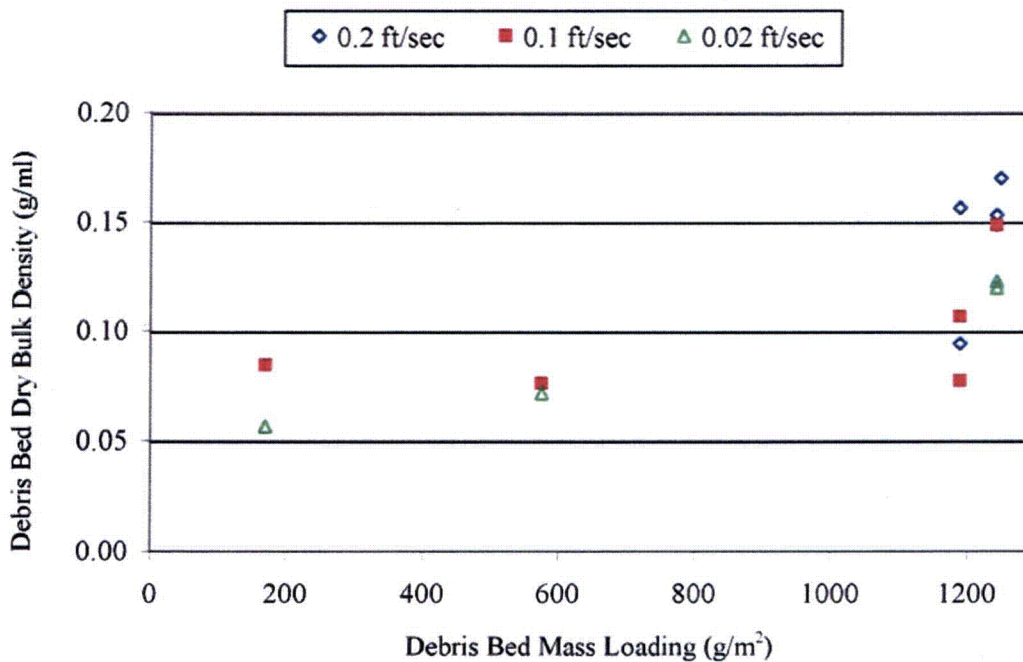


Figure 7.12. Debris Bed Dry Bulk Density as a Function of Mass Loading for the NUKON-Only Debris Beds Created and Tested at Ambient Temperature. The data presented were obtained during the first two cycles of the velocity sequence for each test. For the data plotted, debris beds were formed at 0.1 ft/sec.

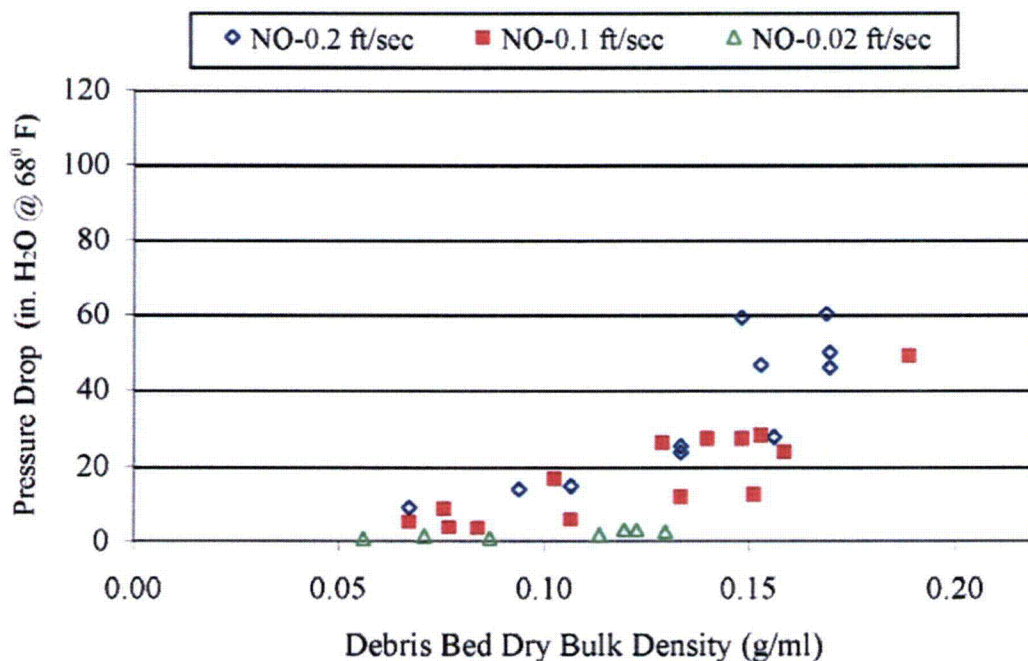


Figure 7.13. Pressure Drop Across NUKON-Only Debris Beds as a Function of Dry Bulk Density for Screen Approach Velocities of 0.02, 0.1 and 0.2 ft/sec. Debris beds were formed at a screen approach velocity of 0.1 ft/sec and tested at ambient temperature.

7.2.2 Temperature Effects on NUKON-Only Debris Beds

The initial Series 2 tests conducted to evaluate the effects of temperature on head loss consisted of elevating the loop temperature after a test at ambient temperature had been completed. The nominal elevated temperatures at which testing was performed were 129°F (54°C) and 180°F (82°C). This resulted in the measurements at elevated temperature being obtained with the debris beds having been subjected to substantially more flow history than when measurements were taken at ambient temperature. For NUKON-only, tests NO3b and NO3c were conducted in this manner. After evaluating the initial results obtained at elevated temperature, it was decided that additional tests should be conducted to further examine the effects of temperature.

For the additional tests, the debris beds were generated at the elevated test temperatures of 129°F (54°C) and 180°F (82°C). The initial head loss measurements were then taken at the temperature at which the debris bed was formed. Following the completion of the initial velocity sequence, the loop temperature was reduced and a truncated velocity sequence was executed. For NUKON-only, tests NO6a through NO7b were conducted in this manner. For Tests, NO6a and NO7a, the debris beds were generated at 129°F (54°C) and 180°F (82°C), respectively, and the full Series 2 velocity sequence was executed. Test NO6b was conducted using the debris bed generated during test NO6a with the loop temperature reduced to 81°F (27°C). Test NO7b was conducted using the debris bed generated during test NO7a with the loop temperature reduced to 131°F (55°C).

It was anticipated, based on conversations with the vendors of the debris material, that fluid temperatures between 68°F (20°C) and 180°F (82°C) would have negligible effects on the physical/chemical makeup of debris material. However, it is unknown what effect the temperature has on the material properties of the fibers (e.g., flexibility). It was also expected that increases in the fluid temperature would decrease the measured head loss due to the reduction in fluid viscosity and density.

The effects of temperature are first evaluated by examining the temperature history for individual tests. Comparisons will then be made for data sets obtained at a similar temperature. Additional parameters impacting the attempt to isolate the effects of temperature include the flow history of a debris bed and the temperature at which the debris bed was generated. For the plots used to present the head loss data, the data sets will be labeled in the legend as NO#-DTC-BF-BTC, where NO# = the test case number, DTC = the temperature at which head loss data were taken (°C), BF stands for bed formation, BTC = the temperature at which the debris bed was formed (°C). For example, NO6b-27C-BF-54C is the data taken at 27°C for test case NO6b, and the debris bed was formed at a temperature of 54°C.

For evaluating temperature effects, three NUKON-only debris beds were generated as part of Tests NO3a, NO6a, and NO7a. Refer to Section 5.3 for a description of how the testing at elevated temperatures was conducted. Figures 7.14, 7.15, and 7.16 contain the head loss data from ramp up 2 for tests NO3a, NO6a, and NO7a along with the corresponding follow-on tests conducted for each debris bed at various temperatures.

In Figure 7.14, it can be seen that the initial increase in temperature from 24° to 53°C was unexpectedly accompanied by a slight increase in head loss. The subsequent rise in temperature to 82°C resulted in a decrease in head loss. For tests NO6a and NO7a, the reduction in loop temperature for the resulting follow-on tests resulted in a corresponding increase in head loss.

Figures 7.14, 7.15, and 7.16 each contain the temperature history for a single debris bed. Each debris bed was generated at a different loop temperature. The expected decrease in head loss for increasing temperature was observed for all test cases except NO3b. The same head loss data is again presented by comparing data sets collected at the same loop temperature. Figures 7.17, 7.18, and 7.19 contain the results obtained at ambient temperature, 54°C, and 82°C, respectively.

The results presented in Figures 7.18 and 7.19 indicate that an increase in the bed formation velocity decreases the resulting head losses. However, the results of Test Case NO6b in Figure 7.17 do not follow this trend. If the calculated dry bulk densities from Table 7.9 are examined, it is observed that the head loss increases with increasing bulk density regardless of the bed formation temperature.

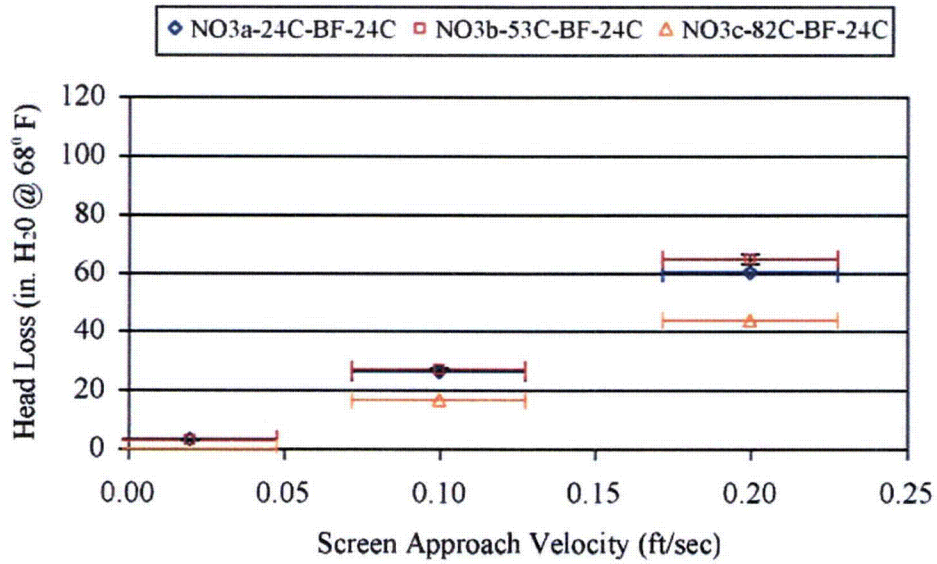


Figure 7.14. Head Loss as a Function of Screen Approach Velocity for the NUKON-Only Debris Bed Formed at 24°C. The retrieved mass loading was 1244 g/m². Tests NO3a, NO3b and NO3c were conducted sequentially at temperatures of 24°, 54°, and 82°C, respectively.

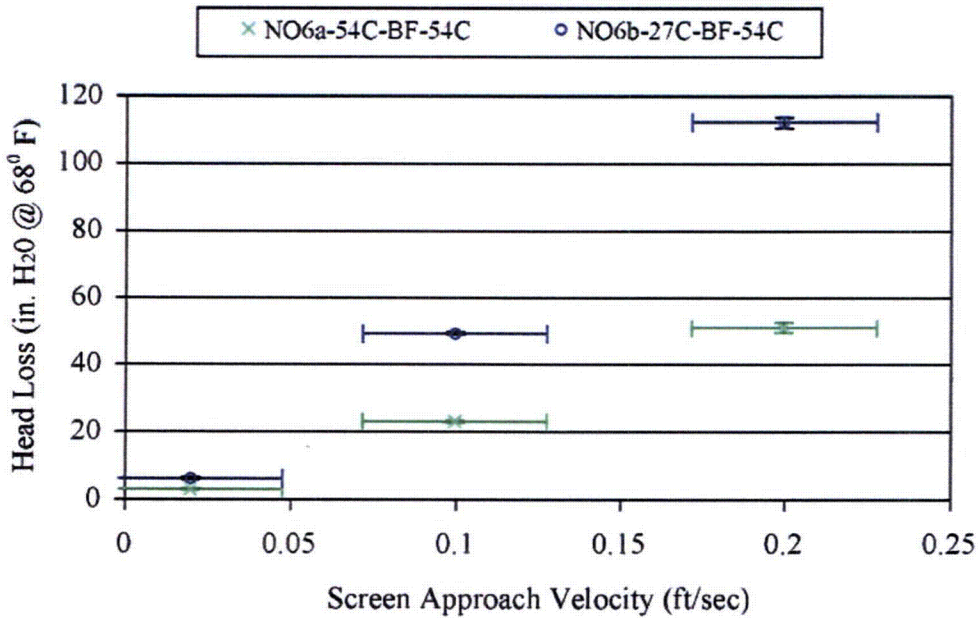


Figure 7.15. Head Loss as a Function of Screen Approach Velocity for the NUKON-Only Debris Bed Formed at 54°C. The retrieved mass loading was 1250 g/m². Tests NO6a and NO6b were conducted sequentially at temperatures of 54° and 27°C, respectively.

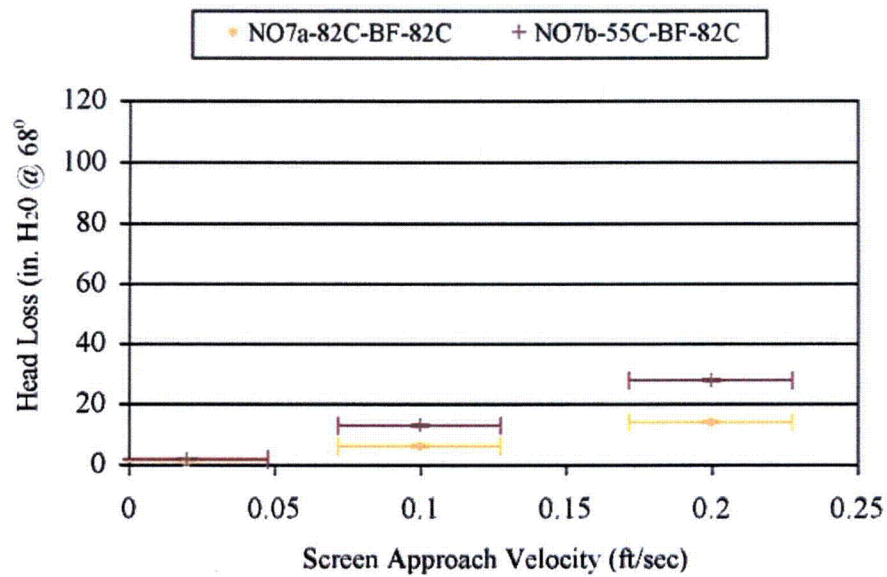


Figure 7.16. Head Loss as a Function of Screen Approach Velocity for the NUKON-Only Debris Bed Formed at 82°C. The retrieved mass loading was 1244 g/m². Tests NO7a and NO7b were conducted sequentially at temperatures of 82° and 55°C, respectively.

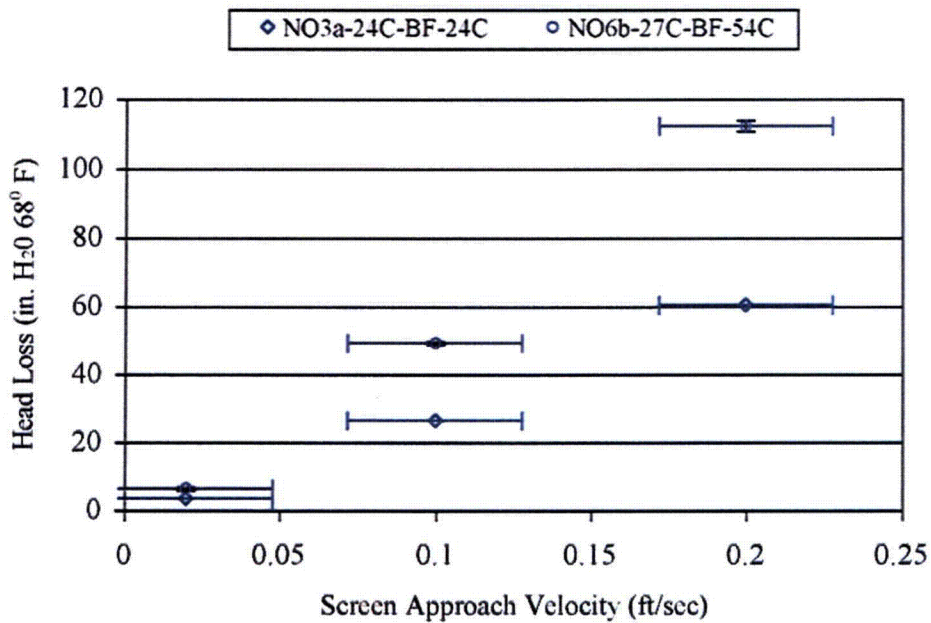


Figure 7.17. Head Loss as a Function of Screen Approach Velocity for the NUKON-Only Debris Bed Tests Conducted at Ambient Temperature. The retrieved mass loading for cases NO3a and NO6b were 1244 g/m² and 1250 g/m², respectively.

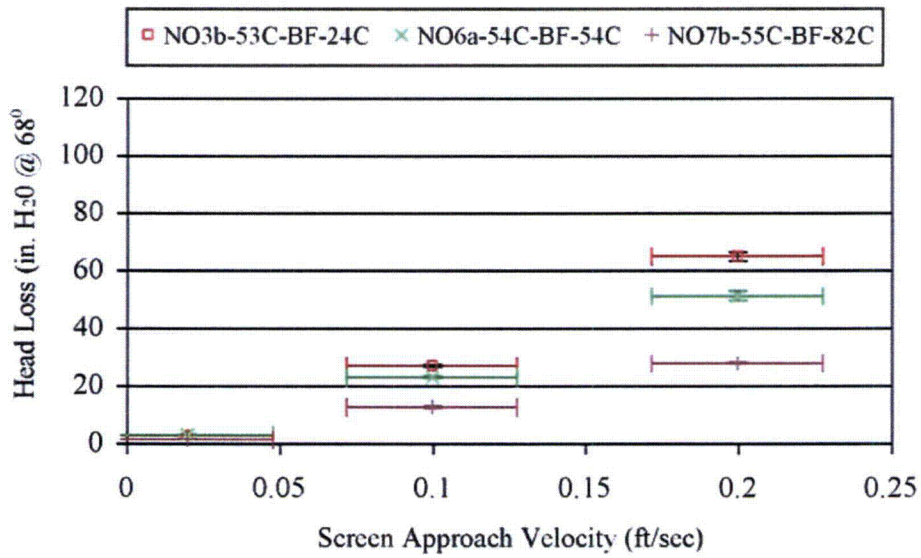


Figure 7.18. Head Loss as a Function of Screen Approach Velocity for the NUKON-Only Debris Bed Tests Conducted at Approximately 54°C. The retrieved mass loading for cases NO3b, NO6a, and NO1 were 1244 g/m², 1250 g/m², and 1191 g/m², respectively.

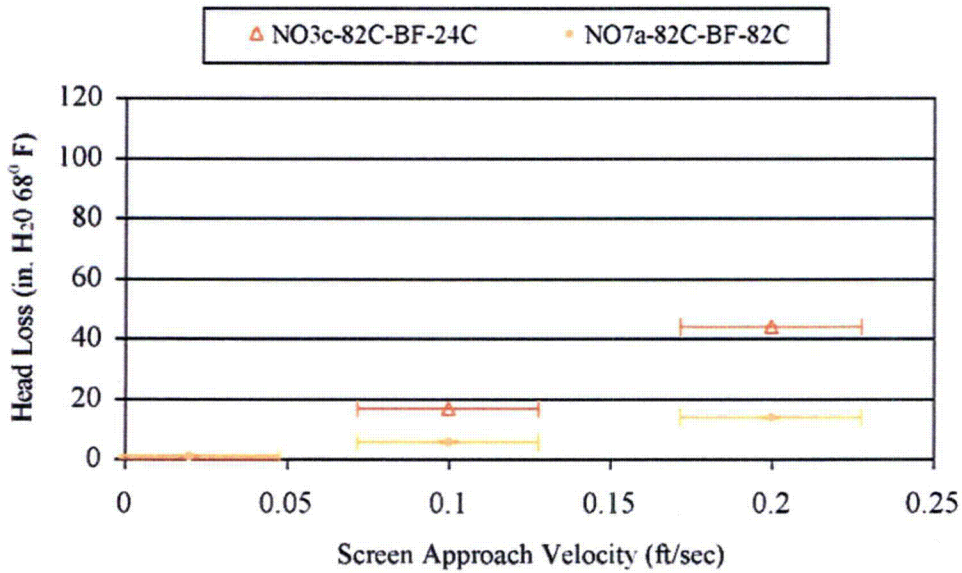


Figure 7.19. Head Loss as a Function of Screen Approach Velocity for the NUKON-Only Debris Bed Tests Conducted at Approximately 82°C. The retrieved mass loading for cases NO3c, and NO7a were 1244 g/m² and 1191 g/m², respectively.

7.3 Results of CalSil-Only Debris Bed Tests

PNNL testing for CalSil-only debris beds was initiated in the benchtop loop to assess what CalSil mass loading would be required to achieve a complete debris bed. The initial benchtop tests were conducted with both the 5-mesh woven cloth and the perforated plate with 1/8-in. holes. Based on the benchtop test results, a mass loading of 4350 g/m² was chosen for the only CalSil-only test condition conducted in the large-scale loop. The large-scale test condition was evaluated for fluid temperatures of 21°, 54°, and 82°C. None of the CalSil target mass loadings tested by PNNL produced a complete debris bed. For all of the CalSil-only tests conducted, the target mass retained on the screen ranged from 5 to 17%.

Tables 7.10 and 7.11 list the large-scale and benchtop CalSil only tests conducted, respectively. The tables include the target mass loadings, retrieved dry mass loadings, and percentages of the target mass loading retrieved on the screen. The benchtop tests are included because their results were used to determine the mass loading for the large-scale tests and are the reason only one large-scale CalSil-only debris bed test was attempted. Test cases are numbered in ascending order of target CalSil mass loading.

The various debris loading scenarios used and the observations obtained from the CalSil tests are presented in Section 7.3.1. The limited head loss measurements from the incomplete CalSil debris beds are presented in Section 7.3.2. Section 7.3.3 discusses the head loss results obtained at elevated fluid temperatures. Because no complete debris beds were formed, none of the photos taken with the optical triangulation system were analyzed for bed height measurements. Therefore, no debris bed height measurements or associated debris bed relative bulk densities are presented for the CalSil-only test cases.

Table 7.10. PNNL Large-Scale CalSil-Only Debris Bed Tests

Test Case	Test Series	Test ID	Target Debris Bed CalSil Loading (g/m ²)	CalSil to NUKON Mass Ratio	Total Target Debris Bed Loading (g/m ²)	Total Retrieved Dry Debris Bed Mass Loading (g/m ²)	Target Mass Loading Retained on Screen (%)	Nominal Temp. (°C)	Screen or Plate	Debris Bed Formed
CO1a	2	060512_CO_8108_LP1	4350	N/A	4350	434	10	21	plate	no
CO1b	2	060512_CO_8108_LP2	4350	N/A	4350	434	10	54	plate	no
CO1c	2	060512_CO_8108_LP3	4350	N/A	4350	434	10	82	plate	no

Table 7.11. PNNL Benchtop CalSil-Only Debris Bed Tests

Test Case	Test Series	Test ID	Target Debris Bed CalSil Loading (g/m ²)	CalSil to NUKON Mass Ratio	Total Target Debris Bed Loading (g/m ²)	Total Retrieved Dry Debris Bed Mass Loading (g/m ²)	Target Mass Loading Retained on Screen (%)	Nominal Temp. (°C)	Screen or Plate	Debris Bed Formed
COBT1 ^(a)	N/A	060406_CO_1176_BP1	1450	N/A	1450	79	5 ^(b)	21	plate	no
COBT2	N/A	060510_CO_1469_BP1	1812	N/A	1812	237	13	21	plate	no
COBT3 ^(b)	N/A	051227_CO_0411x_B1	2174	N/A	2174	184	9 ²	26	screen	no
COBT4	N/A	051227_CO_1763_B2	2174	N/A	2174	279	13	26	screen	no
COBT5	N/A	060510_CO_1763_BP2	2175	N/A	2175	292	13	23	plate	no
COBT6	N/A	060510_CO_2351_BP3	2900	N/A	2900	390	13	22	plate	no
COBT7	N/A	060511_CO_3527_B2	4350	N/A	4350	724	17	22	plate	no

(a) Debris bed disturbed during retrieval. Therefore retrieved mass does include all of the debris material retained on the screen.

(b) Debris incrementally added to the loop in a total of 5 separate batches to obtain the total mass loading.

7.3.1 CalSil Debris Bed Formation

The initial CalSil tests conducted were COBT3 (051227_CO_0411x_B1) and COBT4 (051227_CO_1763_B2). The final target mass loading for both tests was the maximum CalSil loading that had been proposed by the NRC for the Series 1 test matrix. These tests were performed as part of the

load sequence evaluation using the 5-mesh screen. Subsection 6.3.1.2 contains a description of the tests and photos of the two retrieved debris beds (Figures 6.13 and 6.14).

For COBT3, the CalSil debris was added incrementally by recharging the debris injection line five times. For COBT4, the total mass of CalSil was added to the debris injection line at one time and a single debris introduction procedure was executed. While neither test formed a complete debris bed, COBT4 with the single introduction of debris material retained approximately 50% more material than the incremental addition of the debris employed for COBT3. This limited evidence suggests that bulk-loading (single introduction) of the target CalSil mass may have a greater probability of forming a complete CalSil-only debris bed than performing incremental additions to achieve the total target CalSil mass loading. This is the expected result since the bulk-loading would result in the debris having being at a higher concentration when it reached the screen. The higher debris concentration promotes retention on the screen.

Figure 7.20 shows the underside (downstream side, discharge) of the COBT3 debris bed. From the photo one can observe how the CalSil material is wrapped completely around the wires of the screen material. This phenomenon was not observed for the NUKON-only tests presented in Section 7.2.

Test COBT1 was conducted to assess whether the peak CalSil mass loading specified by the NRC in the proposed Series 2 test matrix (NRC 2006) would form a complete debris bed on the perforated plate. The initial screen approach velocity for bed formation was 0.1 ft/sec, which was maintained for approximately 13 calculated loop circulations (approximately 20 minutes) without forming a debris bed. The screen approach velocity was then increased to 0.2 ft/sec for approximately an additional 26 calculated loop circulations (approximately 20 minutes) in an attempt to mobilize any settled CalSil material.

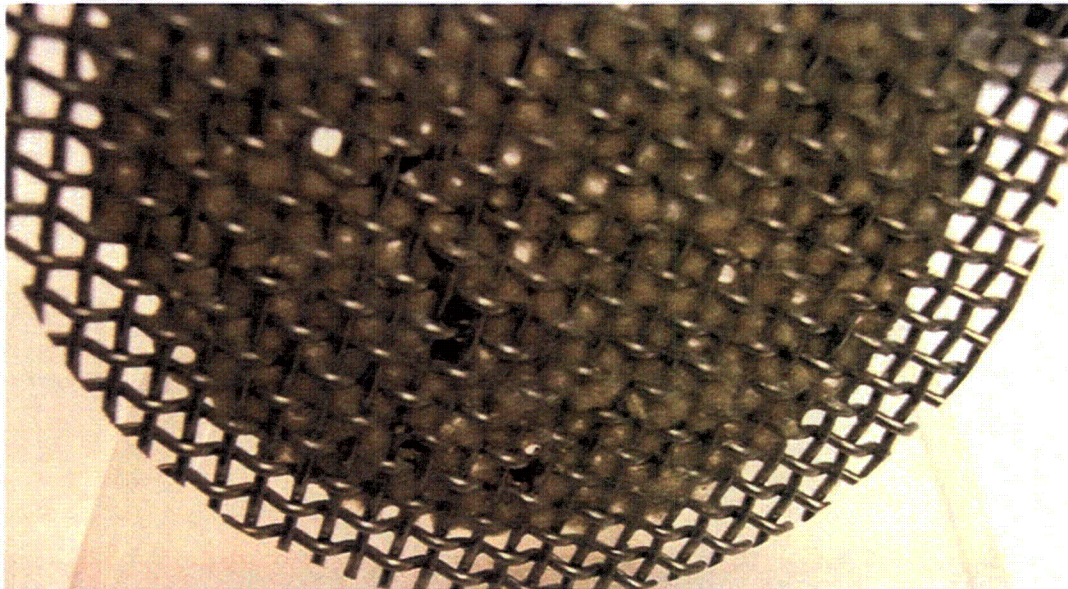


Figure 7.20. Underside of Incomplete Debris Bed from COBT3 Showing How CalSil Material was Completely Entangled with Some Screen Wires in Test 051227_CO_0411x_BP1. Target CalSil mass loading = 2174 g/m², retrieved CalSil mass loading = 184 g/m², 9% of target mass retained on screen, debris bed formed in benchtop test loop.

The higher velocity increased the amount of debris that accumulated on the perforated plate based on visual observations. After about one circulation of the flow loop (approximately 45 sec), the resuspended CalSil material appeared to fill up the holes/openings of the incomplete debris bed. However, a complete debris bed was apparently not sustained. The test section then became very murky, making it extremely difficult to observe the debris bed. The presence of similar amounts (as judged by visual observation) of CalSil debris both above and below the perforated plate may indicate that suspended CalSil was passing uninhibited through the perforated plate or possibly being deposited on the plate but also being lost from the debris bed at a similar rate. Because of the very murky test section, it was not possible to observe whether the holes/openings in the perforated plate were re-exposed. After 20 minutes at 0.2 ft/sec, the debris bed was judged, based on visual observation, to still be incomplete.

During the retrieval of the debris bed for COBT1, a potentially significant portion of the retained CalSil debris was visually observed to be flushed off the screen. Figure 7.20 is a photo of that portion of the retrieved debris bed considered to have experienced the least disturbance. The retrieved mass loading reported in Table 7.11 is known to be less than the amount retained on the screen during the test.

Additional benchtop tests were conducted with progressively larger CalSil mass loadings in an attempt to determine the target mass loading sufficient to generate a complete debris bed in the large-scale test loop. The results of subsequent tests were used to determine the mass loading for the following test. Tests COBT2, COBT5, COBT6, and COBT7 were conducted with target mass loadings 1.25, 1.5, 2.0, and 3.0 times the mass loading of COBT1, respectively. None of the tested mass loadings yielded a complete debris bed. The retrieved debris beds from these tests are pictured in Figures 7.21 through 7.24. The specifications for each test are detailed in the Quick Look reports of Appendix I.

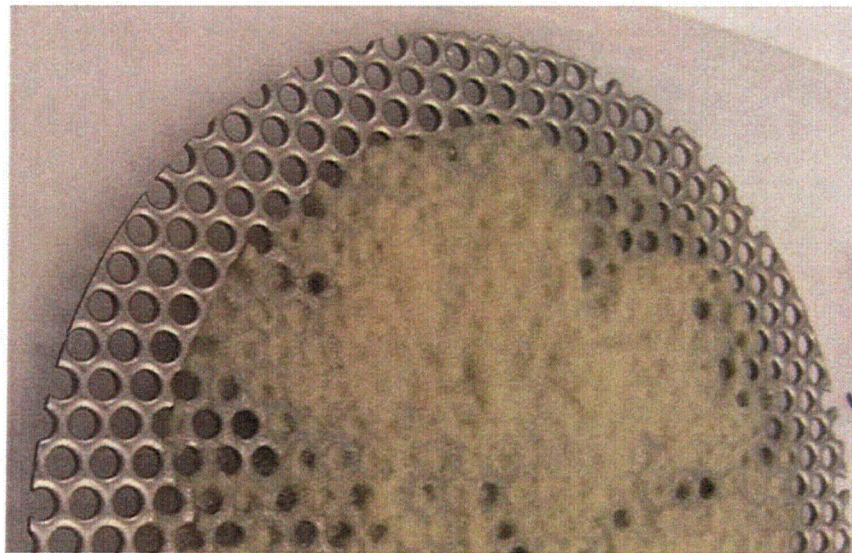


Figure 7.21. Incomplete Debris Bed from COBT1, Test 060406_CO_1176_BP1. NOTE: Debris bed was disturbed during retrieval. The lower half of the photo was not representative of the screen coverage achieved in the test loop and therefore was omitted from the figure. Target CalSil mass loading = 1450 g/m², retrieved CalSil mass loading = 79 g/m² (reduced due to disruption of debris bed during retrieval), 5% of target mass retained on screen, debris bed formed in the benchtop test loop.



Figure 7.22. Incomplete Debris Bed from COBT2, Test 060510_CO_1469_BP1. Target CalSil mass loading = 1812 g/m², retrieved CalSil mass loading = 237 g/m², 13% of target mass retained on screen, debris bed formed in benchtop test loop.



Figure 7.23. Incomplete Debris Bed from COBT5, Test 060510_CO_1763_BP2. Target CalSil mass loading = 2175 g/m², retrieved CalSil mass loading = 292 g/m², 13% of target mass retained on screen, debris bed formed in the benchtop test loop.



Figure 7.24. Incomplete Debris Bed from COBT6, Test 060510_CO_2351_BP3. Target CalSil mass loading = 2900 g/m², retrieved CalSil mass loading = 390 g/m², 13% of target mass retained on screen, debris bed formed in the benchtop test loop.

It was speculated, based on the thickness and appearance of the debris bed retrieved from COBT7, that the potentially nonuniform flow profile in the benchtop loop upstream of the test screen could be creating an uneven distribution of CalSil debris at the surface of the perforated plate. Examining Figure 7.25, the majority of perforated plate appears to be covered with a substantial thickness of debris material. No evidence of the plate hole pattern is observed on the surface of the debris bed. The topography of the surface of the debris bed and the fact that all of the open channels are located on one side of the debris bed indicate the approaching flow stream may have possessed a substantial swirl component that inhibited the formation of a complete debris bed. The relatively longer section of straight pipe upstream of the test screen in the large-scale loop would eliminate this phenomenon. Therefore, it was postulated that a mass loading of 4350 g/m² would be sufficient to generate a complete debris bed in the large-scale loop.

The mass loading of 4350 g/m² was used for conducting CO1a in the large-scale loop. Test cases CO1b and CO1c were conducted with the same debris bed at fluid temperatures of 54° and 82°C, respectively. At no time during any of the three tests was a complete debris bed visually observed. Figure 7.26 is an upstream photo of the retrieved debris bed from test condition CO1. The open channels in Figure 7.26 are distributed throughout the debris bed in contrast to those of the benchtop debris bed pictured in Figure 7.25. The head loss results obtained for CO1a through CO1c are presented in the next two sections.

The CalSil debris beds had debris extruded through the holes of the perforated plate. The majority of the material protruding through the holes appeared to be at the location of open channels. Figure 7.27 is the underside of the perforated plate retrieved from the benchtop test COBT7. Side views of the debris beds and perforated plates from tests COBT7 and CO1 are presented in Figure 7.28. Minimal entangling (attaching to debris from other holes) of the debris material extruded through the holes was observed. This contrasts with the appearance of the material on the underside of the 5-mesh woven wire observed after tests COBT3 and COBT4 in Figure 7.20. The topography of the debris bed surface in the region of the channels can also be seen in Figure 7.28.



Figure 7.25. Incomplete Debris Bed from COBT7, Test 060511_CO_3527_BP2. Target CalSil mass loading = 4350 g/m², retrieved CalSil mass loading = 724 g/m², 17% of target mass retained on screen, debris bed formed in the benchtop test loop.



Figure 7.26. Incomplete Debris Bed from Test Condition CO1, Tests 060510_CO_8108_LP1 Through LP3. Debris bed pictured within TTS, target CalSil mass loading = 4350 g/m², retrieved CalSil mass loading = 434 g/m², 10% of target mass retained on screen, debris bed formed in large-scale test loop.

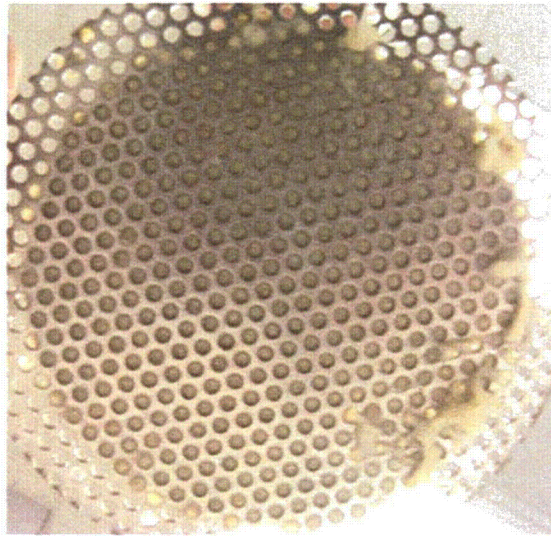
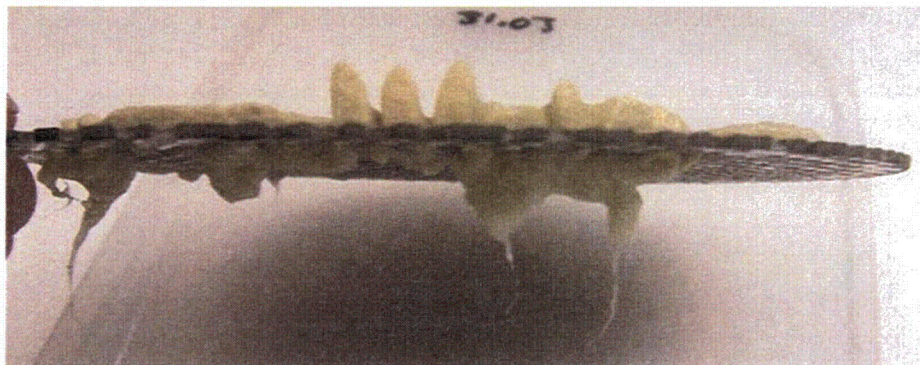
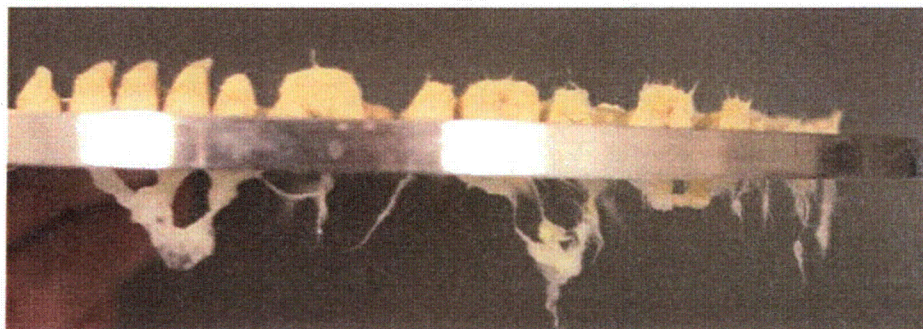


Figure 7.27. Extruded Debris Viewed from the Underside of the Perforated Plate after Benchtop Test COBT7. Retrieved mass loading was 724 g/m^2 , debris extruded through some of the plate holes but was not entangled with the plate (refer to Figure 7.20).



a.



b.

Figure 7.28. Side Views of the Debris Bed and Perforated Plate for Large-Scale and Benchtop Test Cases CO1 and COBT7. Target mass loadings of 4350 g/m^2 debris on the underside of the perforated plate were extruded through the holes in the plate. Figure 7.28a is from COBT 7 with a retrieved mass loading of 724 g/m^2 ; Figure 7.28b is from CO1 with a retrieved mass loading of 434 g/m^2 .

Tables 7.10 and 7.11 also list the percent of the target CalSil mass loading that was retained on each debris screen. Despite significant changes in the target mass loading, test cases COBT2, COBT4, COBT5, and COBT6 all retained 13% of the introduced CalSil. Test Case COBT1 is not a good comparison because it was disturbed during retrieval; neither is Test Case COBT3 because it was formed using incremental addition of the debris. The other benchtop case, COBT7, had a mass loading 2.4 times that of COBT2 and still only retained 17% of the introduced CalSil. In addition, the large-scale test case, CO1, retained 10% of the initial CalSil. This similarity in the retained mass fraction of introduced material indicates that additional CalSil loading does not lead to increased retention.

Having the same fraction of debris retained on the screen over a range of target mass loadings indicates a critical particle size may exist for retention. The CalSil material is made up of 4% by mass fibrous material. If 100% of the CalSil fiber material is retained on the screen, the critical particle size for retention could be approximated using the CalSil particle size data from Section 3.2.2.

7.3.2 Pressure Measurements for CalSil-Only Debris Beds

The benchtop loop had only a single differential pressure transmitter with a range of 0 to 1000 in. H₂O (in. H₂O @ 68°F). Therefore, the resolution and uncertainty of the benchtop measurements are not as good as those obtained from the large-scale loop. The greatest impact is for low pressure drops in the lower 1% of the transmitter range (<10 in. H₂O).

The pressure drop as a function of the screen approach velocity is presented in Figure 7.29 for the large-scale test conducted at ambient temperature, CO1a. The plot contains the data for all four ramp ups in velocity and the first ramp down. Other than ramp up 1, the results were repeatable from one ramp up to another. The increase in pressure observed for the NUKON-only debris beds for repeated cycling of the approach velocity was not observed, which may be because the CalSil-only debris beds were incomplete.

Figure 7.30 compares the pressure drop as a function of the screen approach velocity for benchtop cases COBT2, COBT5, COBT6, and COBT7 and the large-scale case CO1a. The legend of the plot contains the retrieved mass loading after each test case number. The plotted results indicate that, even for the incomplete debris beds, the head loss increases with increasing mass loading.

The pressure drop data for COBT3 and COBT4 was obtained at higher screen approach velocities so a good comparison cannot be made (Section 6.3.1.2). Test Case COBT1 was conducted to determine whether a complete CalSil-only debris bed could be formed, and minimal head loss data were recorded. Following bed formation at 0.1 ft/sec for COBT1, the pressure drop indication was still 0 in. H₂O. After the extended bed formation at 0.2 ft/sec, the indicated pressure drop was 0.1 in. H₂O.

The pressure drop as a function of the retrieved mass loading is plotted in Figure 7.31 for constant velocities of 0.1 and 0.2 ft/sec for the same test cases as plotted in Figures 7.30. The plot in Figure 7.31 indicates how the large-scale and benchtop results compare. Despite the incomplete debris beds, the large-scale data appear to fit well with the benchtop data at both 0.1 and 0.2 ft/sec.

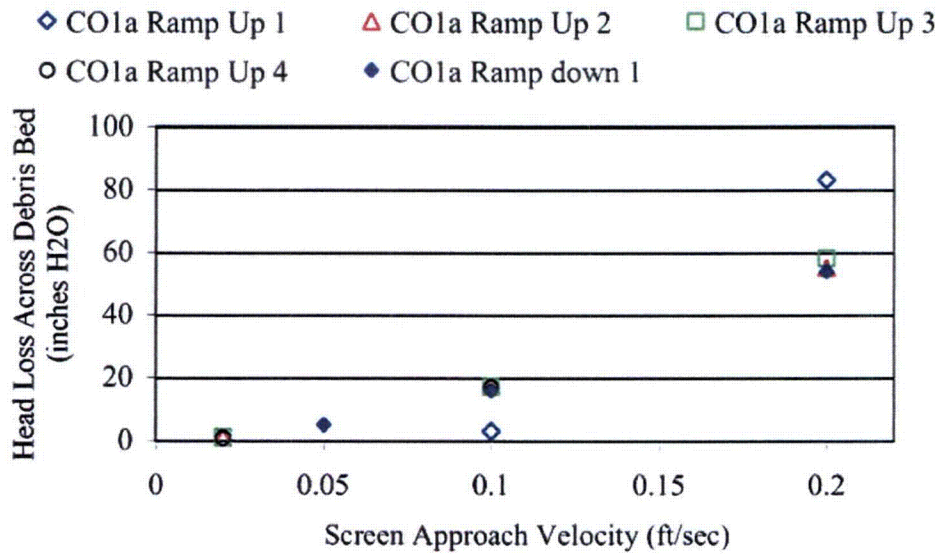


Figure 7.29. Pressure Drop as a Function of the Screen Approach Velocity for CO1a, with a Target CalSil Mass Loading of 4350 g/m² and a Retrieved Mass Loading of 434 g/m². Head loss data are from the Quick Look report for 060512_CO_8108_LP1 in Appendix I.

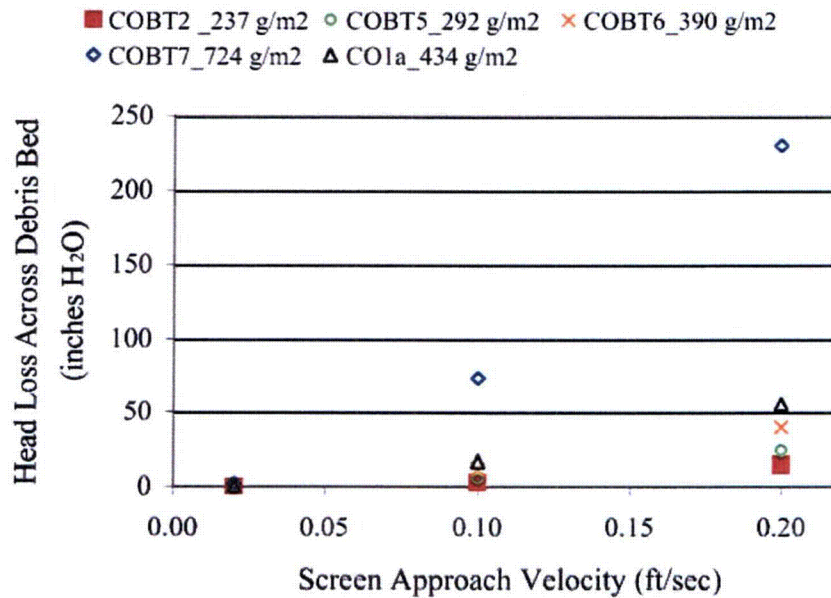


Figure 7.30. Pressure Drop as a Function of Screen Approach Velocity for Benchtop Tests COBT2, COBT5, COBT6, and COBT7 and Large-Scale Test CO1a. Head loss data are from the Quick Look report for 060512_CO_8108_LP1 in Appendix I.

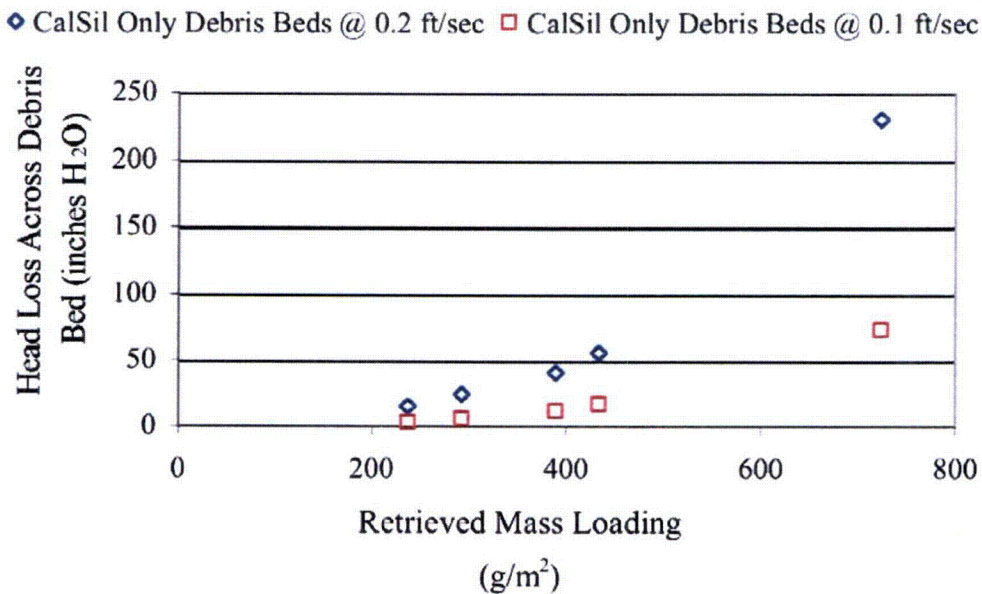


Figure 7.31. Pressure Drop as a Function of Retrieved Mass Loading at Constant Screen Approach Velocities of 0.1 and 0.2 ft/sec. Data plotted for benchtop tests COBT2, COBT5, COBT6, and COBT7 and large-scale test CO1a. Head loss data from Quick Look report for 060512_CO_8108_LP1 in Appendix I.

7.3.3 Temperature Effects on CalSil-Only Debris Beds

The CalSil for test case CO1a was introduced at a fluid temperature of approximately 70°F (21°C). Following the execution of the velocity sequence, the fluid temperature was raised to 129°F (54°C) and the velocity sequence again executed to obtain the steady state measurements for CO1b. The process was again repeated by raising the fluid temperature to 180°F (82°C) to obtain the measurements for CO1c.

The head loss measurements for CO1b were essentially the same as for CO1b without the variations observed in ramp up 1 for CO1a. However, the pressure drop measurements obtained for CO1c yielded an increase in pressure with each velocity cycle. For a screen approach velocity of 0.2 ft/sec, the resulting head loss was 53, 69, and 74 in. H₂O for ramp ups 1 through 3. It is unclear exactly what caused the increase in head loss, and it is assumed that the debris bed retained additional mass, debris material redistributed within the bed (e.g., surface material flowed over an open channel), or the debris properties changed as a function of temperature.

Head loss data are plotted in Figure 7.32 for velocity ramp up 2 of the three temperature cases of test condition CO1. Velocity ramp down 1 has been included for CO1c due to unexplained changes observed for ramp up 2. The other three data sets indicate no measurable change in head loss due to changes in fluid temperature. The effects may be the result of not only the elevated temperature but also the temperature history (i.e., time at temperature and time associated with fluid heat up).

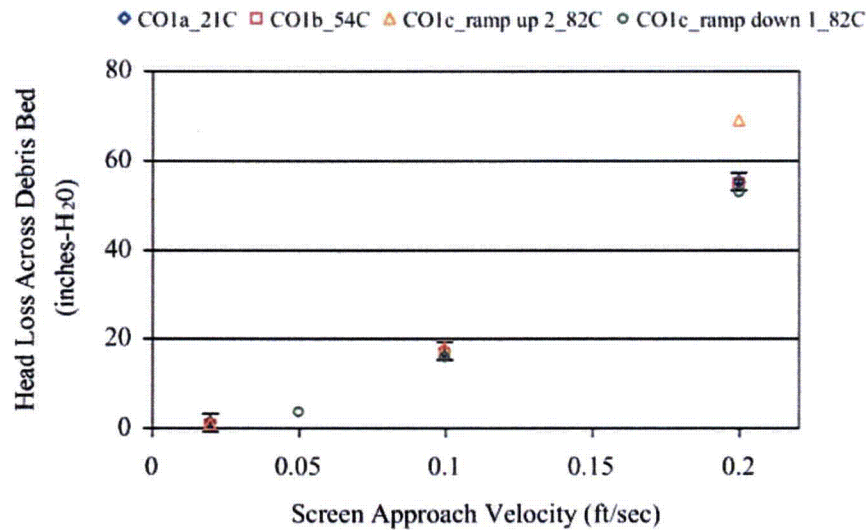


Figure 7.32. Pressure Drop as a Function of Screen Approach Velocity for Test Condition CO1. Target CalSil mass loading was 4350 g/m² and retrieved mass loading was 434 g/m². Test cases CO1a, CO1b, and CO1c were conducted at fluid temperatures of 21°, 54°, and 82°C, respectively. Data for velocity ramp up 2 except as noted for CO1c. Head loss data are from Quick Look report for 060512_CO_8108_LP1 in Appendix I.

7.4 Large-Scale Results for Debris Beds Containing NUKON and CalSil

Sections 7.2 and 7.3 presented the results of the single constituent tests conducted with NUKON-only and CalSil-only debris beds, respectively. The results presented in this section are for tests conducted with both NUKON and CalSil (referred to as NUKON/CalSil or NC) being introduced to the test loop at the same time. Table 7.12 contains the target test matrix for the NUKON/CalSil tests, the dry retrieved mass loadings of the retrieved debris beds, the nominal temperatures at which testing was conducted, the screen materials used, and indication of whether a complete debris bed was formed. An overview of the test matrix completed is provided in Section 7.4.1.

From the results of the NUKON-only tests presented in Section 7.2, it was observed that parameters influencing the debris bed head loss included the mass loading, the flow history, the fluid temperature, the relative bulk density of the debris bed determined from measurements of the debris bed height, and potentially the bed formation velocity. Having a second debris constituent potentially adds the mass loading for the individual constituents and the associated mass ratio of the constituents as parameters influencing the head loss across the debris bed.

The target test matrix was based on a parametric study of the target mass loadings of the constituents and the assumption that the either all of the mass would be retained on the screen or at least the ratio of the debris constituent masses retained on the screen would be similar to the target ratio. In Section 7.2, the results of the NUKON-only tests were presented relative to the retrieved mass loading of NUKON. The same presentation is used for the CalSil in Section 7.3. To evaluate the effects of CalSil being added to the NUKON, the masses of the individual constituents should be determined. Following a preliminary

Table 7.12. Target Test Matrix for Large-Scale NUKON/CalSil Debris Bed Tests

Test Case	Test Series	Test ID	Target Debris Bed NUKON Loading (g/m ²)	Target Debris Bed CalSil Loading (g/m ²)	Target CalSil to NUKON Ratio	Total Target Debris Bed Loading (g/m ²)	Total Retrieved Debris Bed Loading (±8 g/m ²)	Nominal Temp. (°C)	Screen or Plate	Complete Debris Bed Formed
NC1	2	060427_NC_0252_LP1	108	27	0.25	135	56	21	plate	no
NC2	2	060428_NC_0453_LP1	108	135	1.25	243	94	21	plate	no
NC3 ^(a)	1	051110_NC_0595_L1	213	106	0.50	326	217	21	screen	yes
NC4	2	060509_NC_0505_LP1	217	54	0.25	271	209	21	plate	yes
NC5a	2	060426_NC_0708_LP1	217	163	0.75	380	213	21	plate	yes
NC5b	2	060426_NC_0708_LP2	217	163	0.75	380	213	82	plate	yes
NC6a	2	060517_NC_0808_LP1	217	217	1.00	434	297	21	plate	yes
NC6b	2	060517_NC_0808_LP2	217	217	1.00	434	297	82	plate	yes
NC7	1	051121_NC_1586_L1	568	284	0.50	851	729	21	screen	yes
NC8	BM	060323_NC_1619_LP1	724	145	0.20	869	646	21	plate	yes
NC9	2	060331_NC_2024_LP1	724	362	0.50	1086	732	21	plate	yes
NC10 ^(b)	2	060404_NC_2698_LP1	724	724	1.00	1448	862	21	plate	yes
NC11	1	051123_NC_2181_L1	780	390	0.50	1170	1034	21	screen	yes
NC12	1	051117_NC_2776_L1	993	496	0.50	1489	1334	21	screen	yes
NC13	1	051128_NC_2776_L2	993	496	0.50	1489	1260	21	screen	yes
NC14 ^(c)	1	051115_NC_4098_L1	1419	780	0.55	2199	1924	21	screen	yes
NC15a ^(c)	2	060807_NC_0708_LP1	217	163	0.75	380	261	54	plate	yes
NC15b ^(c)	2	060807_NC_0708_LP2	217	163	0.75	380	261	36	plate	yes
NC16a ^(c)	2	060809_NC_0708_LP1	217	163	0.75	380	160	82	plate	yes
NC16b ^(c)	2	060809_NC_0708_LP2	217	163	0.75	380	160	54	plate	yes
NC17a ^(c)	2	060817_NC_2024_LP1	724	362	0.50	1086	811	54	plate	yes
NC17b ^(c)	2	060817_NC_2024_LP2	724	362	0.50	1086	811	29	plate	yes

(a) Initial screen approach velocity during debris-bed formation = 0.2 ft/sec as opposed to a constant 0.1 ft/sec.
(b) Debris bed essentially plugged screen (head loss > 750 in. H₂O) at completion of bed formation process.
(c) Debris bed formed at an elevated fluid temperature.

investigation, the process of dissolving the debris beds in hydrochloric acid and detecting the concentration of calcium using a calcium ISE (Sections 2.5.4.2 and 5.3), was chosen for determining the mass loading of CalSil. The results of this assessment are presented in Section 7.4.2.

Optical triangulation was used to obtain in situ debris bed height measurements for the Benchmark and Series 2 tests. These measurements, along with a comparison of the relative bulk density of the debris beds, are presented in Section 7.4.3. Post-test measurements of the debris bed height are also presented in Section 7.4.3 to provide a comparison of the Series 1 tests, which did not have the optical triangulation system available, and the Benchmark and Series 2 tests. As discussed earlier, in situ manual measurements of the debris bed height could not always be obtained and are not discussed in this section. The data for the NUKON/CalSil debris bed measurements made are in the Quick Look reports in Appendix J.

The head loss measurements obtained for all velocity sequences completed for each NUKON/CalSil debris bed are contained in the Quick Look reports of Appendix J. Section 7.4.4 provides an overview and a comparison of the NUKON/CalSil head loss measurements and is not intended to provide data for all of the measurements, which can be obtained from the Quick Look reports.

As with the NUKON-only tests, fluid temperature effects were evaluated using two different test methods. The results of the testing conducted at elevated fluid temperatures are presented in Section 7.4.5. The test descriptions, initial conditions, debris bed photos, and test measurements for the CalSil/NUKON debris beds are contained in the Quick Look reports of Appendix J.

7.4.1 Overview of the NUKON/CalSil Test Matrix

Debris injection into the large-scale loop was conducted for seventeen NUKON/CalSil debris target conditions. From the 17 debris bed target conditions, 22 tests were conducted. The multiple tests conducted for a single debris bed are the result of changing the test loop fluid temperature and executing a second velocity matrix. The test case numbers for cases NC1 through NC14 are ordered first for ascending target NUKON mass loading followed by increasing target CalSil mass loading. For debris bed conditions having multiple tests conducted with the same debris bed, a lower case letter is used to designate the sequential order of the tests (e.g., Test Cases NC5a and NC5b were conducted with the same debris bed, with Test NC5a being conducted prior to Test NC5b). Test cases 15 through 17 are additional test conditions that are numbered in the order in which they were completed.

For the six Series 1 NUKON/CalSil tests, the CalSil and NUKON were prepared separately and introduced into the loop using independent injection loops for each constituent. The constituents were introduced into the test loop simultaneously but had no interaction prior to entry into the main line of the test loop. Based on the variation in the head loss measurements relative to the target mass loadings obtained between tests from the Series 1 tests, it was postulated that the Series 1 debris introduction procedure created variability in the sequence in which debris arrives at the test screen. To examine the variation observed in the Series 1 head loss measurements, the debris loading sequence investigation presented in Section 6.3 was conducted. Following the investigation of the loading sequence, the NRC staff decided that future tests, Benchmark and Series 2, would be conducted by premixing the debris constituents before introducing them into the test loop. The Series 1 test also used the 5-mesh screen (woven wire cloth), and the Benchmark and Series 2 tests used the perforated plate with 1/8-in. holes.

As discussed, the initial screen approach velocity for bed formation at the start of the Series 1 tests was 0.2 ft/sec (0.06 m/s), which was subsequently changed by NRC staff to a constant 0.1 ft/sec (0.03 m/s) after four large-scale tests were conducted. Two of the NUKON/CalSil tests, NC3 and NC14, had debris beds form with an initial screen approach velocity of 0.2 ft/sec (0.06 m/s). As indicated in Table 7.12, tests NC7 and NC 11 through NC 13 were formed at a constant screen approach velocity of 0.1 ft/sec (0.03 m/s) but with simultaneous introduction (not premixed) of debris constituents.

The two CalSil/NUKON tests with the lowest retrieved mass loading, NC1 and NC2, did not generate complete debris beds. Figures 7.33 and 7.34 are photos of the incomplete debris beds from NC1 and NC2, respectively. The target NUKON loading for both NC1 and NC2 was 108 g/mL while the total retrieved mass loadings were 56.3 and 94.4 g/mL, respectively. Based on the photos, it appears that approximately the same fraction of the screen is covered with debris for both tests despite NC2 having approximately 80% more mass. It appears again, based on the results of Section 7.3, that the formation of a complete debris bed is dependent on the mass loading of NUKON. The lowest target mass loading at which a complete NUKON-only debris bed was formed was 217 g/mL for NO1, which had a total retrieved mass loading of 171 g/mL. The lowest target NUKON loading from the NUKON/CalSil tests that generated a complete debris bed was 213 g/mL from NC13. The retrieved mass loading of NUKON



Figure 7.33. Incomplete Debris Bed Retrieved from Test NC1 with a Retrieved Mass Loading of 56.3 g/m^2 . The target mass loading was 108 g/m^2 NUKON, 27 g/m^2 CalSil, and 135 g/m^2 total.

for Test NC13 is discussed in Section 7.4.2. Testing was not conducted to determine the actual minimum debris loading conditions at which complete debris beds could be formed.

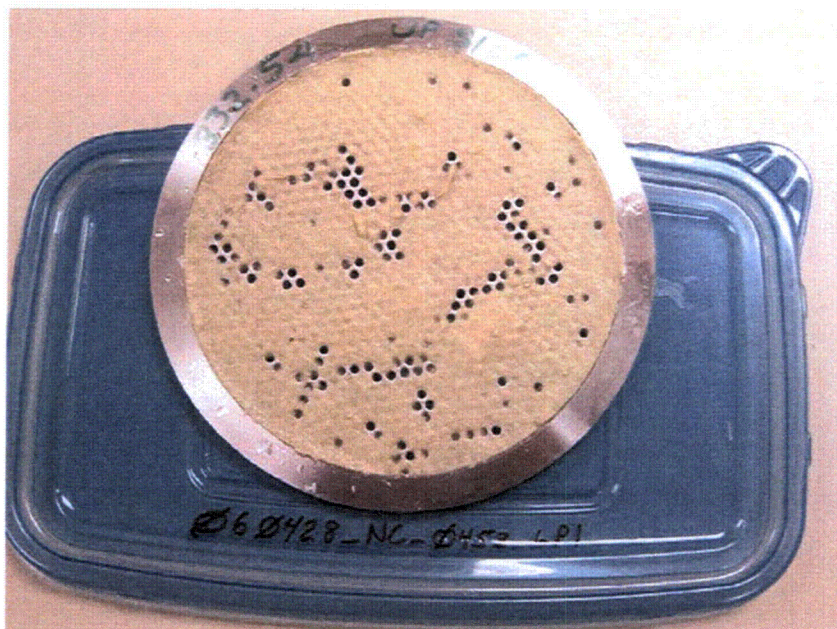


Figure 7.34. Incomplete Debris Bed Retrieved from Test NC2 with a Retrieved Mass Loading of 94.4 g/m^2 . Target mass loading was 108 g/m^2 NUKON, 135 g/m^2 CalSil, and 243 g/m^2 total.

Test NC6a appeared to have formed a complete debris bed at the end of the bed formation process; however, channeling occurred during the initial ramp up in velocity. The target NUKON loading for NC6a was 217 g/mL. The effect of the CalSil loading on the formation of the debris bed is discussed further in Section 7.4.2 with the presentation of the CalSil mass measurements. Due to the effort required to obtain measurements from the CalSil dissolution process, the debris beds from NC1 and NC2 were not assessed for CalSil mass content. Test NC16a yielded the lowest retrieved mass loading for a complete NUKON/ CalSil debris bed at 160 g/mL. Figure 7.35 is a photo of the debris bed retrieved following completion of tests NC16a and NC16b. The hole pattern of the perforated plate is visible on the debris bed surface.

Three tests were conducted for CalSil to NUKON mass ratios greater than 0.75, one of which was the incomplete debris bed of NC2. Of those three tests, NC10 had both the greatest target mass loading, 1448 g/mL, and retrieved mass loading, 862 g/mL. At the completion of bed formation at 0.1 ft/sec (0.03 m/s), the head loss measured for NC10 was 749 in. H₂O at 68°F. The measured head loss was greater than the range of interest for this test program; and therefore, the debris bed was assumed to be plugged and additional measurements were not taken. This test case is discussed further in Section 7.4.2, but head loss measurements from NC10 are not presented in Section 7.4.4.

Head loss measurements were obtained at elevated fluid temperatures (>50°C) for tests NC5b, NC6b, NC15a, NC16a, NC16b, and NC17a; the debris beds for tests NC15a through NC 17b were generated at elevated temperatures. The head loss measurements for the tests conducted at elevated fluid temperatures are presented in Section 7.4.5.



Figure 7.35. Upstream View of Top of Debris Bed from Test Condition NC16. Target mass loadings were 217 g/m² NUKON and 163 g/m² CalSil; total retrieved mass loading was 160 g/m². This is the smallest retrieved mass loading of the CalSil/NUKON test cases to form a complete debris bed. Test cases NC16a and NC16b were completed before bed retrieval. The two divots/craters in the upper of half of the photo are the result of disturbances to the debris bed during post-test retrieval. The surface texture of the debris bed is the hole pattern of the perforated plate being telegraphed through the debris material.

7.4.2 Results of Debris Bed Dissolution to Assess CalSil Mass Content

The mass of CalSil in a retrieved debris bed was determined from two methods referred to as the “mass method” and “chemical dissolution.” The mass method used the dry masses of the constituents introduced to the loop and the dry mass of the retrieved debris bed to calculate an upper and lower bound for the possible quantity of CalSil retained in a debris bed. The predicted CalSil mass loading was obtained from the mass method. Chemical dissolution obtained the final mass from voltage measurements taken with calcium ISE probes in prepared samples of the dissolved debris beds. The ISE probe voltage was experimentally correlated to the CalSil concentration. (See subsection 2.5.4.2 for a brief overview of the ISE probe and Section 5.3 for a summary of the procedure used to determine the CalSil mass in the debris bed.) The calculated CalSil mass loading was obtained from chemical dissolution. The values reported for the retrieved CalSil mass loading and used to compare the NUKON/CalSil test cases are based on the following assumptions.

- No residual CalSil existed in the loop at the start of a test, and the mass of CalSil existing in the debris bed cannot be greater than the mass of CalSil introduced to the loop for the test.
- The mass loading of NUKON in the debris bed is assumed to be equal to the retrieved total dry mass loading minus the CalSil mass loading obtained from chemical dissolution. The minimum mass of CalSil possible in a debris bed can be determined from the post-test measurement of the dry debris bed mass assuming all of the introduced NUKON was retained in the debris bed. The total mass of the retrieved debris bed may be potentially influenced by retained contaminants (debris from previous tests, system debris, etc.), thus affecting the determination of the predicted minimum CalSil mass present in the debris bed. For this section, it is assumed that the debris beds contained no contaminants.
- All of the CalSil fiber material, assumed to be 4% by mass based on information provided by the CalSil vendor during phone conversations with PNNL staff (refer to Section 3), contained in the mass of CalSil introduced into the test loop for a head loss test is retained in a complete debris bed. The performance standards used to generate the correlation between ISE probe voltage and the concentration of CalSil were made with CalSil material having a uniform ratio of calcium silicate to fiber material. Debris beds containing only a fraction of the CalSil introduced into the loop have a different ratio of calcium silicate to fiber material than existed in the performance standards. However, it is assumed the difference in fiber content is not detected by calcium ISE probes. Therefore, the values for CalSil mass loading obtained from the inverse regression have been corrected based on the assumption that 100% of the CalSil fiber material introduced into the test loop was captured by the debris beds.
- Results from earlier “design of experiment” tests indicated that the presence of NUKON during CalSil dissolution can influence the results. Additionally, the amount of hydrochloric acid (HCl) used to dissolve the debris beds may have a slight influence on CalSil mass estimates. For the design of experiment tests, it is not certain whether dissolution kinetics, analysis techniques, or other effects impacted the results. Acknowledging these uncertainties, preliminary unreviewed data from CalSil dissolution in the presence of NUKON indicates that, at lower mass ratios (not quantifiably defined) of CalSil to NUKON the CalSil mass estimates can be lower than the true values. The difference has been indicated to be as much as 35%. The potential effect of the mass of HCl on CalSil mass estimates in debris beds is included in this difference. Additional investigation would be required to quantify these effects. The current analysis has not considered these possible influences.

Based on these assumptions, the CalSil mass loadings for the complete NUKON/CalSil debris beds are presented in Table 7.13. From the mass method, only upper and lower bounding values are presented. Two values for CalSil mass loading obtained from the chemical dissolution method are presented in the table; column 5 contains the CalSil mass loading determined directly from the calcium ISE probe readings, and the values in column six have been corrected assuming 100% of the fiber contained in the CalSil material introduced into the test loop was retained in the debris bed. Upper and lower bounding values are provided for the CalSil mass loadings corrected for the additional CalSil fiber. The lower and upper bound values were obtained from the 95% upper and lower inverse confidence limits obtained for the inverse linear regression used to transform ISE probe voltage readings to CalSil concentration. The CalSil mass loadings provided in Table 7.13 that have been corrected for the additional CalSil fiber are used to present and compare the test results throughout the remainder of the report.

Table 7.13 also includes the mass percent of the target CalSil retained in the debris bed and the mass fraction of retained CalSil predicted to consist of the CalSil fiber. The lower the percent of CalSil retained in the debris bed, the greater the predicted mass fraction of fiber making up the retained CalSil. The predicted NUKON mass loading and the mass ratio of CalSil to NUKON are also included in the table and are obtained from the CalSil mass loading corrected for the additional CalSil fiber. The upper and lower bounds of the CalSil to NUKON mass ratio were obtained from the upper and lower bounding CalSil mass loadings reported in columns 7 and 8, respectively.

Incomplete debris beds were formed for Test Cases NC1 and NC2; therefore, no chemical dissolution of the retrieved debris bed was performed. Test Cases NC1 and NC2 are included in Table 7.13 for completeness and to simplify comparisons with Table 7.12.

Accounting for the additional CalSil fiber has the greatest impact on the results of test cases with the lowest percentage of initial CalSil material introduced into the loop being retained in the debris bed such as cases NC5 and NC16. For both NC5 and NC16, the CalSil assessment predicted that 5% of the initial CalSil material was retained in the debris bed. Correcting for the additional CalSil fiber increased the predicted amount of CalSil retained in both debris beds to 11%, which is a 120% increase. For cases NC8 and NC15, the correction for fiber increased the predicted value for retained CalSil by 25 and 33%, respectively. For all other cases, the correction increased the predicted amount of retained CalSil by 8% or less.

The retrieved CalSil mass loadings determined by chemical dissolution were expected to fall within the range of the minimum and maximum CalSil amounts predicted from the mass method. Twelve of the 15 debris beds that underwent chemical dissolution had predicted CalSil mass loadings falling within the range predicted by the mass method. Of those 12 cases, all but one, NC12, had the upper and lower bounding values based on the 95% confidence interval falling within the range of the mass measurements. Test case NC 12 had a predicted CalSil mass loading of 343 g/m² and a lower limit of 292 g/m² compared to a lower limit of 341 g/m² predicted by the mass method.

NC7, NC11, and NC15 were the three cases with CalSil mass loadings predicted by chemical dissolution to be below the lower bound values for CalSil mass loading determined from the mass method (refer to Table 7.13). For cases NC7 and NC11, the upper bound values of CalSil mass loading lie within the range obtained from the mass method.

Table 7.13. Retrieved Mass Loading of CalSil in the CalSil/NUKON Debris Beds

Test Case	Total Retrieved Debris Bed Loading ($\pm 4 \text{ g/m}^2$)	CalSil Mass Loading Based on Mass Method		CalSil Mass Loading Based on Chemical Dissolution (g/m^2)	Values Below Corrected Assuming 100% of CalSil Fiber Retained in Debris Bed ^(a)								
		Upper Bound (g/m^2)	Lower Bound (g/m^2)		CalSil Mass Loading Based on Chemical Dissolution			Mass of Initial CalSil Retained in Debris Bed (%)	Mass of Retained CalSil Made up of Fiber ^(a) (%)	NUKON Loading (g/m^2)	CalSil to NUKON Mass Ratio		
					Reported CalSil Mass Loading (g/m^2)	Upper Bound from 95% Upper Inverse Confidence Limit (g/m^2)	Lower Bound from 95% Lower Inverse Confidence Limit (g/m^2)				Reported Ratio	Upper Bound	Lower Bound
NC1	56	27	0	N/A	N/A	N/A	N/A	N/A	N/A	N/A	N/A	N/A	N/A
NC2	94	94	0	N/A	N/A	N/A	N/A	N/A	N/A	N/A	N/A	N/A	N/A
NC3 ^(b,c)	217	106	4	47	49	56	42	46	9	168	0.29	0.35	0.24
NC4	209	54	0	25	26	27	25	48	8	183	0.14	0.15	0.14
NC5a	213	163	0	5	11	11	11	7	59	202	0.05	0.06	0.05
NC5b	213	163	0	5	11	11	11	7	59	202	0.05	0.06	0.05
NC6a	297	217	80	80	85	88	83	39	10	212	0.40	0.42	0.39
NC6b	297	217	80	80	85	88	83	39	10	212	0.40	0.42	0.39
NC7 ^(d)	729	284	161	150	155	178	132	55	7	574	0.27	0.32	0.22
NC8	646	145	0	20	25	26	24	17	23	621	0.04	0.04	0.04
NC9	732	362	8	132	141	145	138	39	10	591	0.24	0.25	0.23
NC10 ^(c)	862	724	138	339	354	365	344	49	8	508	0.70	0.73	0.66
NC11 ^(d)	1034	390	254	236	242	279	206	62	6	792	0.31	0.37	0.25
NC12	1334	496	341	337	343	395	292	69	6	991	0.35	0.42	0.28
NC13	1260	496	267	327	334	384	284	67	6	926	0.36	0.44	0.29
NC14 ^(b)	1924	780	505	667	671	772	571	86	5	1253	0.54	0.67	0.42
NC15a ^(d)	261	163	44	18	24	25	23	15	27	237	0.10	0.11	0.10
NC15b ^(d)	261	163	44	18	24	25	23	15	27	237	0.10	0.11	0.10
NC16a	160	160	0	5	11	11	11	7	58	149	0.08	0.08	0.07
NC16b	160	160	0	5	11	11	11	7	58	149	0.08	0.08	0.07
NC17a	811	362	87	120	129	133	126	36	11	681	0.19	0.20	0.18
NC17b	811	362	87	120	129	133	126	36	11	681	0.19	0.20	0.18

(a) CalSil material assumed to contain 4% by mass fiber.

(b) Initial screen approach velocity during debris bed formation = 0.2 ft/sec as opposed to a constant 0.1 ft/sec.

(c) Debris bed essentially plugged screen (head loss > 750 in. H₂O) at completion of bed formation process.

(d) The CalSil mass loading predicted by the chemical dissolution process is less than the lower bound CalSil mass loading determined from the "mass measurements."

Case NC15 provides the one exception in which there is no overlap between the ranges of CalSil mass loading predicted from the mass method and calculated by chemical dissolution. From chemical dissolution, the CalSil mass loading was determined to be $25 \pm 2 \text{ g/m}^2$, compared with the lower and upper bounds from the mass method calculated to be 44 and 163 g/m^2 , respectively. Based on the results of both the mass method and chemical dissolution, the CalSil to NUKON mass ratio was between 0.07 and 0.11, which is one of the four lowest mass ratios obtained. The debris bed was calculated to have retained only 15% of the target CalSil mass. The CalSil mass loading determined from the chemical dissolution is only 57% of the lower bound obtained from the mass method. This deviance significantly exceeds the 35% difference in CalSil estimates compared to true values that was observed during the design of experiment tests for the low CalSil-to-NUKON mass ratios discussed above. Other than uncertainties or chemical effects not investigated, the discrepancy between the CalSil mass loadings obtained from the mass method and chemical dissolution for Test Case NC15 cannot be explained at this time.

Figure 7.36 contains plots of the percent target mass loading obtained, percent target CalSil mass retained, and the CalSil-to-NUKON retrieved mass ratio obtained from the retrieved debris bed as a function of the retrieved dry mass loading. The percent target mass loading obtained is the percentage of the initial mass introduced into the test loop retrieved in the final dry debris bed. The percent target CalSil retained in the debris bed is based on the chemical dissolution calculations of the mass of CalSil retained in the debris bed (corrected for fiber content) and the mass of CalSil initially introduced to the test loop. The CalSil-to-NUKON mass ratio plotted in Figure 7.36 is based on the chemical dissolution measurements of the mass of CalSil retained in the debris bed (corrected for fiber content) and the dry mass of the retrieved debris bed. This is the mass ratio predicted to exist in the final debris bed retrieved from the test loop. From Figure 7.36, the percentage of initial CalSil introduced into the test loop that is retained in the debris bed and the retrieved CalSil to NUKON mass ratio is observed to increase with the retrieved mass loading on the test screen.

The data for NC10, the only large-scale test case that was considered to be plugged, are also included in Figure 7.36. NC10 had 49% of the target CalSil loading retained in the debris bed and a retrieved CalSil-to-NUKON mass ratio of 0.70. This was the largest mass ratio obtained for the 15 debris beds evaluated. NC10 had an initial target CalSil to NUKON mass ratio of 1. In Section 6.3, observations of significant variability in measured head loss for high target CalSil-to-NUKON mass ratio beds obtained during benchtop testing were discussed. During the benchtop tests, extreme variability was observed in the resulting head losses for initial mass ratios greater than 0.5. Debris beds generated with the same initial conditions and target mass loadings were observed to yield head losses that varied by almost an order of magnitude.

The target CalSil-to-NUKON mass loadings are added to the Figure 7.36 plot in Figure 7.37. Inspecting Figure 7.37, the following observations are made:

- The greater the total mass loading, the closer the retrieved CalSil-to-NUKON mass ratio is to the target mass ratio. For case NC14 at a retrieved mass loading of 1924 g/m^2 , the target mass ratio was 0.55 and the retrieved mass ratio was 0.54.
- NC10 had the highest target mass loading of the three cases (NC2, NC6, and NC10; refer to Table 7.12) with target CalSil-to-NUKON mass ratios exceeding 0.75 and was the only test case to have a CalSil-to-NUKON retrieved mass ratio in excess of 0.54, refer to Table 7.13.
- Of the test cases having retrieved mass loadings greater than 900 g/m^2 , none had target CalSil-to-NUKON mass loadings greater than 0.55.

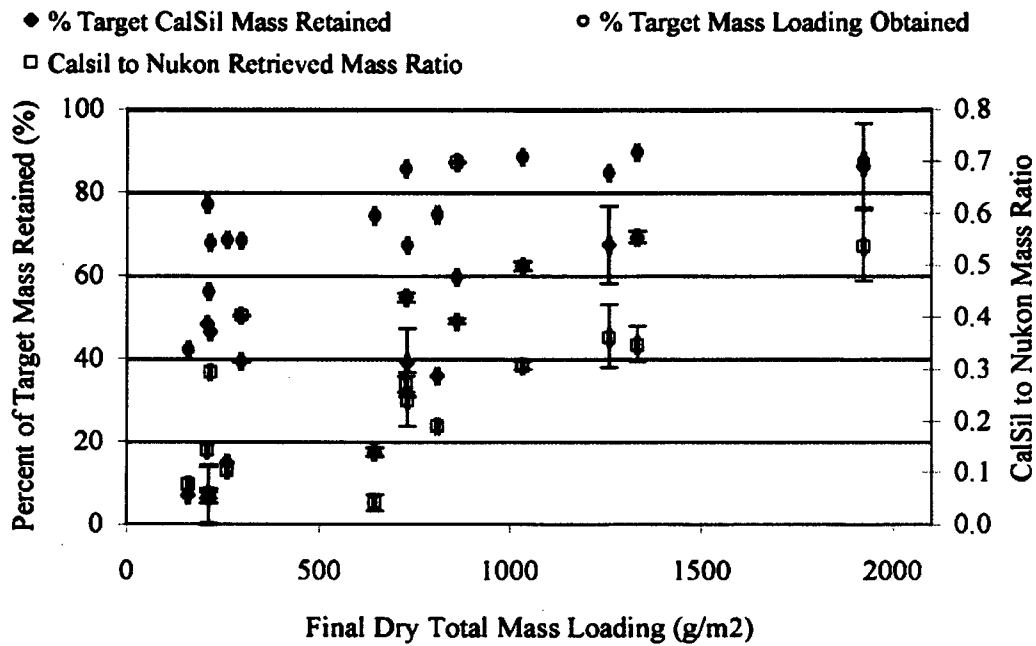


Figure 7.36. Percent Target CalSil Mass and Percent Total Target Mass Loading Retained in the Debris Bed as a Function of the Retrieved Dry Mass Loading. The CalSil-to-NUKON retrieved mass ratio is also plotted. Data are for 15 CalSil/NUKON debris beds that were assessed via chemical dissolution; data presented in Table 7.13

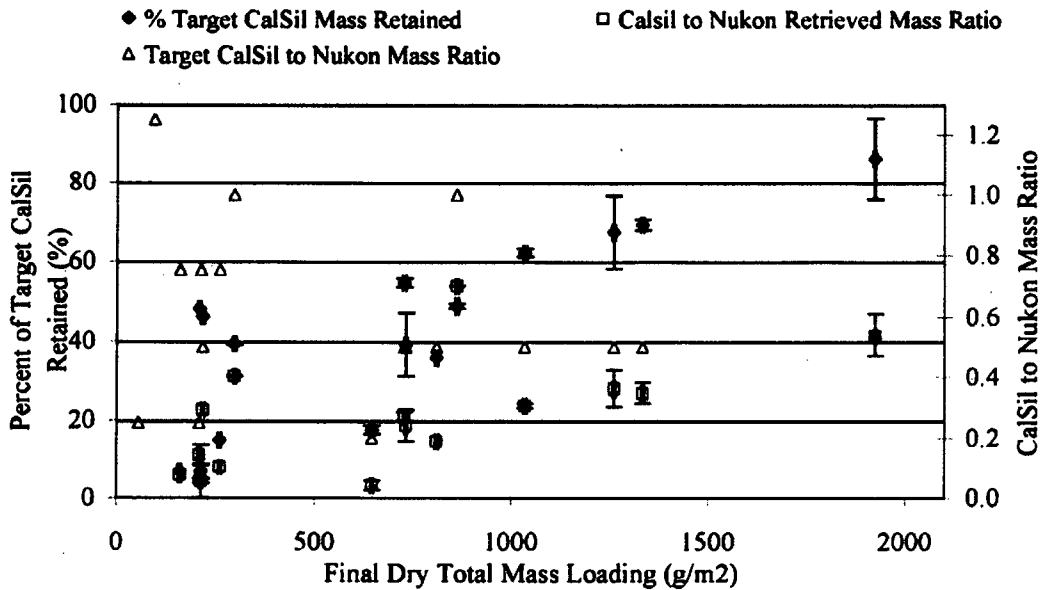


Figure 7.37. Percent Target CalSil Mass and CalSil-to-NUKON Retrieved Mass Ratio Obtained from the Retrieved Debris Bed as a Function of the Total Retrieved Dry Debris Bed Mass Loading. The target CalSil-to-NUKON mass ratio is also plotted as a function of the total retrieved mass loading. Data are for 15 CalSil/NUKON debris beds that were assessed via chemical dissolution; data are presented in Table 7.13

It is unknown whether additional large-scale test cases exhibiting plugged behavior would have been encountered if higher CalSil/NUKON ratios had been tested at the higher mass loadings. The results again indicate that the NUKON mass loading needs to be sufficient to retain the CalSil. The question is again raised as to whether a critical retrieved CalSil/ NUKON mass ratio exists for which the debris bed becomes plugged or saturated. It is unclear to what extent the target CalSil-to-NUKON mass ratio affects the amount of retained CalSil in the debris bed. Test Cases NC3, NC4, NC5, NC15, and NC16 each had a target NUKON mass loading of approximately 217 g/m², and Test Cases NC8, NC9, NC10, and NC17 had a target NUKON mass loading of 724 g/m². Tables 7.14 and 7.15 compare the target mass ratio to the percentage of CalSil retained in the debris bed for the NUKON loadings of 217 g/m² and 724 g/m², respectively.

It was initially postulated that an increase in the CalSil mass loading would increase the amount of CalSil retained in the debris bed. Two scenarios were considered:

- The addition of CalSil to the debris bed would increase the capture efficiency of the debris bed, resulting in a reduction of the average particle size retained in the debris bed.
- The NUKON is only capable of retaining CalSil down to a critical particle size, and additional CalSil does not improve the capture efficiency of the debris bed to act as a filter. This scenario seems more plausible considering the results of Section 7.4.3, in which approximately the same mass fraction of CalSil debris is captured on the perforated plate regardless of the target mass loading of CalSil introduced to the test loop.

Table 7.14. Comparison of Percent of Target CalSil Retained in Debris Bed with Target CalSil-to-NUKON Mass Ratio for a Target NUKON Mass Loading of 217 g/m²

Test Case	Target NUKON Mass Loading (g/m ²)	Target CalSil to NUKON Mass Ratio	Target CalSil Mass Retained in Debris Bed (%)	Retrieved CalSil Mass Loading (g/m ²)	Retrieved Total Mass Loading (g/m ²)
NC4	217	0.25	48	26	209
NC3 ^(a)	213	0.50	46	49	217
NC5	217	0.75	7	11	213
NC16 ^(b)	217	0.75	7	11	160
NC15 ^(b)	217	0.75	15	24	261

(a) Debris bed generated with a bed formation velocity of 0.2 ft/sec.
(b) Debris bed formed at elevated temperature.

Table 7.15. Comparison of Percent of Target CalSil Retained in Debris Bed with Target CalSil-to-NUKON Mass Ratio for Target NUKON Mass Loading of 724 g/m²

Test Case	Target NUKON Mass Loading (g/m ²)	Target CalSil to NUKON Mass Ratio	Target CalSil Mass Retained in Debris Bed (%)	Retrieved CalSil Mass Loading (g/m ²)	Retrieved Total Mass Loading (g/m ²)
NC8	724	0.20	17	25	646
NC9	724	0.50	39	141	732
NC17 ^(a)	724	0.50	36	129	811
NC10 ^(b)	724	1.00	49	354	862

(a) Debris bed formed at elevated temperature.
(b) Debris bed plugged at the completion of debris bed formation.

The results of Table 7.14 do not support the postulated effect of increased CalSil loading on CalSil retention, but instead indicate that an increase in the target CalSil-to-NUKON mass ratio inhibits the

retention of CalSil in the debris bed. However, the results of Table 7.15 indicate the opposite trend; an increase in the target CalSil-to-NUKON mass ratio corresponds to an increase in the percentage of the target CalSil that was retained in the debris bed and an increase in the actual CalSil mass loading. The opposing trends exhibited in these two tables appear to be due to the difference in the retrieved debris bed mass loadings.

Another observation that can be made from the results presented in Tables 7.14 and 7.15 is the similarity in the final CalSil loading obtained from test cases with identical target mass loadings. Cases NC5, NC15, and NC16 formed debris beds at fluid temperatures of 21°, 54°, and 82°C, respectively, but all three had target mass loadings of 217 g/m² NUKON and 163 g/m² CalSil. The three cases retained 7 to 15% of the target CalSil and had CalSil mass loadings between 11 and 24 g/m². NC15 had the largest CalSil mass and total mass loadings of the three cases. However, the increase in total mass loading is not accounted for by the increase in retained CalSil. Additional NUKON should have been retained in the debris bed. It is not known whether the additional CalSil contributed to the retention of the additional NUKON material.

Both of the other two cases presented in Table 7.14, NC4 and NC3, retained more CalSil despite having target CalSil mass loadings 33 and 67% of the target loadings for cases NC5, NC15, and NC16. It appears as if the higher concentration of CalSil present at the initiation of debris bed formation inhibited the NUKON from being as efficient in retaining (filtering) the CalSil. It was observed during benchtop testing that NUKON-only debris beds were fairly durable when retrieved from the test section and readily stayed intact. However, for the same NUKON mass loading, retrieved debris beds seemed to become more fragile and harder to keep intact with increased CalSil mass loading. The observation was that CalSil appeared to weaken or disrupt the structural integrity of the debris bed with respect to post-test handling. It is unclear whether the benchtop test observations are relevant to the results for CalSil retention presented in Table 7.14. Without further investigation, the effect of the target CalSil loading on the amount of CalSil retained in the debris bed is inconclusive. It is speculated that the CalSil may interfere with the interaction of the NUKON fiber.

With regard to the observations of similarity in the final CalSil mass loadings, cases NC9 and NC17 had target mass loadings of 724 g/m² NUKON and 362 g/m² CalSil. These two cases retained 39 and 36% of the target CalSil despite having debris beds generated at different temperatures. Despite NC9 retaining approximately 10% more CalSil than NC17, the total retrieved mass loading for NC9 was approximately 10% less than that of NC17.

7.4.3 Debris Bed Height for NUKON/CalSil Test Cases

As discussed in Section 5, three types of debris bed height measurements were taken during the test program. A description of each of the debris bed height measurements is provided in Section 7.2.1. For review, the three types of height measurements are listed below.

1. Manual post-test debris bed measurements taken with the retrieved debris bed and TTS removed from the test loop
2. In situ manual debris bed height measurements taken by an operator looking (sighting across) through the side of the TTS
3. In situ debris bed measurements obtained via post-test analysis of photos taken during testing using the optical triangulation system.

All of the debris bed height measurements are contained in the Quick Look reports of Appendix J. The optical triangulation system was not operational during the Series 1 NUKON/CalSil tests, which include test cases NC3, NC7, and NC11 through NC14. Like the NUKON-only test cases of Section 7.2.1, the comparison of the optical triangulation measurements is the main focus of this section. The post-test measurements for the debris bed rim and center heights are presented to provide a comparison to the Series 1 tests. The results of the in situ manual measurements are not discussed in this report.

Table 7.16 contains all the bed height measurements obtained with optical triangulation from the NUKON/CalSil test cases. From the measurements of debris bed height and the dry retrieved bed mass, a relative bulk density of the debris material in the bed can be calculated. Table 7.16 contains the calculated bulk dry density of the debris beds for all of the test conditions in which the photo imaging analysis was performed. The values of bulk dry debris bed density reported in Table 7.16 were obtained by calculating the debris bed volume using the product of cross-sectional area of the test section and the average body height obtained from the optical triangulation measurements. The average body height is the average height of the debris bed excluding the area covered by the debris bed rim. Therefore, the volume of debris material included in the rim is excluded from the calculation of the relative density while the mass of the material is included. The calculated density is considered a relative density to be used for comparing test cases and should not be considered an absolute density.

Table 7.16. In Situ Debris Bed Height Measurements and Calculated Density Obtained from Optical Triangulation Measurements

Test Case	Retrieved Debris Bed Mass Loading ($\pm 4 \text{ g/m}^2$)	Screen Approach Velocity ($\pm 0.3 \text{ ft/sec}$)	Test Phase	Rim Height ($\pm 0.03 \text{ in.}$)	Body Center Height ($\pm 0.03 \text{ in.}$)	Average Body Height ($\pm 0.03 \text{ in.}$)	Body Diameter ($\pm 0.03 \text{ in.}$)	Relative Bulk Dry Debris Bed Density Based on Optical Triangulation Bed ht (g/mL)
NC1	56	N/A	N/A	N/A	N/A	N/A	N/A	N/A
NC2	94	N/A	N/A	N/A	N/A	N/A	N/A	N/A
NC3 ¹	217	N/A	N/A	N/A	N/A	N/A	N/A	N/A
NC4	209	0.10	RU1	0.21	0.13	0.11	5.11	0.075
NC4	209	0.20	RU1	0.20	0.11	0.09	5.23	0.091
NC4	209	0.20	RU3	0.18	0.10	0.08	5.38	0.103
NC4	209	0.02	RD3	0.19	0.12	0.10	5.32	0.082
NC4	209	0.10	RU4	0.18	0.11	0.09	5.32	0.091
NC5a	213	0.10	RU1	0.24	0.10	0.08	5.30	0.105
NC5a	213	0.20	RU1	0.22	0.08	0.06	5.18	0.140
NC5a	213	0.02	RD1	0.22	0.10	0.08	5.27	0.105
NC5a	213	0.20	RU2	0.22	0.07	0.05	5.31	0.168
NC5a	213	0.10	RU4	0.22	0.07	0.05	5.25	0.168
NC5b	213	0.20	RU3	0.20	0.06	0.04	5.32	0.210
NC6a	297	0.10	RU1	0.29	0.11	0.09	5.18	0.130
NC6a	297	0.20	RU1	0.21	0.05	0.03	5.42	0.390
NC6a	297	0.02	RD1	0.23	0.09	0.07	5.17	0.167
NC6a	297	0.10	RU2	0.22	0.07	0.05	5.29	0.234
NC6b	297	0.20	RU1	0.23	0.07	0.05	5.19	0.234
NC6b	297	0.02	RD1	0.24	0.10	0.08	5.29	0.146
NC7	729	N/A	N/A	N/A	N/A	N/A	N/A	N/A

Table 7.16 (contd)

Test Case	Retrieved Debris Bed Mass Loading ($\pm 4 \text{ g/m}^2$)	Screen Approach Velocity ($\pm 0.3 \text{ ft/sec}$)	Test Phase	Rim Height ($\pm 0.03 \text{ in.}$)	Body Center Height ($\pm 0.03 \text{ in.}$)	Average Body Height ($\pm 0.03 \text{ in.}$)	Body Diameter ($\pm 0.03 \text{ in.}$)	Relative Bulk Dry Debris Bed Density Based on Optical Triangulation Bed ht (g/mL)
NC8	646	0.10	RD1	0.64	0.36	0.34	4.39	0.075
NC8	646	0.02	RD1	0.59	0.36	0.34	4.44	0.075
NC8	646	0.20	RU2	0.52	0.25	0.23	4.66	0.111
NC8	646	0.10	RU4	0.52	0.25	0.23	4.57	0.111
NC9	732	0.10	RU1	0.40	0.18	0.16	4.61	0.180
NC9	732	0.20	RU1 nf	0.40	0.18	0.16	4.58	0.180
NC9	732	0.02	RD1	0.42	0.26	0.24	4.78	0.120
NC9	732	0.10	RU4	0.36	0.18	0.16	4.60	0.180
NC10	862	0.10	DPI noSS	0.44	0.22	0.20	4.52	0.170
NC10	862	0.01	BF plus	0.40	0.17	0.16	4.72	0.212
NC11	1034	N/A	N/A	N/A	N/A	N/A	N/A	N/A
NC12	1334	N/A	N/A	N/A	N/A	N/A	N/A	N/A
NC13	1260	N/A	N/A	N/A	N/A	N/A	N/A	N/A
NC14	1924	N/A	N/A	N/A	N/A	N/A	N/A	N/A
NC15a	261	0.10	RU1	0.20	0.09	0.07	5.23	0.118
NC15a	261	0.20	RU1	0.21	0.08	0.06	5.27	0.131
NC15a	261	0.02	RD2	0.20	0.08	0.06	5.25	0.132
NC15a	261	0.10	RU3	0.20	0.07	0.05	5.37	0.155
NC15b	261	0.20	RU1	0.17	0.04	0.02	5.42	0.292
NC15b	261	0.10	RU2	0.17	0.05	0.03	5.59	0.254
NC16a	160	0.10	RU1	0.10	0.08	0.06	5.81	0.105
NC16a	160	0.20	RU1	0.09	0.06	0.04	5.78	0.157
NC16a	160	0.20	RU3	0.09	0.06	0.04	5.77	0.157
NC16a	160	0.02	RD3	0.10	0.08	0.06	5.67	0.105
NC16a	160	0.10	RU4	0.09	0.06	0.04	5.85	0.157
NC16b	160	0.20	RU1	0.07	0.05	0.03	5.86	0.210
NC16b	160	0.10	RU2	0.07	0.05	0.03	5.88	0.210
NC17a	811	0.10	RU1	0.40	0.34	0.32	5.48	0.100
NC17a	811	0.20	RU1	0.34	0.28	0.26	5.25	0.123
NC17a	811	0.20	RU3	0.25	0.19	0.17	5.43	0.188
NC17a	811	0.02	RD3	0.28	0.20	0.18	5.47	0.177
NC17a	811	0.10	RU4	0.26	0.20	0.18	5.49	0.177
NC17b	811	0.20	RU1	0.22	0.16	0.14	5.44	0.228
NC17b	811	0.10	RU2	0.22	0.14	0.12	5.56	0.266

Reviewing Table 7.12, five test cases formed complete debris beds, were formed and tested according to Series 2 procedures, and were generated at ambient fluid temperature: NC4, NC5a, NC6a, NC8, and NC9. Three of these, NC4, NC9, and NC8, bound the range of retrieved mass loadings for the five cases, and the debris bed height is plotted for them as a function of the screen approach velocity in Figure 7.38. In the legend of the plot, the test case number is followed by the predicted CalSil mass loading and the total retrieved debris loading. Like the NUKON-only condition, for a specific velocity the debris bed

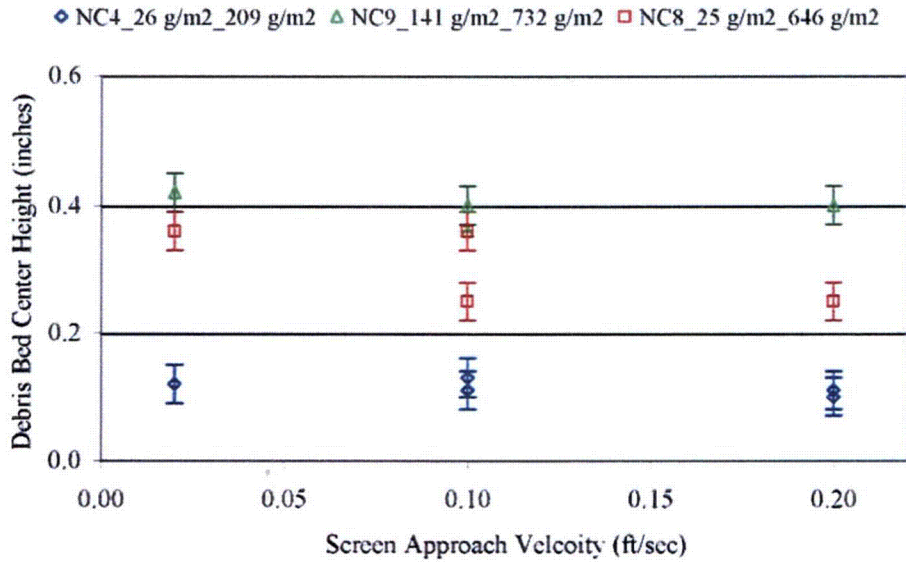


Figure 7.38. Debris Bed Center Height as a Function of Screen Approach Velocity for Three Retrieved Mass Loadings. Data for Series 2 test cases NC4, NC8, and NC9, with debris beds formed at ambient temperature; debris bed height measurements obtained from optical triangulation and presented in Tables 7.16.

height increases with an increase in the total debris bed mass loading. For each debris bed mass loading in Figure 7.38, bed height appears to decrease slightly with an increase in screen approach velocity.

In Section 7.2 the relative debris bed density calculated from the debris bed height appeared to be a significant parameter influencing the pressure drop across the debris bed. For the NUKON/CalSil cases, 6 of the 15 complete debris beds were created from the Series 1 tests, which did not have the capability for optical triangulation to obtain in situ debris bed height measurements. Table 7.17 contains the post-test debris bed height measurements for the 15 complete NUKON/CalSil debris beds and the in situ debris bed measurements obtained at 0.02 ft/sec. The relative debris bed densities have been calculated for both sets of measurements in an attempt to correlate the post-test relative densities with those obtained from measurements made at 0.02 ft/sec.

The test cases in Table 7.17 have been entered in the order of ascending relative bulk density based on the post-test manual measurements. Examining the relative bulk densities obtained from the in situ optical triangulation measurements in the order they are listed, it is apparent that no correlation can be made between the post-test debris bed measurement and the optical triangulation measurements obtained at 0.02 ft/sec. No agreement is observed in the ordering of the relative density obtained from the two debris bed height measurement techniques. It is unknown whether the retrieval process, which requires draining the test section, or simply the relaxation of the debris beds following the removal of the pressure differential unpredictably changes the relative density of the post-test debris beds. This lack of a correlation means only the Series 2 test cases can be used to evaluate the effects of the relative debris bed density on the pressure drop across the debris bed.

Table 7.17. Comparison of Post-Test Manual Measurements and In Situ Measurements from Optical Triangulation of Debris Bed Height and the Corresponding Calculated Relative Densities. Test cases arranged by ascending relative bulk density calculated from post-test measurements.

Test Case	Retrieved Debris Bed Mass Loading ($\pm 4 \text{ g/m}^2$)	CalSil Mass Loading Based on ISE Readings (g/m^2)	Based on In Situ Optical Triangulation Measurements			Based on Post Test Manual Measurements		
			Debris Bed Center Height (in.)	Debris Bed Rim Height (in.)	Relative Bulk Dry Debris Bed Density (g/mL)	Debris Bed Center Height (in.)	Debris Bed Rim Height (in.)	Relative Bulk Dry Debris Bed Density (g/mL)
NC15a	261	18	0.08	0.20	0.171	0.15	0.40	0.068
NC7	729	150	#N/A	#N/A	#N/A	0.36	0.13	0.080
NC14	1924	667	#N/A	#N/A	#N/A	0.92	0.36	0.082
NC13	1260	327	#N/A	#N/A	#N/A	0.55	0.25	0.090
NC12	1334	337	#N/A	#N/A	#N/A	0.47	0.23	0.112
NC11	1034	236	#N/A	#N/A	#N/A	0.35	0.12	0.116
NC8	646	20	0.36	0.59	0.075	0.21	0.51	0.121
NC17a	811	120	0.20	0.28	0.177	0.23	0.29	0.139
NC3 ¹	217	47	#N/A	#N/A	#N/A	0.06	0.16	0.142
NC6b	297	80	0.10	0.24	0.146	0.08	0.12	0.146
NC6a	297	80	0.09	0.23	0.167	0.08	0.12	0.146
NC4	209	25	0.12	0.19	0.082	0.05	0.22	0.164
NC9	732	132	0.26	0.42	0.120	0.15	0.33	0.192
NC5a	213	5	0.10	0.22	0.105	0.04	0.12	0.210
NC16a	160	5	0.08	0.10	0.105	#N/A	N/A	#N/A
NC10	862	339	0.17	0.40	0.212	#N/A	N/A	#N/A
NC1	56	#N/A	#N/A	#N/A	#N/A	#N/A	#N/A	#N/A
NC2	94	#N/A	#N/A	#N/A	#N/A	#N/A	#N/A	#N/A

In Section 7.2.1, Figure 7.12, the larger relative bulk densities ($> 0.1 \text{ g/mL}$) only occurred at the higher debris bed mass loadings ($> 1100 \text{ g/mL}$). Figure 7.39 plots the debris bed bulk density as a function of the retrieved debris bed mass loading for constant screen approach velocities of 0.02, 0.1, and 0.2 ft/sec from the Series 2 test cases for debris beds formed at ambient temperature. Test Cases NC4, NC5a, NC6a, NC8, and NC9 are included in the plot, and data are presented in Table 7.16. These five test cases were all formed at a constant 0.1 ft/sec and at ambient temperature, according to the Series 2 test procedures and subjected to the same velocity sequence (see Section 5.3). No indication of a trend in the data is observed.

The Series 2 NUKON/CalSil tests consisted of lower retrieved mass loadings than were obtained for the NUKON-only tests. Any effect of mass loading on the bulk density may not occur except at higher mass loadings. The bulk densities of the NUKON/CalSil tests were also higher than those of the NUKON-only test, which is expected with the addition of the CalSil particulate material. Both the CalSil mass loading and the CalSil-to-NUKON mass ratio are additional parameters for the NUKON/CalSil cases that did not exist for the NUKON-only tests. Figures 7.40 and 7.41 contain the same test conditions from Table 7.16 that were presented in Figure 7.39 to evaluate the bulk debris bed density as a function of the CalSil mass loading and CalSil/NUKON mass ratio, respectively. No trend is observed for the bulk density as a function of the CalSil mass loading; however, Figure 7.41 indicates the bulk density increases with an increase in the CalSil/NUKON mass ratio. This trend is expected due to the potential for CalSil particulate to be captured in the interstitial space of a NUKON debris bed. However, additional data points are needed before a definitive conclusion can be drawn.

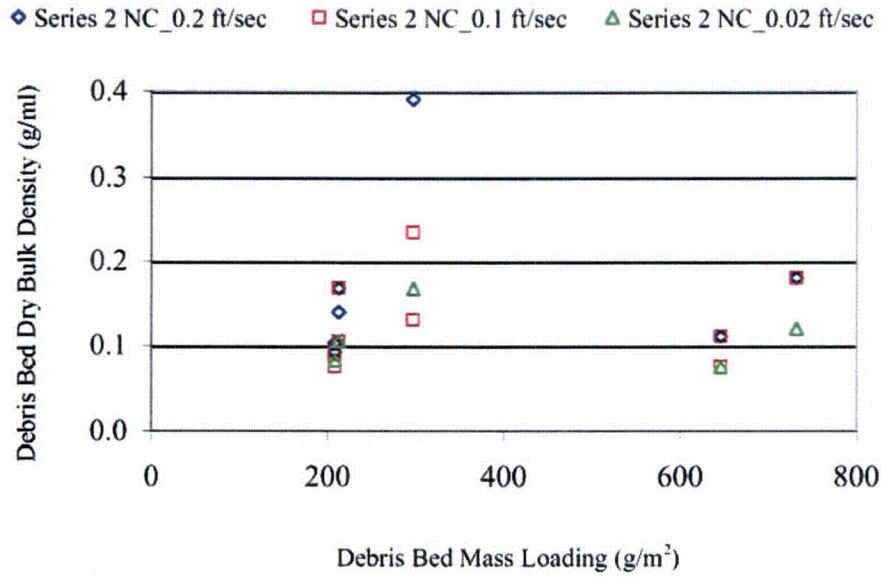


Figure 7.39. Debris Bed Dry Bulk Density as a Function of the Retrieved Debris Bed Mass Loading for Constant Screen Approach Velocities of 0.02, 0.1, and 0.2 ft/sec. Data are from Table 716 for Test Cases NC4, NC5a, NC6a, NC8, and NC9, which are all Series 2 test cases with debris beds formed at ambient temperature.

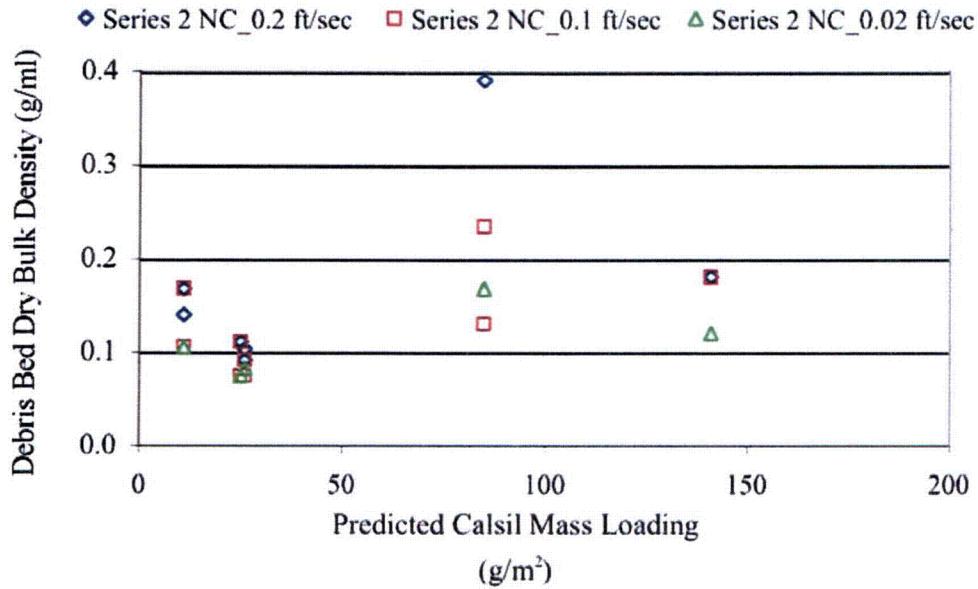


Figure 7.40. Debris Bed Bulk Density as a Function of the Predicted Calsil Mass Loading for Constant Screen Approach Velocities 0.02, 0.1, and 0.2 ft/sec. Data are from Table 716 for Test Cases NC4, NC5a, NC6a, NC8, and NC9, which are all Series 2 test cases with debris beds formed at ambient temperature.

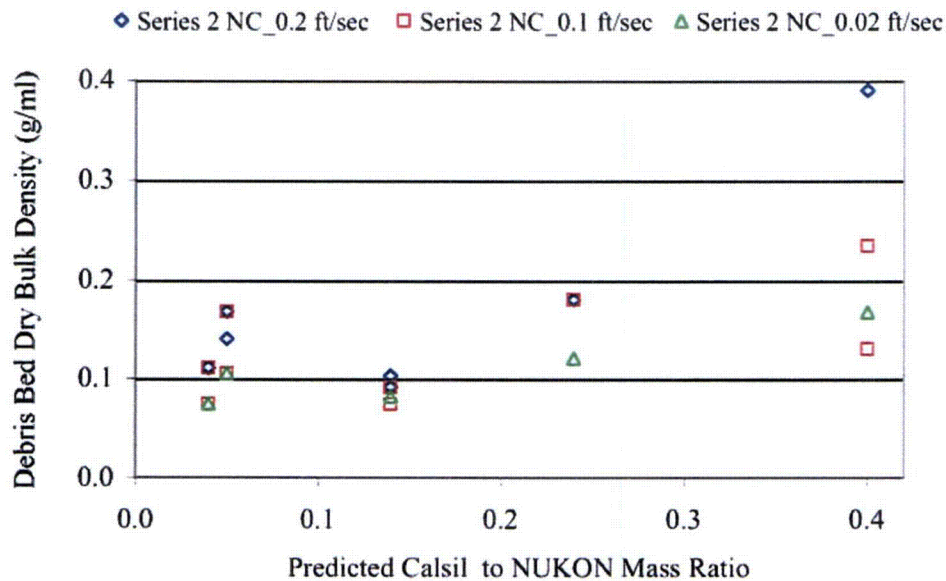


Figure 7.41. Debris Bed Bulk Density as a Function of the Predicted CalSil to NUKON Mass Ratio for Constant Screen Approach Velocities of 0.02, 0.1, and 0.2 ft/sec. Data are from Table 716 for Test Cases NC4, NC5a, NC6a, NC8, and NC9, which are all Series 2 test cases with debris beds formed at ambient temperature.

Based on these results, the effects of the bulk density and CalSil mass ratio on the debris bed pressure drop are examined in the next section.

7.4.4 Head Loss Measurements for NUKON/CalSil Debris Beds at Ambient Temperature

This section provides an overview of the head loss data obtained at ambient fluid temperature for debris beds generated at ambient fluid temperatures. The pressure drop measurements obtained at elevated fluid temperatures or for debris beds generated at elevated temperatures are presented in Section 7.4.5. Test cases NC1 and NC2 did not generate complete debris beds, so pressure drop data for these cases are not included. The debris bed formed for case NC10 essentially plugged the test section during debris bed formation. A head loss of 749 in. H₂O was measured at a screen approach velocity of 0.1 ft/sec near the end of the bed formation process. Due to the high pressure drop, the planned velocity sequence was not executed for case NC10.

Based on the distribution of retrieved debris bed mass loadings, the test cases are separated into three groups for presenting results. Group 1 test cases have retrieved mass loadings between 160 and 297 g/m² and consist of cases NC3, NC4, NC5a, and NC6a. The elevated temperature cases for test condition NC15 and NC16 also fall into the range of Group 1. Group 2 cases have retrieved mass loadings between 646 and 811 g/m² and consist of cases NC7, NC8, and NC9. The elevated temperature cases for test condition NC17 also fall into the range of Group 2. Group 3 test cases have retrieved mass loadings between 1034 and 1924 g/m² and consist of cases NC11 through NC14. Group 3 consists of only Series 1 test cases, which have no optical triangulation measurements from which to calculate the debris bed relative bulk density. There are also no elevated temperature cases associated with Group 3.

Tables 7.18, 7.19, and 7.20 contain the retrieved mass loading, CalSil mass loading, NUKON mass loading, CalSil-to-NUKON mass ratio, and debris bed bulk densities at 0.02, 0.1, and 0.2 ft/sec for test case groups 1, 2, and 3, respectively. Each test case was subjected to a velocity sequence that consisted of cycling the screen approach velocity up and down (refer to Section 5.3).

Table 7.18. NUKON/CalSil Group 1 Test Case Debris Bed Properties (total mass loadings between 160 and 297 g/m²)

Test Case	Nominal Temp (°C)	Retrieved Mass Loading	Calculated CalSil Loading (g/m ²)	Calculated NUKON Loading (g/m ²)	Calculated CalSil to NUKON Mass Ratio	Bulk Densities Calculated from Optical Triangulation Debris Bed Heights ^(a)		
						@ 0.02 ft/sec (g/mL)	@ 0.1 ft/sec (g/mL)	@ 0.2 ft/sec (g/mL)
NC3 ^(b,c)	21	217	49	168	0.29	N/A	N/A	N/A
NC4	21	209	26	183	0.14	0.082	0.075 0.091	0.091 0.103
NC5a	21	213	11	202	0.05	0.105	0.105 0.168	0.140 0.168
NC6a	21	297	85	212	0.40	0.167	0.130 0.234	0.390
Elevated Temperature Cases								
NC15b	36	261	24	237	0.10	N/A	0.342	0.513
NC15a	54	261	24	237	0.10	0.171	0.147 0.205	0.171
NC16b	54	160	11	149	0.08	N/A	0.210	0.210
NC5b	82	213	11	202	0.05	N/A	N/A	0.210
NC6b	82	297	85	212	0.40	0.146	N/A	0.234
NC16a	82	160	11	149	0.08	0.105	0.105 0.157	0.157 0.157
(a) Multiple densities are listed for velocities that had multiple optical triangulation photos analyzed from different velocity cycles. The densities are listed in the order they occurred in the velocity sequence.								
(b) Test case from Series 1, no optical triangulation measurements								
(c) Debris bed formed at an initial screen approach velocity of 0.2 ft/sec.								

Table 7.19. NUKON/CalSil Group 2 Debris Bed Properties (total mass loadings between 646 and 811 g/m²)

Test Case	Nominal Temp (°C)	Retrieved Mass Loading	Calculated CalSil Loading (g/m ²)	Calculated NUKON Loading (g/m ²)	Calculated CalSil to NUKON Mass Ratio	Bulk Densities Calculated from Optical Triangulation Debris Bed Heights ^(a)		
						@ 0.02 ft/sec (g/mL)	@ 0.1 ft/sec (g/mL)	@ 0.2 ft/sec (g/mL)
NC7 ^(b)	21	729	155	574	0.27	N/A	N/A	N/A
NC8	21	646	25	621	0.04	0.075	0.075 0.111	0.111 0.111
NC9	21	732	141	591	0.24	0.120	0.180 0.180	0.180 0.180
Elevated Temperature Cases								
NC17b	29	811	129	681	0.19	N/A	0.266	0.228
NC17a	54	811	129	681	0.19	0.177	0.100 0.177	0.123 0.188
(a) Multiple densities are listed for velocities that had multiple optical triangulation photos analyzed from different velocity cycles. The densities are listed in the order they occurred in the velocity sequence.								
(b) Test case from Series 1, no optical triangulation measurements.								

Table 7.20. NUKON/CalSil Group 3 Debris Bed Properties (total mass loadings between 1034 and 1924 g/m²)

Test Case	Nominal Temp (°C)	Retrieved Mass Loading	Calculated CalSil Loading (g/m ²)	Calculated NUKON Loading (g/m ²)	Calculated CalSil to NUKON Mass Ratio	Bulk Densities Calculated from Optical Triangulation Debris Bed Heights ^(a)		
						@ 0.02 ft/sec (g/mL)	@ 0.1 ft/sec (g/mL)	@ 0.2 ft/sec (g/mL)
NC11 ^(a)	21	1034	242	792	0.31	N/A	N/A	N/A
NC12 ^(a)	21	1334	343	991	0.35	N/A	N/A	N/A
NC13 ^(a)	21	1260	334	926	0.36	N/A	N/A	N/A
NC14 ^(a,b)	21	1924	671	1253	0.54	N/A	N/A	N/A

(a) Test case from Series 1, no optical triangulation measurements.
(b) Debris bed formed at an initial screen approach velocity of 0.2 ft/sec.

Like the NUKON tests, in these tests the pressure drop continued to increase with each cycling of the velocity. Based on the cycling of the debris bed height measured with the optical triangulation and the visual observations of fine debris material periodically exiting from the downstream side of the debris bed, it is postulated that the cycling of the screen approach velocity allowed the CalSil material within the debris bed to migrate deeper into the bed and possibly to be transported through the debris bed. This rearranging of the debris constituents may account for the increase in head loss with each velocity cycle.

Figures 7.42 and 7.43 are plots of head loss as a function of screen approach velocity for several velocity cycles. These figures provide examples of the increase in head loss experienced with each velocity cycle. NC7 is a Series 1 test case; NC9 is a Series 2 test case. For Series 2, the test fluid was filtered after ramp up 1. No filtering occurred during the Series 1 tests. The Series 2 results from Figure 7.43 indicate that increases in head loss following ramp up 1 during the Series 1 tests were not due entirely to the addition of recirculated debris material. The increase in head loss with each velocity cycle demonstrates the impact of flow history on the pressure drop across the debris bed. (For additional discussion of the effects of flow history; see Section 6.5.) To reduce the effects of flow history and minimize the effects of recirculated debris addition, the head loss measurements obtained during ramp up 2 of the velocity sequence are used throughout this section to compare results from different test cases.

Based on the results presented in Sections 7.2, 7.4.2, and 7.4.3, the head loss across the debris bed is evaluated as a function of the retrieved debris bed mass loading, the debris bed relative bulk density, and the calculated (based on chemical dissolution) CalSil-to-NUKON mass ratio in Figures 7.44, 7.45, and 7.46, respectively. The data used to generate the three figures are from Table 7.13, Table 7.16, and the Quick Look reports in Appendix J and are plotted for constant screen approach velocities of 0.02, 0.1, and 0.2 ft/sec. The plots of the debris bed head loss as a function of mass loading and of CalSil-to-NUKON mass ratio, Figures 7.44 and 7.46, contain Series 1 data, which has been identified on the plots. The Series 1 debris beds were generated using simultaneous introduction of debris constituents, while pre-mixed constituents were used for the Series 2 tests. Test cases NC3 and NC14 have been omitted from the Series 1 data used to generate the plots because the debris beds for these cases were formed with an initial screen approach velocity of 0.2 ft/sec (0.06 m/s). The pressure drop as a function of mass ratio has been plotted both with and without Series 1 data for clarity because Series 2 data were obtained over a lower range of head losses.

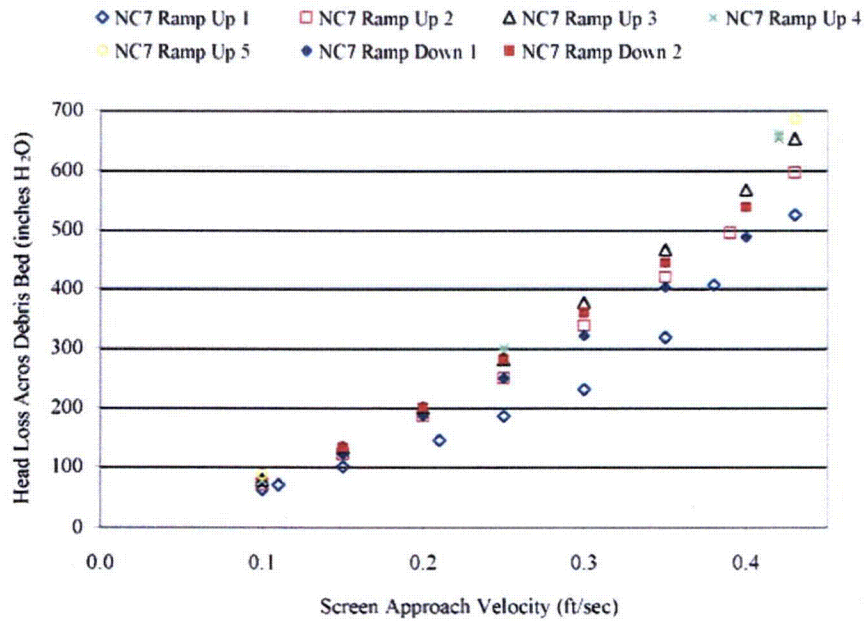


Figure 7.42. Debris Bed Head Loss from NC7 as a Function of Screen Approach Velocity for Five Ramp ups and the First Two Ramp Downs in the Screen Approach. NC7 is a Series 1 test case with data presented in the Quick Look report for PNNL Test 051121_NC_1586_L1, which is included in Appendix J.

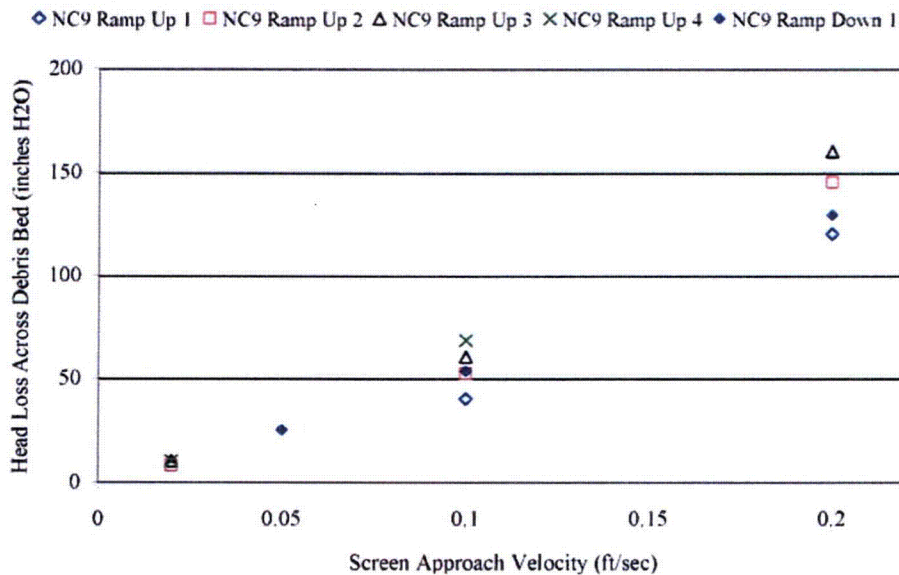


Figure 7.43. Debris Bed Head Loss from NC9 as a Function of Screen Approach Velocity for Four Ramp ups and the First Ramp Down in the Screen Approach Velocity. NC9 is a Series 2 test case with data presented in the Quick Look report for PNNL Test 060331_NC_2024_L1, which is included in Appendix J.

The head loss as a function of the debris bed relative bulk density presented in Figure 7.45 contains only Series 2 data since the optical triangulation measurements were not available for the Series 1 tests. The plot was created using the results of Test Cases NC4, NC5a, NC6a, NC8, and NC9.

From Figure 7.44, definitive trend in the data for the head loss as a function of the retrieved mass loading is observed for either the Series 1 or Series 2 data. As was observed for the NUKON-only test cases, Figure 7.45 indicates that for the NUKON/CalSil test cases the resulting pressure drop across the debris bed increases with an increase in the relative bulk density of the debris bed. The relationship between the debris bed pressure drop and the CalSil-to-NUKON mass ratio is not as obvious in Figure 7.46. Examining the Series 2 data in Figure 7.46b, the pressure drop appears to increase with an increase in the mass ratio. However, due to the limited number of points and the spread in the data further investigation is needed to draw final conclusions. No trend was observed between the debris bed pressure drop and calculated CalSil mass loading (plot not shown).

The individual test cases in each group of tests defined by Tables 7.18 through 7.20 will be compared using the ramp up 2 pressure data in Figures 7.47 through 7.50. For each test case listed in the legend of the plots, the calculated CalSil loading, the total mass loading, and the CalSil-to-NUKON mass ratio follows the test case. For example, NC4_26 g/m²_209 g/m²_0.14 is for test case NC 4, which had a CalSil mass loading of 26 g/m², a total retrieved mass loading of 209 g/m², and a CalSil to NUKON mass ratio of 0.14.

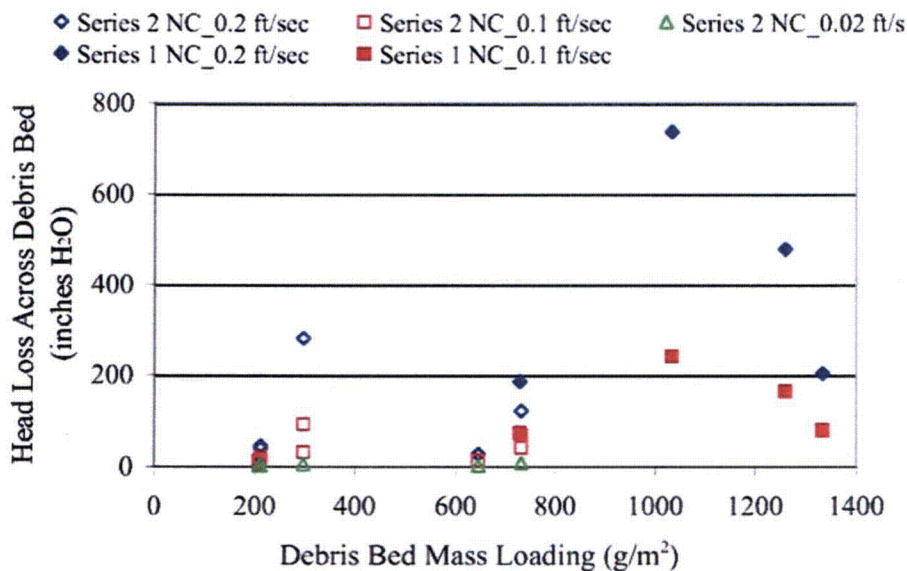


Figure 7.44. Plot of the Pressure Drop Across the Debris Bed as a Function of the Retrieved Debris Bed Mass Loading for Constant Screen Approach Velocities of 0.02, 0.1, and 0.2 ft/sec. Data from both Series 1 and 2 test cases for debris beds formed at ambient temperature and a screen approach velocity of 0.1 ft/sec. Test Cases NC4, NC5a, NC6a, NC7, NC8, NC9, NC11, NC12, and NC13 are included in the plot; head loss data are from the Quick Look reports in Appendix J.

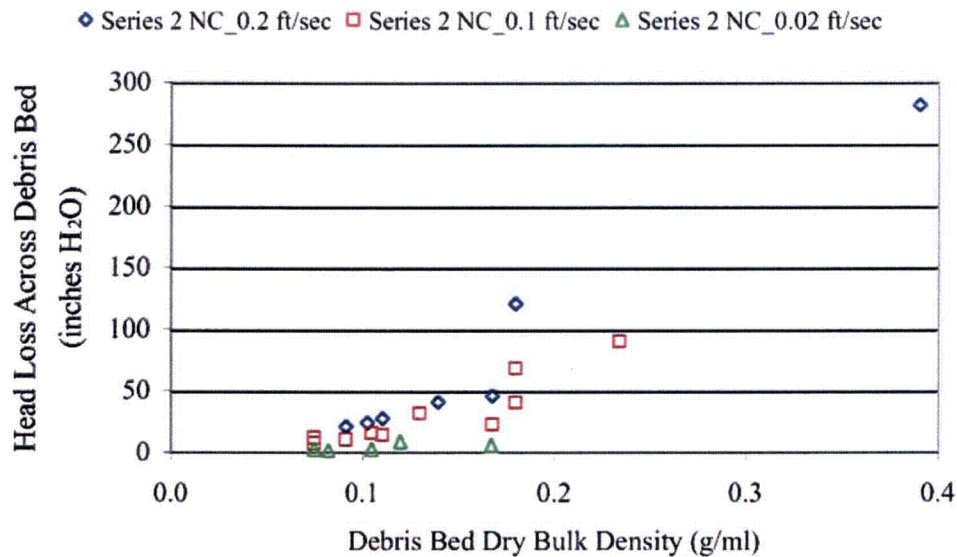
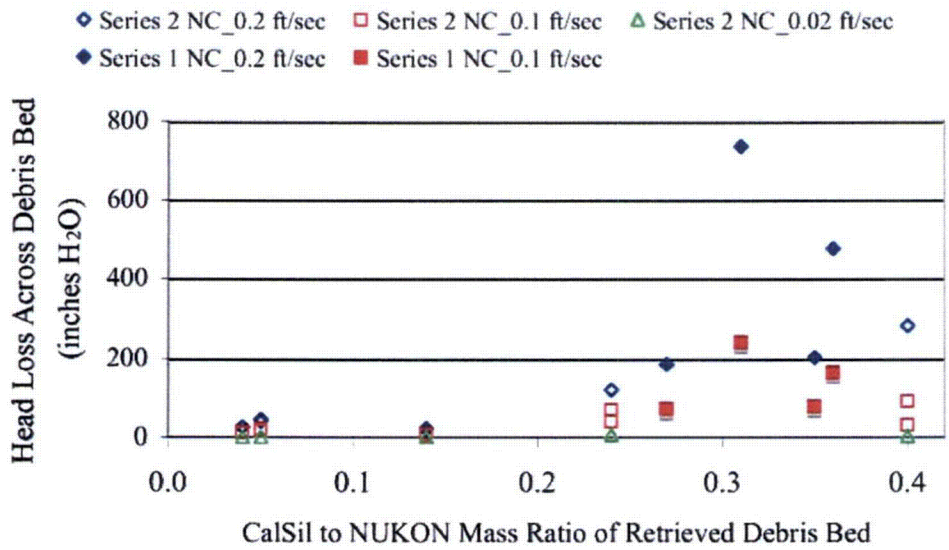


Figure 7.45. Plot of Debris Bed Pressure Drop as a Function of the Relative Debris Bed Bulk Density for Constant Screen Approach Velocities of 0.02, 0.1, and 0.2 ft/sec. Data from the Series 2 test cases with debris beds formed at ambient temperature. Test Cases NC4, NC5a, NC6a, NC8, and NC9 are included in the plot; data are from Table 7.16 and the Quick Look reports in Appendix J.

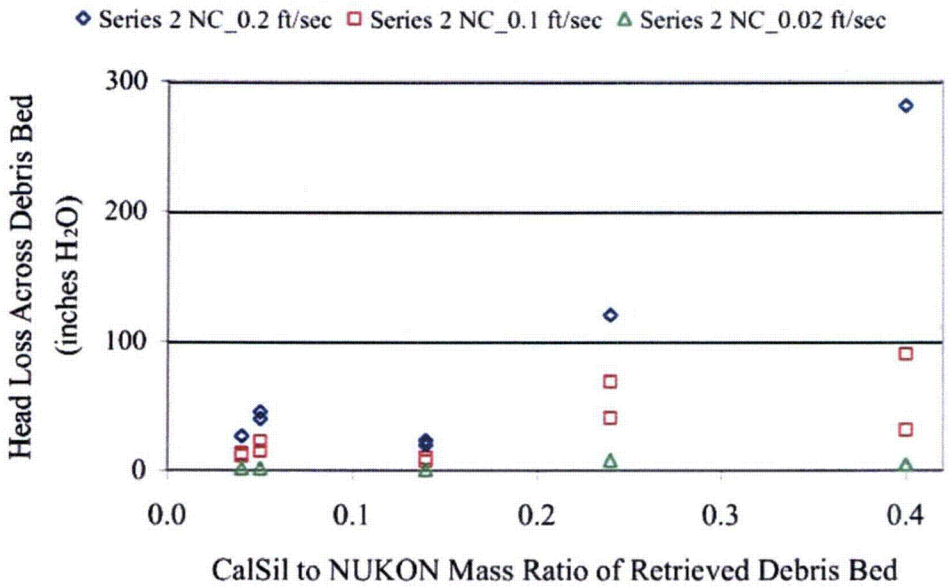
The head loss across the debris bed as a function of the screen approach velocity is plotted for Group 1 test cases in Figures 7.47 and 7.48. Figure 7.47 contains the Series 1 test case NC 3, which has been excluded from Figure 7.48 for simplifying the comparison between the remaining test cases. The NC3 debris bed was formed at an initial screen approach velocity of 0.2 ft/sec (0.06 m/s) and tested over a different range of screen approach velocities, which could skew the comparison with the other cases. There are also no optical triangulation debris bed heights and associated debris bed densities for NC3.

The four parameters considered in comparing the pressure drop measurements from the various test cases were the total mass loading, the CalSil mass loading, the CalSil-to-NUKON mass ratio, and the debris bed relative bulk density. The four test cases for Group 1 ranked from highest to lowest pressure drop are NC6a, NC5a, NC3, and NC4. Table 7.21 lists the 4 test cases of Group 1 and their ranking with respect to the four parameters listed above. Of the four parameters, only the ranking of the relative bulk densities corresponds to the order of the measured head losses. If NC3 is excluded due to the difference in the debris bed formation approach velocity, then the ranking of total mass loading also corresponds to the order of the measured head losses.

The head loss across the debris bed as a function of the screen approach velocity is plotted for Group 2 test cases in Figure 7.49. The four test cases for Group 2 ranked from highest to lowest pressure drop are NC17b, NC7, NC9, and NC8. Table 7.22 lists the 4 test cases of Group 2 and their ranking with respect to the four parameters listed above. Of the four parameters, only the ranking of the relative bulk densities corresponds to the order of the measured head losses. As with Group 1, if the Series 1 case, NC7, is excluded due to the difference in the screen approach velocity used for debris bed formation, then the ranking of retrieved total mass loading also corresponds to the order of the measured head losses.



(a) Includes both Series 1 and Series 2 data



(b) Includes only Series 2 data

Figure 7.46. Pressure Drop Across the Debris Bed as a Function of the Retrieved CalSil-to-NUKON Mass Ratio for Constant Screen Approach Velocities of 0.02, 0.1, and 0.2 ft/sec. Data provided from both Series 1 and 2 test cases with debris beds formed at ambient temperature and a screen approach velocity of 0.1 ft/sec. Test Cases NC4, NC5a, NC6a, NC8, and NC9 from Series 2 and NC7, NC11, NC12, and NC13 from Series 1 are included in the plot. Head loss data are from Quick Look reports in Appendix J.

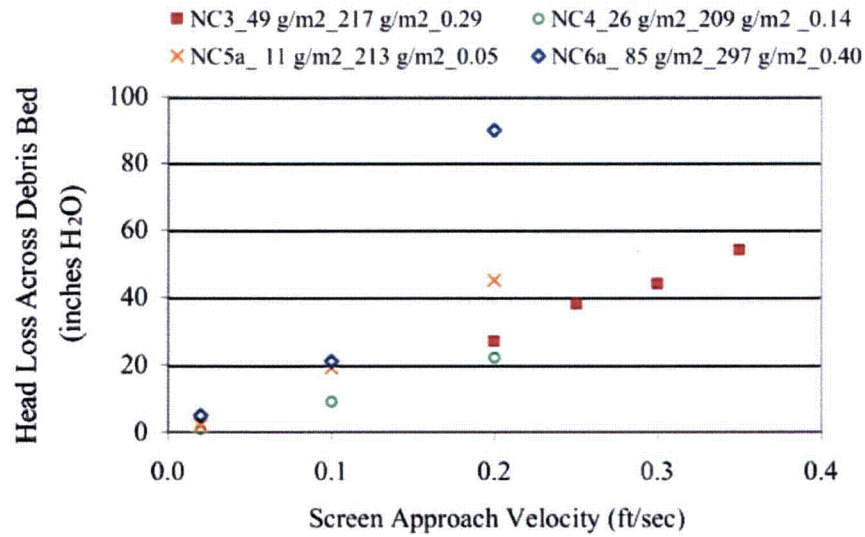


Figure 7.47. Pressure Drop Across the Debris Bed as a Function of the Screen Approach Velocity for Group 1 NUKON/CalSil Test Cases. Test Cases NC4, NC5a and NC6a are from Series 2 and were formed at ambient temperature with a screen approach velocity of 0.1 ft/sec. Test Case NC3 is from the Series 1 tests and was formed at ambient fluid temperature with an initial screen approach velocity of 0.2 ft/sec. The head loss data are from the Quick Look reports in Appendix J.

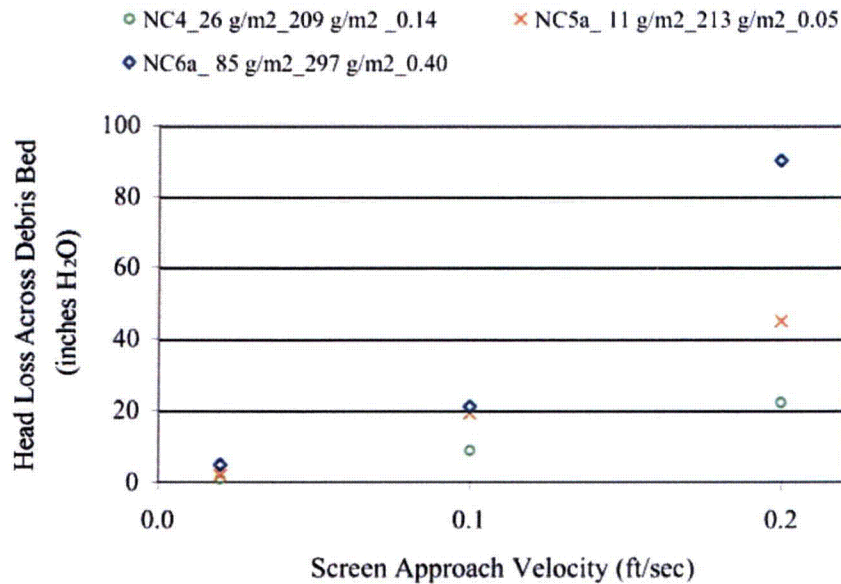


Figure 7.48. Pressure Drop Across the Debris Bed as a Function of the Screen Approach Velocity for Group 1, Series 2, NUKON/CalSil Test Cases. All debris beds were formed at ambient temperature with a screen approach velocity of 0.1 ft/sec. The head loss data are from the Quick Look reports in Appendix J

Table 7.21. Comparative Ranking (highest to lowest) of the Group 1 Test Cases with Respect to Head Loss Across the Debris Bed, Total Mass Loading, CalSil Mass Loading, CalSil-to-NUKON Mass Ratio, and Relative Bulk Density

Test Case Ranked in Order of Pressure Drop	Head Loss Across Debris Bed at 0.2 ft/sec (in. H ₂ O)	Ranking of Total Retrieved Dry Mass Loading	Ranking of Calculated CalSil Mass Loading	Ranking of CalSil- to-NUKON Mass Ratio	Ranking of Debris Bed Bulk Density
NC6a ^(a)	90	1	1	1	1
NC5a ^(a)	45	3	4	4	2
NC3 ^(b,c)	27	2	2	2	N/A
NC4 ^(a)	22	4	3	3	3

(a) Test case from Series 2.

(b) Test case from Series 1.

(c) Debris bed formed at an initial screen approach velocity of 0.2 ft/sec.

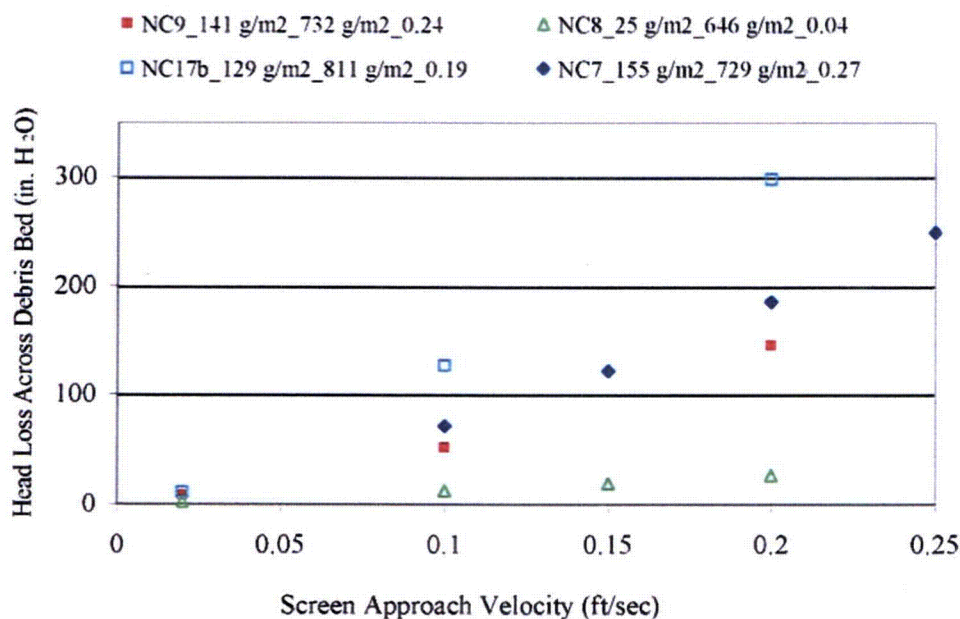


Figure 7.49. Pressure Drop Across the Debris Bed as a Function of the Screen Approach Velocity for Group 2 NUKON/CalSil Test Cases. Test Cases NC8, NC9 and NC17b are from Series 2 and were formed with a screen approach velocity of 0.1 ft/sec. Debris beds for NC8 and NC9 were formed at ambient temperature and the one for NC17b was formed at 54°C. Test Case NC7 is from the Series 1 tests and was formed at ambient fluid temperature with an initial screen approach velocity of 0.2 ft/sec. The head loss data are from the Quick Look reports in Appendix J.

Table 7.22. Comparative Ranking (highest to lowest) of the Group 2 Test Cases with Respect to Head Loss Across the Debris Bed, Total Mass Loading, CalSil Mass Loading, CalSil-to-NUKON Mass Ratio, and Relative Bulk Density

Test Case Ranked in Order of Pressure Drop	Head Loss Across Debris bed at 0.2 ft/sec (in. H ₂ O)	Ranking of Total Retrieved Dry Mass Loading	Ranking of Calculated CalSil Mass Loading	Ranking of CalSil-to-NUKON Mass Ratio	Ranking of Debris Bed Bulk Density
NC17b ^{(a)(b)}	298	1	3	3	1
NC7 ^(c)	185	3	1	1	N/A
NC9 ^(a)	145	2	2	2	2
NC8 ^(a)	26	4	4	4	3

(a) Test case from Series 2.
 (b) Debris bed formed at a fluid temperature of 54°C.
 (c) Test case from Series 1.

The head loss across the debris bed as a function of screen approach velocity is plotted for Group 3 in Figure 7.50. All four test cases are from Series 1 with the debris bed for NC14 formed at an initial screen approach velocity of 0.2 ft/sec compared to 0.1 ft/sec for the other three. No optical triangulation bed heights or associated densities are available for Group 3. The Group 3 test cases ranked from highest to lowest pressure drop are NC11, NC13, NC14, and NC12. Table 7.23 lists the relative ranking of the Group 3 test cases with respect to total retrieved mass loading, CalSil mass loading, and CalSil-to-NUKON mass ratio. Based on these rankings, no trend is observed. However, if NC14 is excluded due to its different bed formation velocity, both total mass loading and calculated CalSil loading decrease with increasing pressure drop. Analysis of these cases led to evaluation of the debris loading sequence discussed in Section 6.3. No elevated temperature cases were conducted for the mass loading range of Group 3; therefore, no discussion of Group 3 results is included in Section 7.4.5.

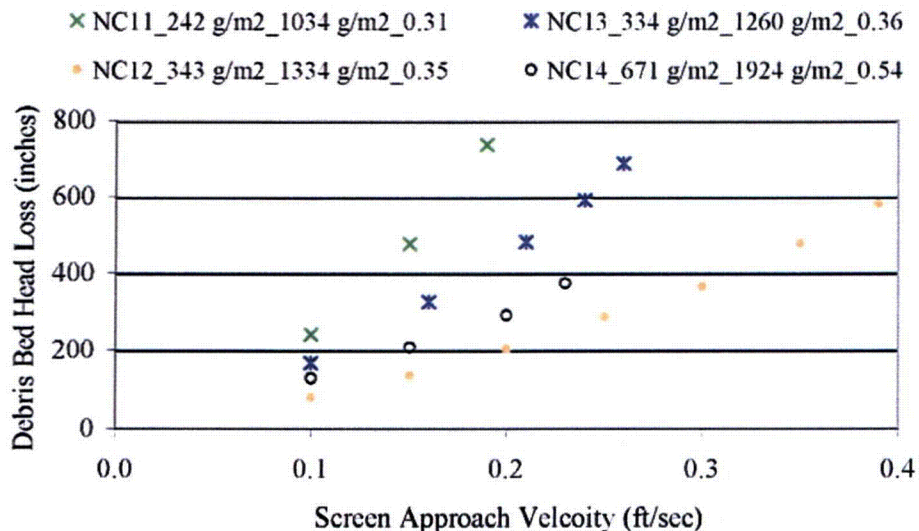


Figure 7.50. Pressure Drop Across Debris Bed as a Function of Screen Approach Velocity for Group 3, Series 1, NUKON/CalSil Test Cases. All debris beds were formed at ambient temperature with a screen approach velocity of 0.1 ft/sec. Head loss data are from the Quick Look reports in Appendix J.

Table 7.23. Comparative Ranking (Highest to Lowest) of the Group 3 Test Cases with Respect to Head Loss Across the Debris Bed, Total Mass Loading, CalSil Mass Loading, and CalSil-to-NUKON Mass Ratio

Test Case Ranked in order of Pressure drop	Head Loss Across the debris bed at 0.2 ft/sec (in. H ₂ O)	Ranking of Total Retrieved Dry Mass Loading	Ranking of Calculated CalSil Mass Loading	Ranking of CalSil to NUKON Mass Ratio	Ranking of Debris Bed Bulk Density
NC11 ^(a)	735	4	4	4	N/A
NC13 ^(a)	477	3	3	2	N/A
NC14 ^{(a)(b)}	292	1	1	1	N/A
NC12 ^(a)	203	2	2	3	N/A

(a) Test case from Series I.
(b) Debris bed formed at an initial screen approach velocity of 0.2 ft/sec.

7.4.5 Head Loss Measurements for NUKON/CalSil Debris Beds at Elevated Temperatures

Two types of elevated temperature tests were conducted with NUKON/CalSil debris beds. The first elevated temperature tests were conducted by forming the debris bed at ambient fluid temperature, executing the velocity sequence at ambient fluid temperature, and then elevating the fluid temperature with the screen approach velocity maintained at approximately 0.1 ft/sec (0.3 m/s) and again taking data for the velocity sequence at the elevated temperature. Test cases NC5b and NC6b were performed this way to obtain data at 82°C and are part of Group 1 with their debris bed properties presented in Table 7.18. The results of elevated temperature tests NO4 and NO5 (refer to Section 7.2.2) raised concerns that the effects of flow history were masking any effects on the measured head loss resulting from the higher fluid temperature. Therefore, additional elevated temperature tests were conducted with debris beds formed at elevated temperatures.

The later elevated temperature tests consisted of raising the fluid temperature to the desired conditions prior to the introduction of debris material. The debris bed was formed and the velocity sequence executed at the raised temperature. At the completion of the first pass through the velocity sequence, the fluid temperature was cooled and a truncated velocity sequence executed at the reduced temperature. The debris beds for NC15a and NC16a had the same target debris loadings as test case NC5a and were formed at 129° and 180°F (54° and 82°C), respectively. NC15a and NC16a are part of Group 1. Their debris bed properties are presented in Table 7.18. The debris bed for NC17a was formed at 129°F (54°C) and had the same target mass loading as NC9. NC17a is part of Group 2; its associated debris bed properties are presented in Table 7.19.

The test cases listed in Tables 7.18 and 7.19 with identification numbers ending in “b” (e.g., NC5b) represent test cases that were conducted after an initial test and associated velocity sequence were run at a different temperature. The debris beds for these cases were also subjected to a prolonged period of flow (> 45 minutes) during fluid heat up or cool down prior to executing the velocity sequence and taking the associated steady-state pressure measurements. Test cases NC5b, NC15b, NC16b, and NC17b all yielded higher relative debris bed densities than the corresponding test cases conducted first with the same debris beds. The increase in the relative densities is another indication of the effect the flow history can have on the debris beds. Test Case NC6b was the lone exception, with debris bed densities less than those obtained from the bed height measurements for NC6a.

Identification of test cases used in the legends of plots are the same as described in Section 7.4.4 with the fluid temperature at which the head loss data was obtained added to the end of the identification. The reader is again reminded that all of the head loss data are reported in inches of H₂O @ 68°F. Figure 7.51 is a plot of the debris bed head loss as a function of the screen approach velocity for all the test conditions from Group 1 that include a test conducted at an elevated temperature. The results from four debris beds (test conditions NC5, NC6, NC15, and NC16) and eight test cases are presented in Figure 7.51. The same geometric shape is used to represent data points for the same debris bed. The hollow shape represents the test case conducted at the lower temperature and the filled in data point represents data obtained at the higher temperature. Despite the differences in flow history for all four debris beds, the lower temperature (i.e., higher fluid viscosity) test case yielded the higher pressure drop.

The Group 1 test cases conducted at 180°F (82°C) listed from highest to lowest pressure drop were NC6b, NC5b, and NC16a. Comparing the debris bed properties from Table 7.18 for the three test cases, the ranking from highest to lowest for the relative debris bed density and total mass loading corresponds to the order obtained for the pressure drop measurements.

Test cases NC15a and NC16b were conducted at 129°F (54°C) with NC15a producing the higher measurements for pressure drop. NC16b had a relative density greater than that for NC15a; however, the total mass loading for NC15a was 168% that for NC16b, 261 g/m² compared to 160 g/m².

The test cases conducted at ambient temperature from highest to lowest pressure drop were NC6a, NC15b, and NC5a, which corresponds to the ranking for total mass loading, CalSil mass loading, and CalSil-to-NUKON mass ratio. The relative density for the three debris beds did not correspond to the order of the pressure drops at an approach velocity of 0.2 ft/sec (0.06 m/s); however, it should be noted that test case NC15b, which had the largest relative density, was conducted at 97°F (36°C) compared to approximately 70°F (21°C) for test cases NC6b and NC16a. The greater fluid temperature of NC15b corresponds to a reduced fluid viscosity, which may account for the greater density case not yielding the largest pressure drop at 0.2 ft/sec (0.06 m/s). However, the highest pressure drop was obtained for test case NC15b at screen approach velocity of 0.1 ft/sec (0.03 m/s) (see Figure 7.51).

Visual observations indicated the debris beds generated at elevated temperatures did not appear to have rims as pronounced as comparable beds formed at ambient temperature. This observation could impact the relative densities calculated from the optical triangulation debris bed heights. The relative density measurements are obtained from the total retrieved mass, the debris bed volume calculated from the test section diameter, and the average body height obtained from the optical triangulation measurements. The average body height is the average height of the debris bed excluding the area covered by the debris bed rim. Therefore, the volume of debris material included in the rim is excluded from the calculation of the relative density, while the mass of the material is included.

The debris beds formed at an elevated fluid temperature, test cases NC15A, NC16a and NC17a, had relative rim heights that were a smaller percentage of the debris bed center height than those formed at ambient fluid temperatures. From Group 1, debris beds NC5a and NC6a formed at ambient temperature both had rims heights measured at 0.1 ft/sec that were 3.1 times the center height, respectively. In comparison, the Group 1 debris beds NC15a and NC16a formed at fluid temperatures of 129° and 130°F (54° and 82°C), respectively, had rims heights measured at 0.1 ft/sec that were 2.8 and 1.5 times the

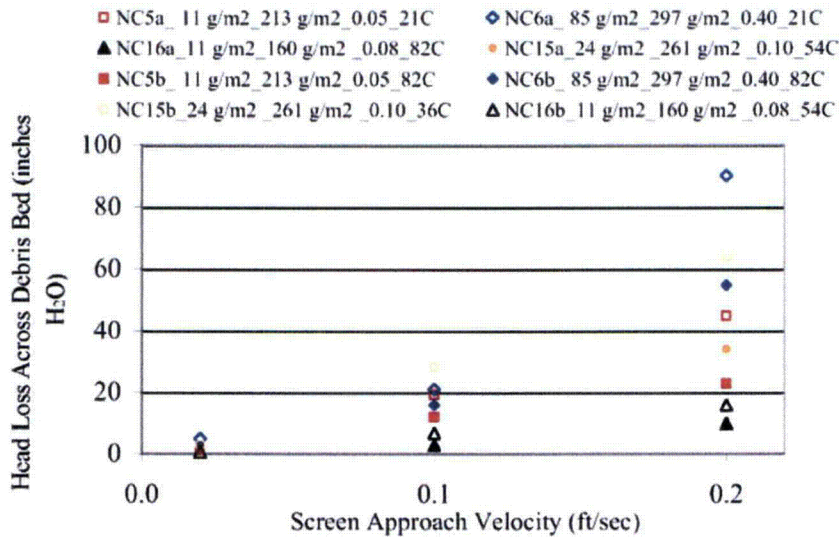


Figure 7.51. Plot of Pressure Drop Across the Debris Bed as a Function of Screen Approach Velocity for Group 1 Debris Beds Subjected to Testing at Elevated Fluid Temperatures. All test cases are from Series 2. The debris beds for conditions NC5 and NC6 were formed at ambient fluid temperature; debris beds for test conditions NC15 and NC16 were formed at fluid temperatures of 129° and 130°F (54° and 82°C), respectively. Head loss measurements are from Quick Look reports in Appendix J.

center height, respectively. Group 2 debris bed NC9 formed at ambient temperature had rim heights measured at 0.1 and 0.2 ft/sec that were 1.4 and 2.2 times the center height, respectively. In comparison, the Group 2 debris bed NC17a formed at a fluid temperature of 129°F (54°C) and had rim heights measured at 0.1 and 0.2 ft/sec that were 1.3 and 1.2 times the center height, respectively. The calculated densities are relative measurements used for comparing the different test cases and are not expected to represent true bulk densities. The variations in the relative rim height observed between debris beds formed at the different fluid temperatures indicate additional caution should be used when using the relative density to compare debris beds formed at different temperatures.

Figure 7.52 plots the debris bed head loss as a function of the screen approach velocity for the Group 2 test cases NC9, NC17a, and NC17b. The debris bed for NC17a was formed at a fluid temperature of 129°F (54°C) with the same target mass loading as NC9. For test condition NC17, the lower temperature (higher viscosity) case, NC17b, yielded larger pressure drop measurements. Comparing the ambient temperature cases of NC9 and NC17b, the test case with the larger mass loading and relative density, NC17b, yielded the higher head loss. Again, it is likely that the increased relative density obtained for NC17b is the result of the additional flow history resulting from the cool-down period and execution of the second velocity sequence.

The elevated temperature cases continue to support the trend that, for comparable mass loadings, the debris beds with the largest relative bulk density yielded the largest pressure drop measurements. The flow history resulting from periods of heating up and cooling down and repeating velocity sequences appears to impact the head loss measurements by increasing the relative density of the beds. Other than visual observations of the change in relative debris bed rim height, no conclusions have been drawn regarding changes to the debris bed resulting from forming it at an elevated temperature.

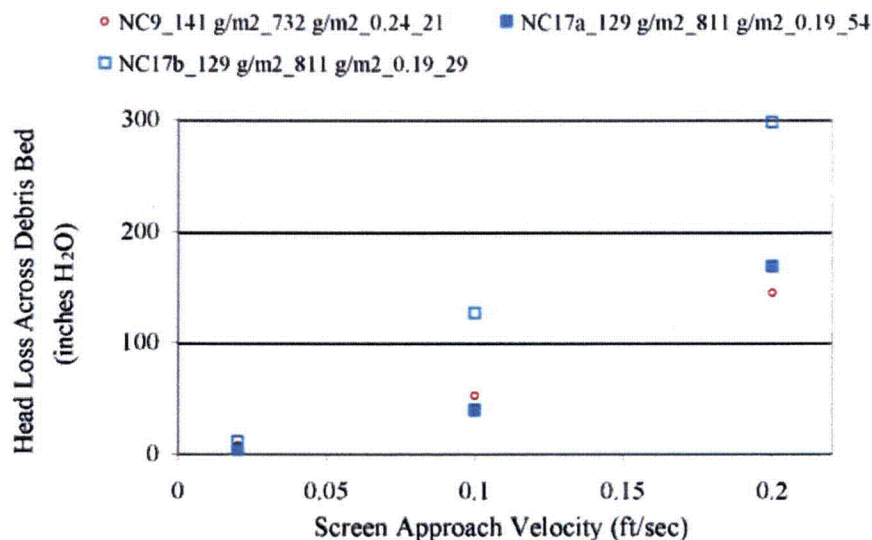


Figure 7.52. Pressure Drop Across Debris Bed as a Function of Screen Approach Velocity for Group 2 Debris Beds Associated with Elevated Temperature Test NC17a. Debris bed NC17 was formed at a fluid temperature of 129°F (54°C) and the same target mass loading as NC9, which was formed at a fluid temperature of 70°F (21°C). Head loss measurements are from Quick Look reports in Appendix J.

7.5 Coating Debris Bed Results

PNNL evaluated debris bed head loss for Ameron's Amercoat 5450 alkyd topcoat (ALK) and Ameron's Dimetcote 6 inorganic zinc primer with Amercoat 90 epoxy topcoat (ZE) coatings as a function of screen approach velocity, flow history, and fluid temperature. The debris material was prepared as described in Section 4 to create processed and ¼-in. square chips for each coating type. The processed debris was the finer material with major and minor axis dimensions on the order of 0.05 to 0.15 in. (1.3 to 3.8 mm) and 0.05 to 0.10 in. (1.3 to 2.5 mm), respectively, for both the ALK and ZE coatings. The ¼-in. square chips were obtained by sieving and had major and minor axis dimensions on the order of; 0.1 to 0.45 in. (2.5 to 11 mm) and 0.1 to 0.3 in. (2.5 to 7.6 mm) for ALK and 0.3 to 0.6 in. (7.6 to 15 mm) and 0.15 to 0.3 in. (3.8 to 7.6 mm) for ZE, respectively. Size distributions for the four coating debris tested are provided in Appendix O.

Tests conducted with the ALK and ZE coatings are listed in Table 7.24. An ALK coating benchtop test, ALKBT, was initially conducted as a scoping test at 700 g/m² each of blender processed coating and ¼ in. square (also referred to as chips) coating (Section 4). Three large-scale tests, ALK1a, ALK1b, and ZE1, were conducted in the large-scale loop with equal target concentrations, 700 g/m² each, of processed coating and ¼ in. square coating (see Section 4). Test ALK1b is a continuation of test ALK1a at an elevated fluid temperature. One additional test, ALK2, was conducted with only processed coating at the total target loading of 1,400 g/m².

In Section 7.5.1, determinations from the ALKBT benchtop test regarding the debris bed formation process are listed, and large-scale debris bed formation test procedures and observations are discussed. Coatings test results are discussed in Section 7.5.2.

Table 7.24. PNNL Coating Debris Tests Conducted

Test Case	Test ID	Target Debris Bed Processed Coating Loading (g/m ²)	Target Debris Bed ¼-in. sq. Coating Loading (g/m ²)	Total Debris Bed Loading (g/m ²)	Total Retrieved Debris Bed Loading (±8 g/m ²)	Nominal Fluid Temp. (°C)	Screen or Plate	Debris Bed Formed
ALK1a	060501 PQC 2609 LP1	700	700	1,400	807	18	plate	incomplete
ALK1b	060501 PQC 2609 LP2	700	700	1,400	807	82	plate	incomplete
ZE1	060504 PQZ 2609 LP1	700	700	1,400	794	21	plate	incomplete
ALKBT	060428 PQC 1136 BP1	700	700	1,400	762	21	plate	incomplete
ALK2	060502 POC 2609 LP1	1400	0	1,400	850	21	plate	incomplete

7.5.1 Coating Debris Bed Formation

The following items were determined from the initial ALKBT benchtop test:

- The paint chips when wet have a tendency to adhere easily to surfaces. Therefore, when premixing constituents, 1/4-inch square chips were placed dry in a mixing container and the other slurried constituents were added wet.
- A screen approach velocity of 0.1 ft/sec was not fast enough to transport the coating debris to the test screen. Initially, the benchtop injection line velocity was set to 0.8 ft/sec with a screen approach velocity of 0.1 ft/sec. Negligible paint chip material was visually observed to be transported to the test screen, even with significant line agitation. The paint chips exited the injection line as a saltation-type flow and immediately settled upon being introduced into a horizontal section of the main line. Some coating debris transport was achieved when the screen approach velocity was increased to approximately 1.5 ft/sec. Screen approach velocities for the coatings tests were greater than those used for the insulation materials (Sections 7.2–7.4)

From the latter observation in the benchtop test, the screen approach velocity for bed formation for the ALK1a and ALK1b coating test was set to the maximum velocity of the test matrix, 0.20 ft/sec (see Section 5 for test velocity matrixes). Some of the debris introduced to the loop was judged by visual observation of the flow to settle within the piping as opposed to collecting on the perforated plate. Thus, settled material was mobilized into the flow by tapping the horizontal flow region of the test loop at the debris injection level with a rubber hammer. Hammering was continued until some (usually a small amount) additional debris was observed to be mobilized. This hammer mobilization technique was conducted intermittently for approximately 20 minutes after debris injection.

Based on the debris bed formation conditions for tests ALK1a and ALK1b, the initial screen approach velocity for test ALK2 with processed-only coating debris was set to 0.30 ft/sec. At this screen approach velocity, essentially no debris was observed to be mobilized in the flow. Additionally, minimal processed ALK debris was visually observed retained on the perforated plate after the debris bed formation time of one hour. As noted for the ALK1a and ALK1b test, settled material was mobilized into the flow by tapping the horizontal flow region of the test loop at the debris injection level with a rubber hammer. This methodology, though apparently successful at mobilizing some portion of the particulate, was not used for test ALK2 because it was observed that the tapping released the processed-only particulate from the plate. Additional testing was conducted after completion of the truncated velocity matrix (see Section 5).

The additional testing for ALK2 consisted of incrementally raising the screen approach velocity to identify, if possible, when the settled (as inferred from the visually observed lack of debris on the plate or in the flow) was mobilized. The flow was then held for 45 minutes at this mobilization velocity to form, if possible, a complete debris bed, and filtration was again conducted. The maximum limit for flow rate was set to 140 gpm (corresponds to a screen approach velocity of 1.55 ft/sec) to preserve bag-filter integrity (see Section 2 for bag-filter description).

Cursory calculations were performed during the test in an attempt to quantify the expected solid volume fraction at complete mobilization of the injected debris into the flow. With a flowing loop volume of approximately 85 gallons, total processed ALK debris mass of 26.09 g (neglecting filtering given the limited indication of mobilization), and measured ALK density of approximately 1.04 g/mL, the solid volume fraction in the flow with homogenous mixing was calculated to be $< 0.01\%$ (mass fraction $8.1E-5$). Visual observation is therefore inadequate to determine total mobilization of the complete debris mass. Thus, the relative visually observed change in the solids content of the flow was used solely to judge mobilization effect. For a limited range of approach velocities (not thoroughly quantified) coatings material would appear to be entrained and held up (accumulate) in turbulent eddies just below the bed. Therefore, consideration was also given to ensuring an approach velocity sufficient to negate the trapping of debris particulate in the turbulence of the plate discharge. This was desired to ensure transport to the filter and negate the potential for settling upon reduction of the flow velocity.

The previous test conditions indicated that 0.3 ft/sec (all subsequently referenced velocities refer to the screen approach velocity) was insufficient to maintain suspension of the debris. Thus, it was not expected that 0.3 ft/sec would mobilize the settled particulate, and 0.4 ft/sec was selected as the initial elevated velocity. Limited particulate (hereafter to be taken as visually observed to be on the order of the prepared debris in size) was observed to be mobilized into the flow. The quantity of debris above and below the plate was judged to be similar, and no buildup was observed on the plate. Particulate was trapped below the screen. At this and subsequent velocities, the debris appeared to be evenly distributed throughout the loop; i.e., the observed concentration appeared constant for successive circulations (with time).

At 0.5 ft/sec, the quantity of particulate was observed to increase, a slight difference in concentration was observed in the upper (above the plate) and lower (below the plate) test sections, a slight buildup was observed on the plate, and particulate was trapped below the screen. At 0.6 ft/sec, the quantity of particulate in the flow was observed to significantly increase, a difference in concentration was observed between the upper and lower test sections, gradual buildup was observed on the plate, and the quantity of particulate trapped (mobilized) below the screen was reduced as trapped particulate was transported downstream.

The increase in particulate in the flow from 0.6 to 0.7 ft/sec was not as substantial as the increase from 0.5 to 0.6 ft/sec, particulate buildup was observed on the plate, and particulate was mobilized below the screen. Thus, the 45-minute second bed formation period was initiated. At the end of the 45 minute period, the particulate concentration was significantly reduced and particulate coated the plate surface leaving the majority of the perforations open. A velocity of 0.8 ft/sec was subsequently achieved. No increase in particulate concentration was observed, the flow was returned to 0.7 ft/sec, and the incomplete debris bed velocity test matrix was again employed.

The initial debris bed formation screen approach velocity for test ZE1 was maintained at 0.3 ft/sec. As with previous benchtop and large-scale coating debris tests, the mobilized debris for flow circulations immediately after the introduction of debris into the loop was judged by visual observation to be reduced by settling rather than collection on the plate. Thus, settled material was mobilized into the flow by

tapping the horizontal flow region of the test loop at the debris injection level with a rubber hammer. Eight tapping periods were conducted within 5 minutes of the debris introduction. By the eighth tapping period, material mobilization to the test section/plate was minimal as judged by visual observation.

At the end of the debris bed formation period at a screen approach velocity of 0.3 ft/sec, 1/4-in. square ZE debris on the perforated plate was visually observed to approximate the loaded amount. The debris bed was incomplete, with ~20% of the plate area exposed. The processed debris was visually observed to be passing through the plate (and the 1/4-in chips were retained thereon) during the early portion of the bed formation test phase. This processed debris concentration in the flow was visually observed to decrease with time without readily apparent buildup on the debris bed. Thus, it was judged to have settled in the loop. The screen approach velocity was therefore increased to 0.7 ft/sec (per test ALK2 description above). The processed particulate concentration in the flow was visually observed to increase, minimal 1/4-in. chip debris appeared mobilized, and the processed particulate collected on the plate over the 45-minute hold period, as judged by the visually observed increase on the plate and reduction of debris in the flow. The measured debris bed head loss increased by 60% (10 to 16 in. H₂O) over this period. The incomplete debris bed velocity matrix was subsequently employed.

7.5.2 Coating Debris Bed Results

A Quick-Look report providing the data sets for tests ALK1a, ALK1b, ZE1, and ALKBT is provided in Appendix K. The current presentation of results will focus on the effects of coating preparation, test repeatability, coating type comparison, and test fluid temperature. The effect of coating preparation is considered in subsection 7.5.2.1 for tests ALK1a and ALK2; test repeatability is examined through tests ALK1a and ALKBT in Section 7.5.2.2; coating type comparison (e.g., ALK to ZE) is provided in Section 7.5.2.3; and temperature effects are considered in Section 7.5.2.4. The uncertainties for the Coatings test are similar to those presented in Sections 7.2 through 7.4. Given that incomplete debris beds were formed for each test, uncertainties in the presented data are not detailed.

7.5.2.1 Coating Preparation

The effect of coating preparation (i.e., processed or 1/4-in. square chips debris) may be considered with regard to tests ALK1a and ALK2. The 3°C temperature difference for the nominal fluid temperature between the tests is neglected (Table 7.5.1).

As specified in Table 7.5.1, the total target debris loading for these tests was 1,400 g/m². Test ALK1a had 700 g/m² each of processed and 1/4-in. square chips coating, while the entire loading for ALK2 consisted of -processed coating. Differences in debris behavior during the debris bed formation periods are noted in Section 7.5.1. No data are available to evaluate or quantify the possible effects of flow histories.

Each debris bed was incomplete, as shown in Figures 7.53 and 7.54. The debris bed for test ALK2 was an extreme case, with the bulk of the perforations in the plate open to flow.¹ As expected due to the bed formation behavior, the combination of processed coating and 1/4-in. square chips for test ALK1a resulted in a larger head loss across the debris bed than for test ALK2 (Figure 7.55).² Test phase ramp up 2 for ALK1a and ramp up 1 of the truncated velocity matrix employed for ALK2 are shown.

¹ In Figure 7.54, the observable areas of blocked perforations were observed to be caused by contamination with 1/4-in. square coating ALK from the prior ALK1a and ALK1b test mobilized out of the test loop by the increased screen approach velocities used during debris bed formation for ALK2 (see Section 7.5.1).

² Results from the second test period (Section 7.5.1) of ALK2 are presented.



Figure 7.53. ALK1a Debris Bed After Retrieval from Test Section, Top View

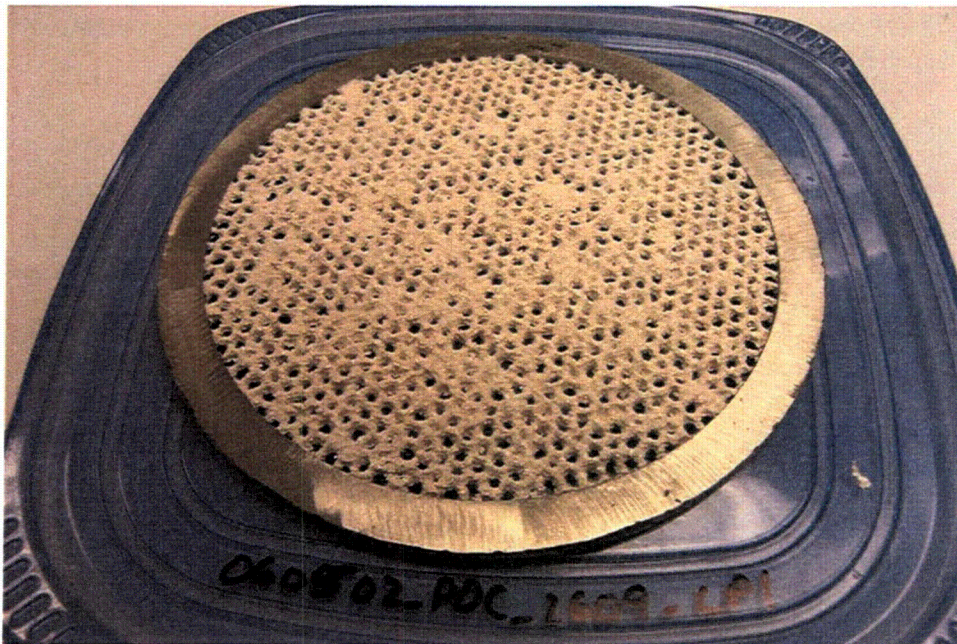


Figure 7.54. ALK2 Debris Bed After Retrieval from Test Section, Top View

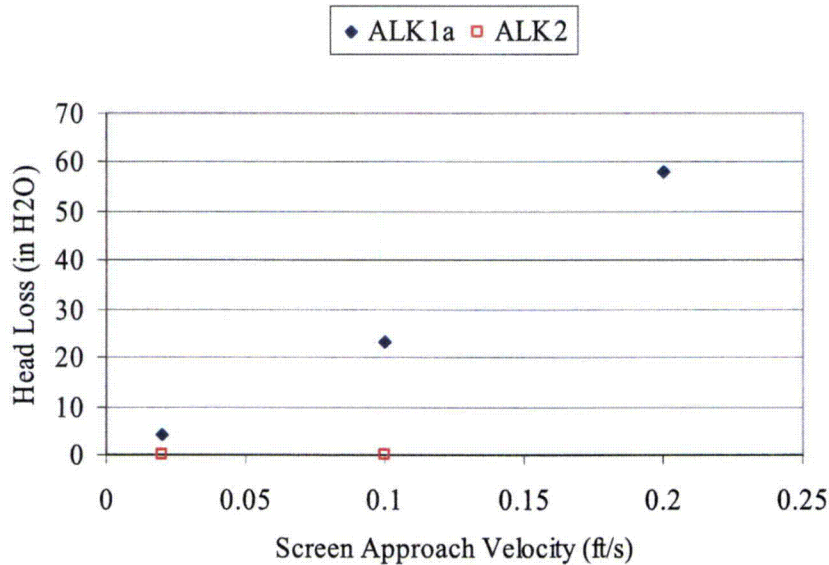


Figure 7.55. Head Loss Results for ALK1a and ALK2

The retrieved debris bed mass loadings for ALK1a and ALK2 were within about 5% of each other. The incomplete and varying debris bed surfaces preclude considerations based on the debris bed heights.

7.5.2.2 Coating Test Repeatability

Coating test repeatability, in terms of measured head loss for a given screen approach velocity, is considered for repeat velocity cycles within a single test and for repeated tests. Multiple velocity cycles were performed for tests ALK1a and ALK1b. As shown in Figure 7.56, the variability between the velocity cycles (ramp up 2 and 3 results are plotted for each test) is relatively minor (absolute value ~ 0 (10%) at 0.1 ft/sec, ~ 0 (5%) at 0.2 ft/sec), indicating stability (i.e., constant mass, porosity, etc. at or over the screen approach velocities) for the debris bed.

Repeat tests for the ALK coating were performed in the large scale, ALK1a, and benchtop, ALKBT, loops. The 3°C temperature difference for the nominal fluid temperature between the tests is neglected (Table 7.24). Each test had 700 g/m² each of processed coating and 1/4 in. square coating chips. The debris beds were formed under different flow conditions, and no data are available to evaluate or quantify the possible effects of the bed formation and flow histories.

As may be observed by comparison of Figures 7.53 and 7.57, the incomplete debris beds were similar in appearance, although the open channels and perforations were noticeably fewer for ALKBT. In Figure 7.58, test phase ramp up 2 head loss results are provided for each test. The higher head loss results for ALKBT are somewhat surprising given the higher retrieved debris bed loading of ALK1a, refer to Table 7.24, but may be expected with the relative completeness of the debris beds indicated above. This observation may be supported by considering that the maximum variability in the presented results. The variability of approximately 55% is up to 25% larger than that observed for comparisons of the NUKON-only large-scale and benchtop tests (Section 7.2). This difference is also substantially larger than the benchtop test comparisons in Section 6.1. The incomplete and varying debris bed surfaces preclude investigation of the head loss results based on the debris bed heights.

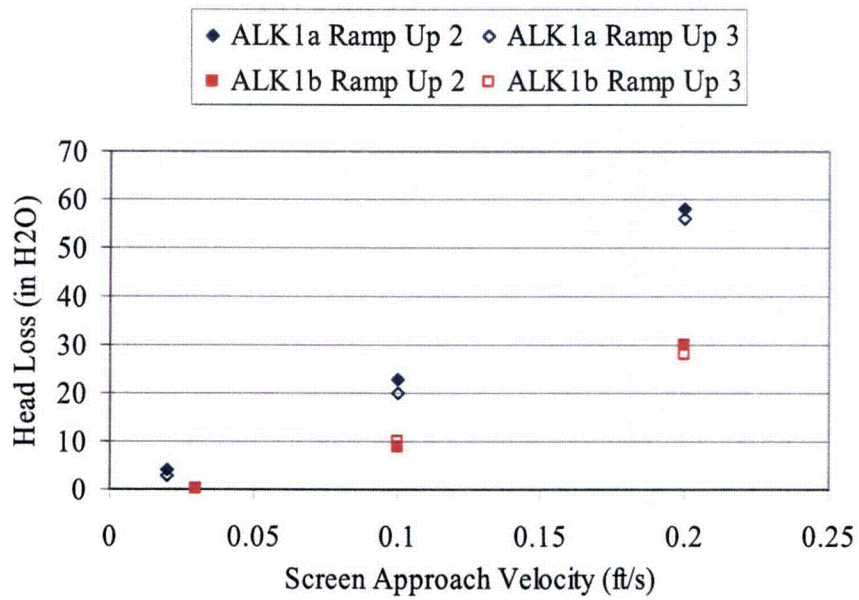


Figure 7.56. Head Loss Results for ALK1a and ALK2, Repeat Velocity Cycles

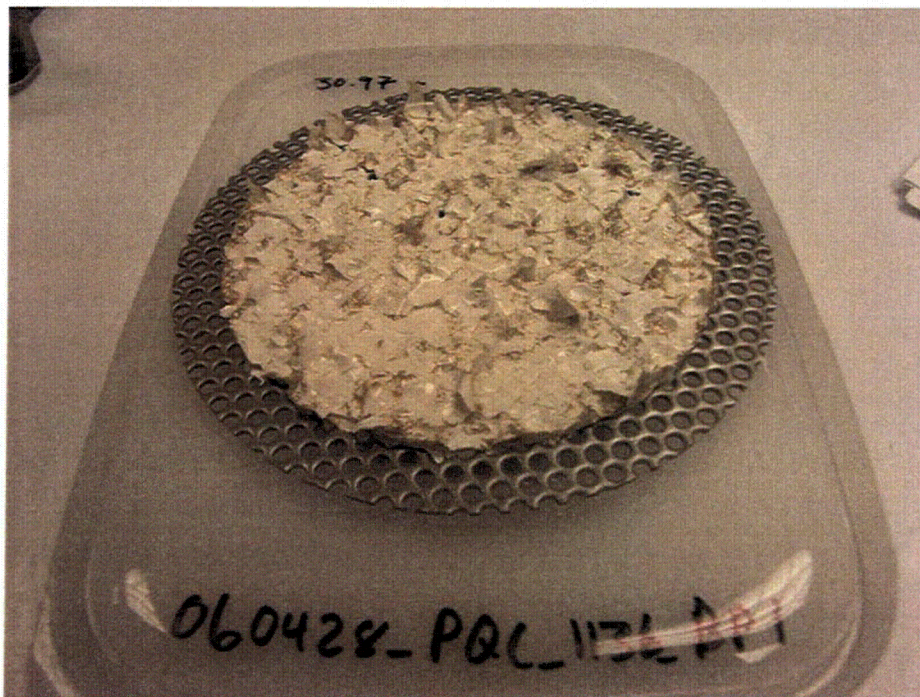


Figure 7.57. ALKBT Debris Bed After Retrieval from Test Section, Top View

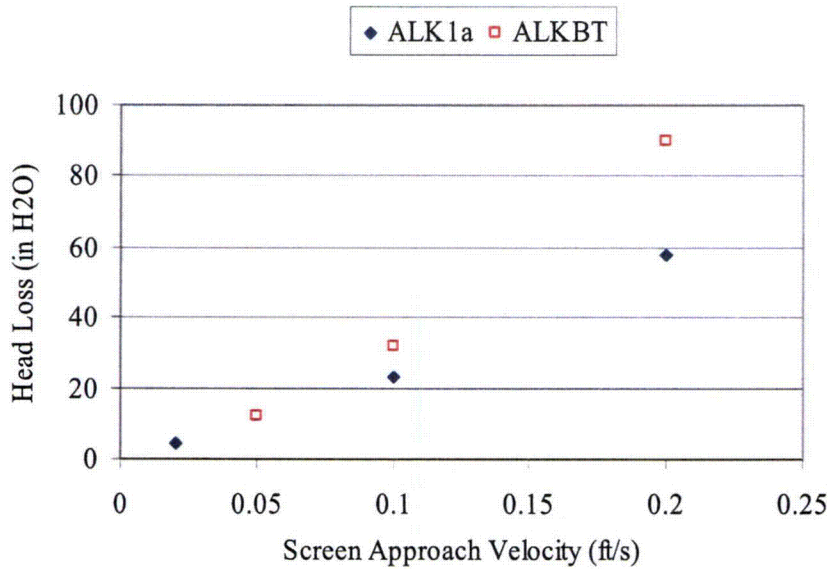


Figure 7.58. Head Loss Results for ALK1a and ALKBT

7.5.2.3 Coating Type Comparison

The head loss performance of debris beds with the same target debris loading and preparation but different coating materials was investigated. ALK was used for test ALK1a, and ZE was used for ZE1. ALK1a and ZE1 had 700 g/m² each of processed coating and 1/4-in. square coating chips for a total target debris loading of 1,400 g/m². The nominal fluid temperature difference, 3°C (from Table 7.24), is neglected. No data are available to evaluate or quantify the possible effects of bed formation and flow histories.

As described in Section 7.5.1, significantly different flow conditions were required for debris bed formation. The ALK coating debris types are thought to have been more homogeneously transported to and collected on the screen, while the ZE debris appeared to be segregated by the flow conditions. The ZE1 debris bed thus formed by deposition of the 1/4-in. square coating chips, and the processed coating was deposited only after a substantial increase in the screen approach velocity (Section 7.5.1).¹ Insufficient data exist to evaluate the possible effect of this observed variation.

The ZE1 debris bed shown in Figure 7.59 was substantially less complete than the ALK1a debris bed in Figure 7.53. Further, while the ALK1 debris bed was relatively easily removed from the screen as a complete intact bed after drying, the ZE1 debris bed was essentially a collection of separate debris pieces with no cohesiveness. It is uncertain what effect this observed integrity of the debris bed had on the resultant head loss, but clearly, as shown in Figure 7.60, the ALK1a debris bed head loss was substantially greater than that for ZE1. The head loss results presented are for test phases ramp up 2 and ramp up 1 for the ALK1a and ZE1 tests, respectively. The retrieved debris bed loading for ALK1a was 2% greater than that for ZE1. Considerations based on the debris bed heights are precluded by the incomplete and varying debris bed surfaces.

¹ It has been shown (see Section 6.3) that small variations in the loading sequence of fibrous and particulate insulation debris can have a significant impact on head loss results. Thus it may be reasonable to assume that a similar effect, uncertain in magnitude, may be achieved with coating debris. The varied nature of the ALK and ZE coating debris, and more significantly the incompleteness of the coating debris beds formed, possibly renders comparison of the loading sequence effects for ALK1a and ZE1 moot.

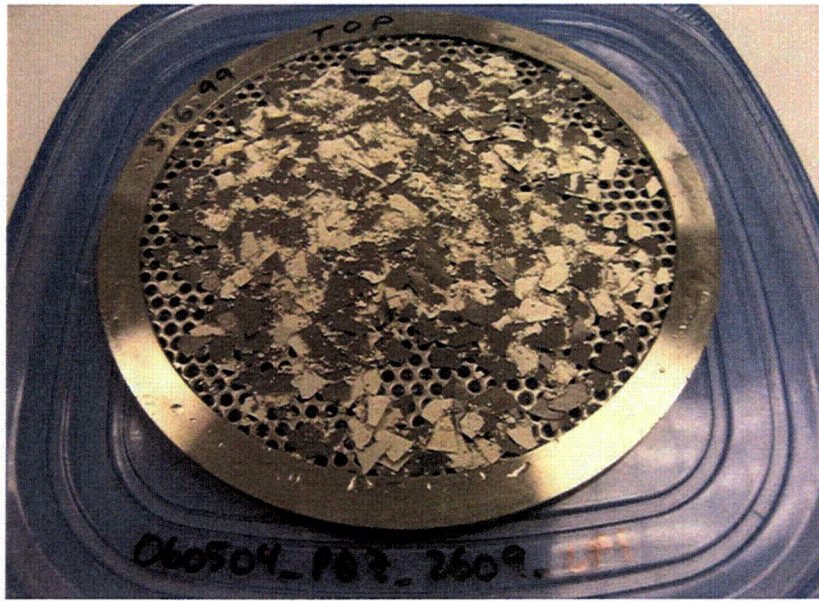


Figure 7.59. ZE1 Debris Bed After Retrieval from Test Section, Top View

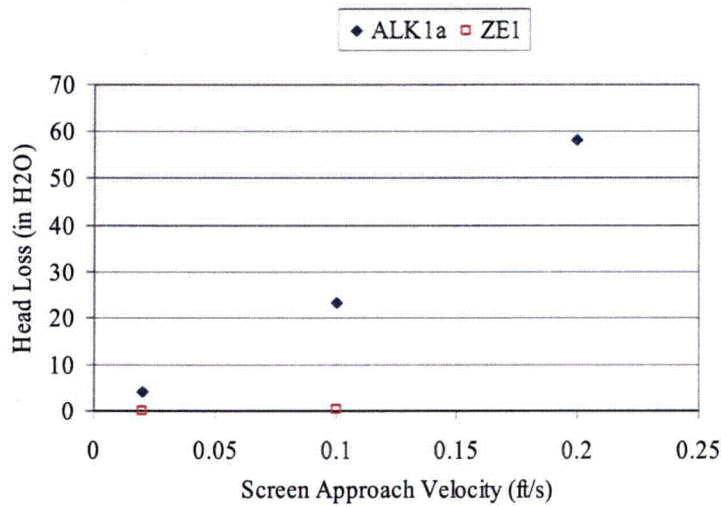


Figure 7.60. Head Loss Results for ALK1a and ZE1

7.5.2.4 Temperature Effects

The effect of varied fluid temperature on head loss as a function of screen approach velocity was investigated with tests ALK1a and ALK1b. As with specific NUKON-only and NUKON/CalSil debris beds, temperature effects testing was first conducted by performing debris bed formation and the completion of the velocity test matrix at ambient conditions (test ALK1a). The loop fluid was then heated to 82°C, whereupon the velocity matrix was repeated (test ALK1b). The effect of the flow history resulting from this approach is uncertain.

The head loss for ALK1b was reduced as compared to that for ALK1a, Figure 7.61. Data for test phase ramp up 2 is shown for each temperature.

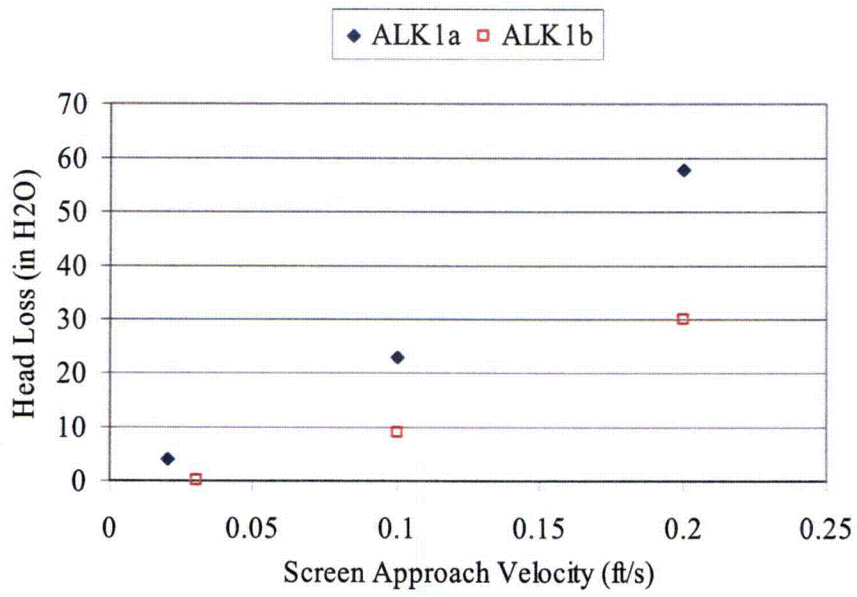
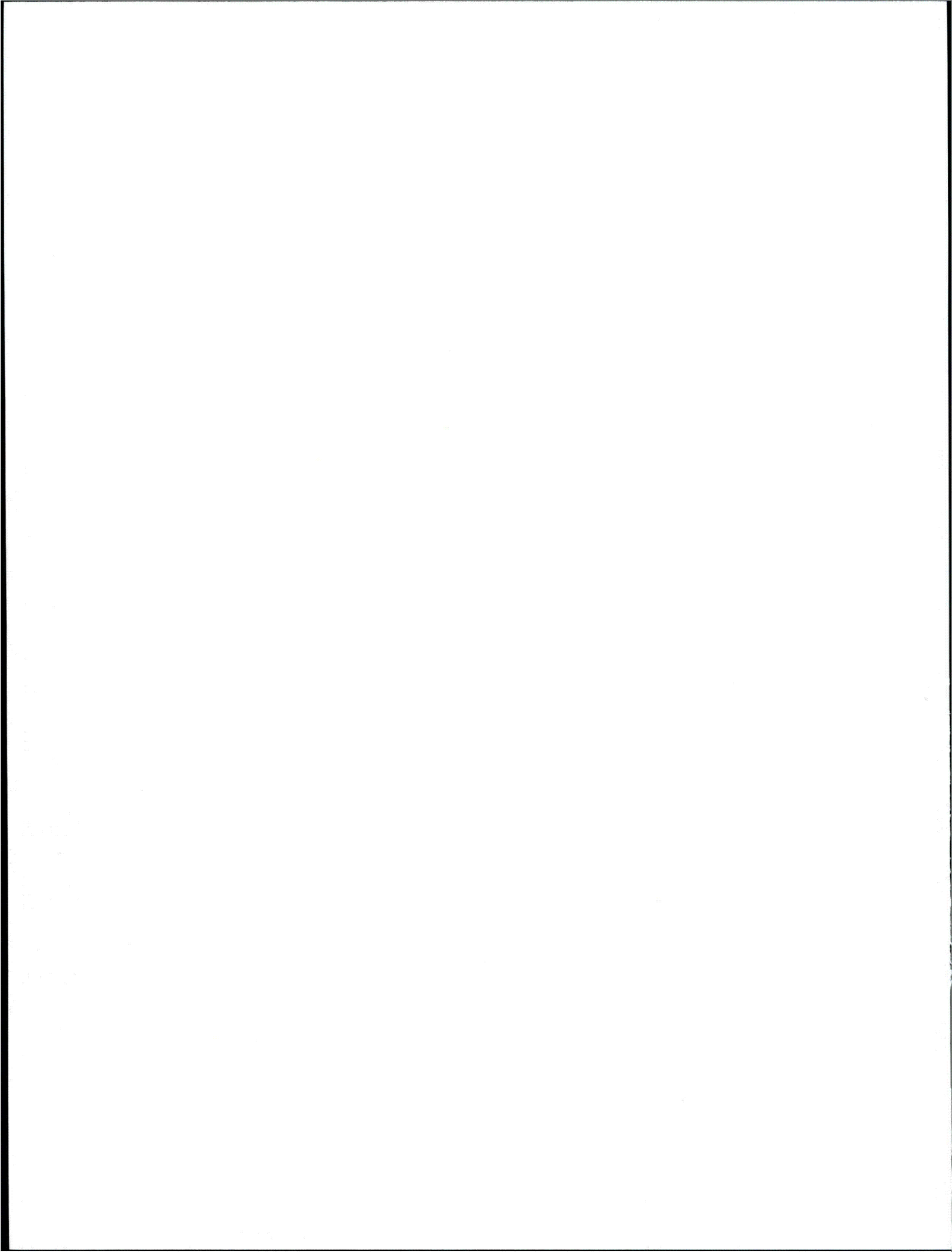


Figure 7.61. Head Loss Results for ALK1a and ALK1b



8.0 Discussion of Large Scale Results

This section discusses the results obtained from large-scale testing that were presented in Section 7. Comparisons are made between the results for different types of debris beds and test conditions. Final conclusions are presented in Section 9.

Under clean, debris-free conditions, the perforated plate with 1/8-inch holes had a greater resistance to flow than the 5-mesh woven wire cloth screen (referred to as the 5-mesh screen); however, the difference in pressure drop was small. At a screen approach velocity of 2.0 ft/sec, the perforated plate had a head loss of 3.7 in. H₂O (referenced to 68°F) compared with 2.3 in. H₂O for the 5-mesh screen. For a screen approach velocity of 0.2 ft/sec, both screen materials yielded head loss measurements on the order of 0.1 ± 0.1 ft/sec for clean water. Based on how the debris bed formed on the two types of screen material, it is unclear which material contributed higher flow resistance to a debris bed. The NUKON and NUKON/CalSil debris beds formed on the surface of the perforated plate with minimal material protruding through the perforations. The debris beds were easily removed from the perforated plates. For the CalSil-only tests (no complete debris beds formed), the debris appeared to have been extruded through holes in the perforated plate in the vicinity of open flow channels, but minimal entangling of the extruded material occurred.

On the 5-mesh screen, the debris appeared to become entangled with the woven wire. The least entanglement was experienced with NUKON-only debris beds. Additional effort was required to remove the debris beds from the 5-mesh woven wire screens, and after removal of a debris bed, additional effort was required to remove residual debris material that remained entangled with the woven wire.

For the bare screen materials, no significant changes in head loss were observed at elevated fluid temperatures of 129°F (54°C) and 180°F (82°C). Any difference in the measured pressure drop with respect to fluid temperature is considered to be indistinguishable within the resolution of the DAS at low head loss values.

The pressure drop data presented for ambient fluid temperatures (approx. 68° to 82°F [20° to 28°C]) were obtained for conditions of either fully turbulent or fully laminar pipe flow upstream of the debris bed. Only the data obtained at 0.05 ft/sec (0.02 m/s) for ambient fluid temperatures were predicted to have transition flow conditions upstream of the test screen. For the elevated fluid temperature tests at 129° and 180°C (54° and 82°C), the data presented for 0.02 ft/sec (0.01 m/s) were predicted to potentially have transition pipe flow conditions upstream of the debris bed. Higher approach velocities at the elevated temperature were predicted to produce fully turbulent pipe flow upstream of the test screen.

For the NUKON-only and NUKON/CalSil debris beds, the steady-state head loss achieved for each velocity condition tested tended to increase with each cycle of the velocity sequence. The continual changes observed in the pressure drop with each velocity cycle were greater than the uncertainty of the measurements. This phenomenon complicates the assessment of test repeatability. Because the debris beds were observed to compress and relax with changes in the screen approach velocity over multiple cycles, the potential existed for the structure of the debris beds to continually change as finer material migrated through the debris bed with oscillations in the debris bed height and associated bulk porosity.

For the NUKON-only tests, repeatability was obtained between large-scale tests NO4 and NO5, with both test cases exhibiting a similar increase in pressure drop with each velocity cycle. The large-scale results also compared well with benchtop loop results with similar mass loadings. All of the test cases used to assess the repeatability of the NUKON-only debris beds had an initial screen approach velocity of 0.2 ft/sec. After this assessment, the screen approach velocity for bed formation was changed to 0.1 ft/sec.

Based on the comparison made for the measured debris bed height as a function of screen approach velocity presented in Figures 7.10 and 7.11, the initial screen approach velocity used for bed formation appears to impact the resulting debris bed height and, hence, the relative bulk density. The debris bed in test NO5, which was formed with an initial screen approach velocity of 0.2 ft/sec, had a bed height similar to that of NO2 despite having a mass loading approximately three times greater.

Several factors may contribute to the differences observed in results obtained for the various screen approach velocities used for debris bed formation. At greater approach velocities, debris beds were observed to compress. The variation in the compression of a debris bed changes the filtration efficiency of the debris bed. Changes in the screen approach velocity may change the mass fraction of material that is retained within a debris bed. If a debris bed captures fewer fines during the initial stages of the bed formation process, a higher fraction of the smaller size material may not be captured until the bulk of the debris bed is formed or the screen approach velocity is increased. This would result in a higher fraction of fine debris being available for deposition in a thin surface layer, as discussed in Section 6.4.

Variations in the results obtained between test cases with different bed formation velocities may also be the result of the test loop geometry. A reduction in the screen approach velocity also reduces the flow rate throughout the test loop. The reduction in the flow rate may lead to material holdup or settling within the test loop. The size distribution of the held-up or settled material would differ from that of the bulk material introduced to the loop. This segregation of material would create a change in the debris loading sequence, which, based on the results of Section 6.3, can have a significant effect on the pressure drop across the debris bed. For the same screen approach velocity, the bed formation process could be altered depending on the line sizes of the test loop.

For the NUKON/CalSil tests, NC3 and NC14 were formed at the higher initial bed formation velocity of 0.2 ft/sec. Due to the potential differences in the debris load sequence and in the CalSil mass loadings compared with other NUKON/CalSil test cases, it is difficult to draw final conclusions regarding the impact of the initial bed formation velocity on the resulting head loss across the debris bed. NC14 had the greatest retrieved mass loading of any debris bed tested, but the measured pressure drops at 0.1 and 0.2 ft/sec were approximately 50 and 40% those obtained for NC11, which had approximately half the mass loading of NC14. These results indicate the importance of knowing the conditions for debris bed formation when comparing the results of different test cases.

For the same debris bed formation process, the pressure drop across the NUKON-only and CalSil-only debris beds increased with an increase in the retrieved mass loading. Figure 8.1 is a plot of the head loss across the debris bed as a function of the retrieved mass loading for the NUKON-only (denoted NO) and CalSil-only (denoted CO) test cases. The data are plotted for constant screen approach velocities of 0.1 and 0.2 ft/sec. The data plotted in Figure 8.1 are for the debris beds formed at ambient fluid temperatures. While none of the CalSil-only mass loadings tested developed complete debris beds, for the same retrieved mass loading the CalSil-only test cases still generated higher pressure drops than the NUKON-only cases, which were for complete debris beds (i.e. no channeling).

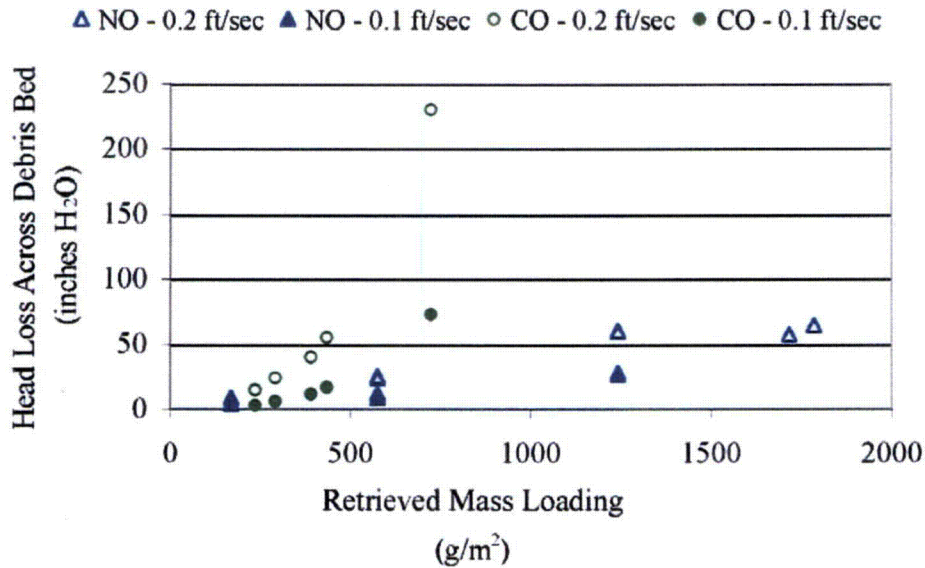


Figure 8.1. Pressure Drop Across the Debris Bed as a Function of the Retrieved Mass Loading for NUKON-Only (NO) and CalSil-Only (CO) Test Cases at Constant Velocities of 0.1 and 0.2 ft/sec. Test cases conducted at elevated fluid temperatures or with debris beds formed at elevated temperatures are excluded from the data. Data are from Tables 7.6 and 7.12 and the Quick Look reports in Appendixes H and I.

The pressure drops obtained for the CalSil-only tests combined with the results of the debris loadings, sequence investigation demonstrate what a difference the rearrangement of the debris constituents can have on the resulting pressure drop. In the benchtop loop, complete NUKON-only debris beds were formed on the 5-mesh screen that had retrieved mass loadings of 56 and 102 g/m². Thin fibrous beds such as these can provide a support structure for capturing CalSil, potentially creating a two-layer bed that, based on the test results, can have a significantly higher pressure drop than one using debris constituents that were premixed before introduction into the test loop.

For the loading sequence investigation, four scenarios were evaluated.

1. Formation of a NUKON-only debris bed prior to CalSil material being introduced into the test loop.
2. Premixing of the NUKON and CalSil debris constituents prior to introduction into the loop.
3. Formation of a CalSil-only debris bed followed by the addition of NUKON debris.
4. The addition of CalSil to the test loop with the addition of NUKON debris following after a short time (referred to as the lag time). The intent was to evaluate the formation of a debris bed resulting from the addition of NUKON to a flow stream that already contained well-dispersed CalSil material.

Scenario 4 yielded the highest-pressure drop measurements of the scenarios tested with the pressure drop reaching approximately 1000 in. H₂O in the benchtop loop and essentially exceeding the pump capacity. Scenario 1 yielded the next highest pressure drop measurements, followed by the results for the premixed condition of Scenario 2. As stated earlier, the results of Scenario 3 were not fully evaluated because a complete CalSil debris bed was never formed. The Series 2 tests were conducted using premixed debris for the NUKON/CalSil test cases.

The Series 1 tests attempted to simultaneously inject the separated debris constituents into the test loop. It is postulated that the variation in the resulting head loss with respect to the mass loading observed for the Series 1 NUKON/CalSil tests was due to variations created in the loading sequence of the debris on the screen. The simultaneous injection of the debris constituents was determined to create variations in the relative concentrations of the constituents in the main line just downstream of the point of debris injection. The loading sequence investigation not only demonstrated a variation in pressure drop resulting from changes in the debris loading sequence, it also demonstrated that repeatable results can be obtained for various loading sequences as long as the introduction sequence of the debris materials was controlled.

In Figure 8.2, the data from Figure 8.1 are plotted along with the pressure drop data from the NUKON/CalSil (denoted NC) debris beds formed under similar conditions. The head loss data presented in Figure 8.2 as a function of the retrieved debris bed mass loading is plotted for constant screen approach velocities of 0.1 ft/sec (0.03 m/s) and 0.2 ft/sec (0.06 m/s). Figure 8.2a includes both the Series 1 and Series 2 test cases; Figure 8.2b contains only the Series 2 test cases. The retrieved mass loadings of Series 1 tests are higher than those of Series 2 with minimal overlap between the two test series. Therefore, a good comparison of the pressure drop measurements obtained for the two debris-loading procedures cannot be made. The variations in the head loss measurements relative to the retrieved mass loading for the NUKON/CalSil test cases could be impacted by both the debris loadings sequence and the variations in the CalSil-to-NUKON mass ratio for each retrieved debris bed.

The results of Figure 8.2a and the fact that no complete CalSil-only debris beds were formed make it difficult to determine which debris bed condition would yield the highest pressure drop. Based on the results of the loading sequence evaluation, it is postulated that higher pressure drops can be obtained from a NUKON/CalSil debris bed then from a CalSil-only debris bed.

In both Sections 7.2 and 7.4, the pressure drop was shown to increase with an increase in the relative bulk density of the debris bed for the Series 2 test cases. Figure 8.3 compares the pressure drop across the debris bed as a function of the debris bed relative bulk density for both the NUKON-only and NUKON/CalSil debris beds. From Figure 8.3, the trend appears to hold for all of the Series 2 test cases, with the NUKON/CalSil debris beds appearing to yield a slightly higher pressure drop at a given mass loading (see Figure 8.2). Comparing Figures 8.2 and 8.3, it appears the pressure drop across the debris bed for a given bed formation procedure trends better with the debris bed relative bulk density than with the retrieved mass loading of the debris bed.

The pressure drop across a debris bed was anticipated to decrease with an increase in the fluid temperature due to the reduction in the fluid viscosity and density. While this was observed for a majority of the test cases, several instances occurred where the pressure drop increased with an increase in the fluid temperature. For both the NUKON-only and the NUKON/CalSil debris beds, these discrepancies in the measured head loss across a debris bed relative to the fluid temperature were accounted for by observed changes in the relative bulk density of the debris beds. It is assumed the change in debris bed density observed for some of the elevated temperature tests was the result of the additional flow history to which the debris bed was subjected.

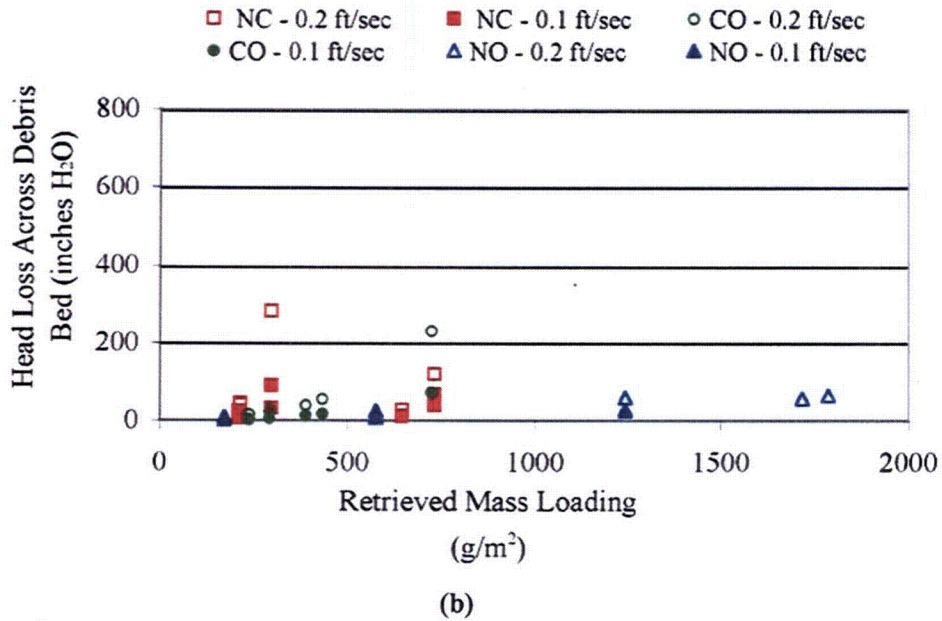
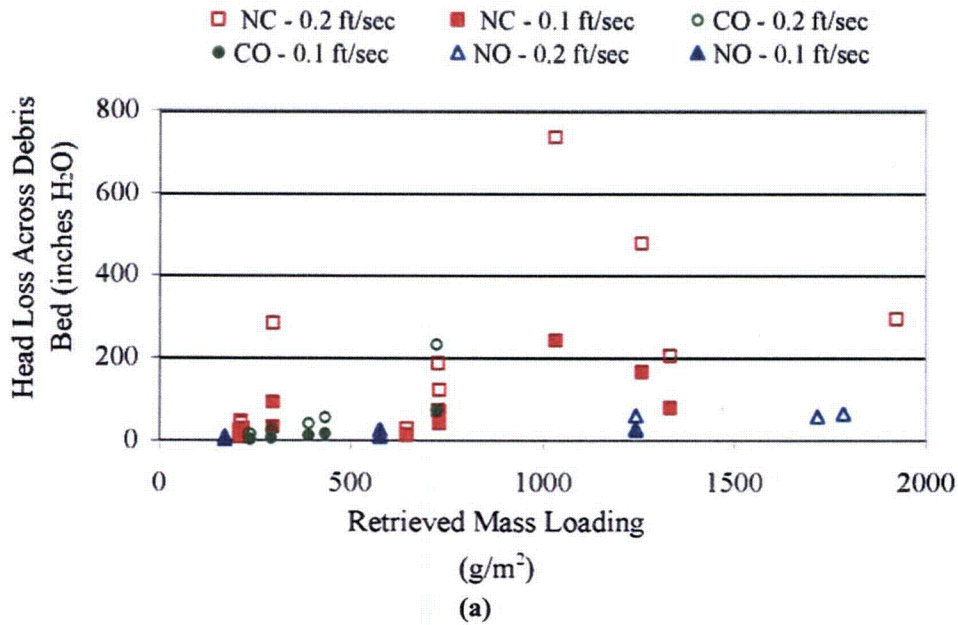


Figure 8.2. Pressure Drop Across the Debris as a Function of the Retrieved Mass Loading for NUKON-Only, CalSil-Only, and NUKON/CalSil (NC) Test Cases at Constant Velocities of 0.1 and 0.2 ft/sec. Test cases conducted at elevated fluid temperatures or with debris beds formed at elevated temperatures are excluded from the data. Figure 8.2a contains data from both Series 1 and 2 tests; Figure 8.2b contains only Series 2 data. Data taken from Tables 7.6, 7.10, 7.11, and 7.12 and Quick Look reports in Appendixes H, I, and J.

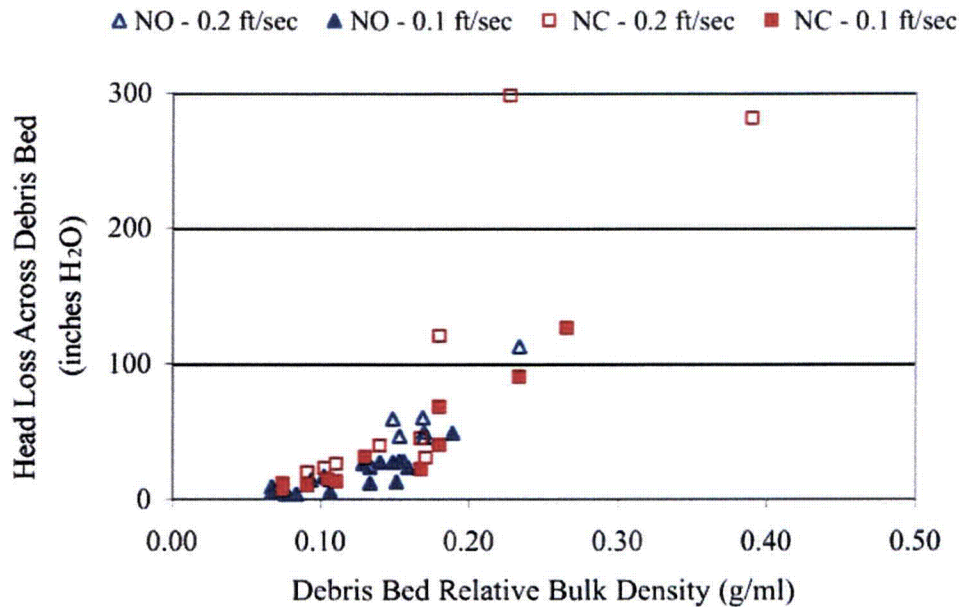


Figure 8.3. Pressure Drop Across the Debris Bed as a Function of the Debris Bed Relative Bulk Density for NUKON-Only and NUKON/CalSil Test Case at Constant Velocities of 0.1 and 0.2 ft/sec. Test cases conducted at elevated fluid temperatures or with debris beds formed at elevated temperatures are excluded from the data. The NUKON/CalSil Series 1 tests have not been included because no optical triangulation bed height measurements or associated densities exist. Data are from Tables 7.9 and 7.16 and the Quick Look reports in Appendixes I and J.

In Section 6.3, an example was provided to demonstrate that two debris beds of similar porosity (similar bulk density) could have significantly different flow resistances. However, these debris beds were generated using different load sequences. Based on the results of Sections 6.3, 7.2.1, 7.2.2, 7.4.4, and 7.4.5, it is postulated that, if two debris beds are formed with the same bed formation process, an increase in the relative density of the debris beds will correspond to an increase in the flow resistance.

The pressure drop measurements obtained from the two test scenarios used for the elevated temperature tests provided no indication of whether the fluid temperature had a significant effect on the formation of the debris bed. However, it is unclear whether subjecting the debris bed to an elevated temperature between 129° and 180°F (54° and 82°C) affects the CalSil content of the retrieved bed. Table 7.14 lists the percent of the target CalSil mass retained and the calculated retrieved CalSil mass loading for each of the Group 1 debris beds with a target NUKON mass loading of 217 g/m². Based on the results of Table 7.14, it appears that an increase in the CalSil-to-NUKON mass ratio reduced the mass of CalSil retained in the debris bed despite the target CalSil mass loading being higher.

The debris beds for NC4 and NC3 had CalSil-to-NUKON mass ratios of 0.25 and 0.50, respectively, and retained CalSil mass loadings of 26 and 49 g/m², respectively, which correspond to 48 and 46% of the target CalSil being retained. This compares to NC5, NC15, and NC16, which all had target CalSil-to-NUKON mass ratios of 0.75 and retained 11, 24, and 11 g/m² CalSil and 7, 15, and 7% of the target

CalSil, respectively. It has also been noted that the physical integrity (qualitatively assessed) of the retrieved NUKON/CalSil debris beds was observed to degrade with an increase in the CalSil mass loading. It is unclear whether this observed phenomenon is related to the ability of the debris material to form a debris bed.

However, the reduced retention of CalSil may be the result of testing at elevated fluid temperatures. The debris beds from NC5 and NC16 were subjected to a maximum fluid temperature of 180°F (82°C) and NC15 to a maximum fluid temperature of 129°F (54°C). The debris beds from NC3 and NC4 were only subjected to ambient temperature. Based on the Group 1 results, the higher the temperature, the lower the CalSil mass loading in the retrieved debris beds.

The debris bed from test condition NC17 was the other NUKON/CalSil bed subjected to an elevated temperature, 129°F (54°C). NC17 had a NUKON target mass loading of 724 g/m² and a target CalSil-to-NUKON mass ratio of 0.5. The same dramatic drop in retained CalSil was not observed for test condition NC17. This may be because the CalSil and NUKON mass loadings of NC17 were over twice and three times those of NC5, NC15, and NC16. The higher CalSil loading may result in a saturation level being reached, or the increased NUKON loading may counteract the reduction of CalSil at the elevated temperature by increasing the capture efficiency of the debris bed. The difference may also be due to the lower CalSil-to-NUKON mass ratio of 0.5. Due to the number of parameters in play, the limited number of test cases and limited ranges of parameters insufficient results were obtained to determine what caused the dramatic reduction in CalSil retention for test conditions NC5, NC15, and NC16.



9.0 Conclusions

To meet the objectives of this test program, PNNL fabricated large-scale and supporting benchtop test loops. A total 156 tests were conducted consisting of the following test conditions: 5 screen-only tests, 11 CalSil-only tests, 90 NUKON-only tests, 45 NUKON/CalSil tests, and 5 Coatings tests. Of the 156 tests, 43 were performed in the large-scale test loop, and 16 of those tests were conducted at elevated temperatures of 129° and 180°F (54° and 82°C). The large-scale tests were conducted in three series. The first series duplicated test conditions from the previous study conducted by LANL at the University of New Mexico (Shaffer et al. 2005).

All of the tests were conducted and completed according to documented test procedures. Test facility fabrication and operation was performed according to PNNL's Standards Based Management System. All safety, health, and environmental related requirements were satisfied in the execution of this test program, and no work-related injuries or instances of environmental impact occurred.

The following head loss data are provided for test cases with mass loadings on the order of 200 and 1300 g/m² for test cases of NUKON-only and NUKON/CalSil to provide a comparison of the differences observed between the two test conditions.

PNNL testing of NUKON-only debris beds with retrieved mass loadings of 171 and 1244 g/m² produced pressure drops of 0.3 psi (9 in. H₂O @ 68°F [23 cm H₂O @ 20°C]) and 2.2 psi (60 in. H₂O @ 68°F [152 cm H₂O @ 20°C]), respectively, at screen approach velocities of 0.2 ft/sec (0.06 m/s). Repeatable head loss measurements were obtained for the NUKON-only results. The flow history effects created slight increases in pressure drop with each velocity cycle, but these increases were observed in repeat tests. Good comparisons were also obtained between the pressure drop measurements from the large-scale and benchtop loops.

The NUKON/CalSil debris bed with a retrieved mass loading of 209 g/m² (containing 183 g/m² NUKON and 26 g/m² CalSil) and a screen approach velocity of 0.2 ft/sec (0.06 m/s) yielded a pressure drop of 0.8 psi (23 in. H₂O @ 68°F [58 cm H₂O @ 20°C]). For the CalSil/NUKON test cases, there were fewer opportunities to evaluate repeatability because the introduction of a target mass loading does not guarantee the same retained mass loading or ratio of constituents in the debris bed. To obtain a repeat case for a NUKON/CalSil debris bed, both the NUKON and CalSil mass loadings should be repeated. In addition, variations in the debris bed formation for cases of similar mass loadings can have significant effects on the resulting pressure drop. NUKON/CalSil debris beds having retrieved mass loadings of 1260 (926 g/m² NUKON and 334 g/m² CalSil [27 wt% CalSil]) and 1334 g/m² (991 g/m² NUKON and 343 g/m² CalSil [26 wt% CalSil]) produced pressure drops of 17.2 psi (477 in. H₂O @ 68°F [1212 cm H₂O @ 20°C]) and 7.3 psi (203 in. H₂O @ 68°F [516 cm H₂O @ 20°C]), respectively, at a screen approach velocity of 0.2 ft/sec.

Adjusting the debris loading procedure reduced variations in the results obtained for NUKON/CalSil debris beds and allowed comparable results in the benchtop loop to be obtained for various debris loading sequences. However, the CalSil content of the benchtop debris beds was not evaluated.

The work presented in Section 3 demonstrates that the debris preparation procedures yielded repeatable results. The R4 metric, while not quantifiable against other metrics used for debris characterization, provided a relative metric that allowed the debris preparation procedure to be adjusted, based on the debris concentration and the equipment being used, to yield prepared debris of similar consistency.

The particle size analysis conducted for CalSil debris demonstrated that similar particle size distributions were obtained over the range of CalSil concentrations prepared for introduction into the test loop.

The term complete is used to define debris beds that completely covered the screen and had no channeling through the debris bed. Debris beds that did not cover the entire screen or had channels (open flow passages) are referred to as incomplete. The appearance of the complete debris beds was uniform with a rim around the edge (at the wall of the test section) representative of what is expected for material deposited from a uniform steady pipe flow. The complete debris beds filled the entire cross-sectional area of the test section, with no gaps for flow to bypass the debris bed.

The increase in static pressure applied to the large-scale loop with the cover gas pressure maintained gas in solution with increases in the pressure drop across the debris bed. Therefore, the pressure drops measured in the large-scale loop are for two-phase (liquid and solids) flow with no gas present.

The in situ debris bed height measurements obtained with the optical triangulation system demonstrated that debris beds continued to compress and relax with changes in the screen approach velocity. The center height of a debris bed was observed to change typically on the order of 30% for an order of magnitude change in the screen approach velocity (0.2 to 0.02 ft/sec) with changes in bed height as much as 80% for some cases.

Post-test filtration and inspections of the test loop indicated that negligible amounts of NUKON and CalSil debris were left in the test loop. Test observations indicate that debris material was being held up within the loop during portions of the test. However, the peak flow rates appeared to be sufficient to transport the debris material within the test loop. The peak flow rates used during testing did not appear to be high enough to fully mobilize and transport all of the coatings materials.

The minimum retrieved mass loading obtained for a complete large-scale NUKON debris bed was 171 g/m^2 on the perforated plate, which was created with a target mass loading of 217 g/m^2 . In the bench-top loop, complete debris beds were formed on the 5-mesh screen with target mass loadings of 107 g/m^2 , which yielded retrieved mass loadings of 56 and 102 g/m^2 . The minimum retrieved mass loading that formed a complete NUKON/CalSil debris bed was 160 g/m^2 on the perforated plate, which was calculated to have a NUKON mass loading of 149 g/m^2 . This was the smallest NUKON mass loading obtained for any complete debris bed generated in the large-scale loop. NUKON/CalSil tests conducted with NUKON target debris loadings of 108 g/m^2 and target CalSil loadings of 27 and 135 g/m^2 failed to generate complete debris beds. Testing was not performed to determine the minimum mass loading at which debris beds could be formed.

Visual observations of the retrieved debris beds noted that the NUKON-only debris beds were very durable—they could be removed from the test screen and handled. However, for the same NUKON mass loading, the addition of CalSil debris appeared to reduce the durability or the physical integrity of the retrieved debris bed. It is unknown whether this observation has any relevance to the conditions

necessary to generate a complete debris bed. Similar target NUKON mass loadings for NUKON-only test conditions that generated complete debris beds were not adequate to form complete debris beds when additional CalSil mass was mixed with the NUKON prior to introduction into the loop for the NUKON/CalSil test cases.

PNNL CalSil-only tests with CalSil target mass loadings ranging from 1450 to 4350 g/m² yielded incomplete debris beds with retrieved mass loadings from 79 to 724 g/m². No complete CalSil-only debris beds were generated during this test program. All of the CalSil-only debris beds that were undisturbed during the retrieval process only retained from 10 to 17% of the target debris loading. The results of the CalSil-only and NUKON/CalSil tests indicate sufficient NUKON mass loading is necessary for a complete debris bed to be formed. The test plan was not designed to determine the minimum NUKON mass loading required for bed formation, nor could it be ascertained from the completed test matrix.

The results presented in Sections 3 and 6 demonstrate that the debris preparation procedure strongly influenced the resulting pressure drop across the debris bed. Other parameters shown to influence the head loss across the debris bed for a given retrieved mass loading include:

- The sequence in which debris material is loaded onto the screen. The loading sequence investigation and Series 1 NUKON/CalSil tests demonstrated that, for the same mass loading, the sequence in which the debris material was loaded on the screen could change the resulting head loss by more than an order of magnitude. The higher pressure drops were not fully quantified because they exceeded the limits of the instrumentation for both test loops and the pump capacity of the benchtop loop.

The debris loading sequence influenced multiple-constituent debris bed as well as the single-constituent beds. The CalSil-only test cases, COBT3 and COBT4, had the same target mass loading; however, the bulk loading in COBT4 (single introduction of debris) resulted in approximately 50% more mass being retained than the incremental loading of COBT3.

- The screen approach velocity used during debris bed formation. It is unclear how much of the influence of bed formation velocity is an artifact of test loop geometry. It has been postulated that if holdup or settling of debris occurs within the test loop during the test, the effect on the measured pressure drop may be as much as that of a change in the debris loading sequence due to segregation of material. All changes in the bed formation velocity may not result in a change in the measured pressure drops. A notable impact would occur if velocities within the test loop dropped below a critical velocity for transport or mobilization for the size range of a debris constituent.
- The flow history to which the debris bed has been subjected. The parameters contributing to the flow history include the magnitude of the screen approach velocity, the duration for which the debris bed is subjected to a flow condition, and the cycling or history of the screen approach velocity. The flow history contributes to changes in the debris bed structure. For the tested conditions the greatest impact appears to be that caused by cycling of the screen approach velocity.

It is postulated that the relaxing and contracting of the debris bed allows material to migrate through the bed. Some of the migrating debris may be released from the debris bed, circulate through the loop, and be recaptured by the debris bed. The migration of material could allow the debris bed to reorganize in a way which increases flow resistance. The migrating particulate would continue to pass through the debris bed until the flow carried individual particles to locations where they were

completely trapped despite relaxation of the debris bed. The returning particulate will enter the debris bed at points of preferential flow. As more and more material becomes permanently trapped within the debris bed, the head loss increases.

- The initial target mass loading. The initial target mass loading may impact the results in two ways. The absolute mass of material in the flow determines the amount of material present for a given size range. A critical size may exist for retention, and all smaller material may continue to pass through the debris bed with the flow or migrate through the bed with some critical holdup. The effects of the target mass could also impact the formation of the debris bed based on the effect of the concentration of debris material in the flow. The same target mass loadings may yield different results depending on the concentration of the debris approaching the screen. While the target mass loading appears to affect the results, it is unknown which phenomenon has the most significant effect.

The in situ bed height measurements obtained from optical triangulation allowed the relative bulk density of the debris beds to be calculated. The calculated density is associated with the bulk porosity of the debris bed and can be used to compare test cases and test conditions because the structure of the debris bed appears to change with changes in the screen approach velocity. The bulk density is not a controllable parameter but is a result of the bed formation process, flow history, and mass loading. The head loss for both the NUKON and NUKON/CalSil debris beds formed at ambient fluid temperature with a constant screen approach velocity of 0.1 ft/sec (0.03 m/s) increased with an increase in the relative bulk density. The trend also appeared to hold when NUKON-only and NUKON/CalSil beds were compared. The NUKON/CalSil debris beds tended to form debris beds with larger relative bulk densities. Over the entire range of Series 2 testing the trend appears to hold. The comparison could only be made for debris beds with in situ bed height measurements obtained from optical triangulation.

In most instances, an increase in fluid temperature (decrease in fluid viscosity) resulted in a decrease in pressure drop across the debris beds. The results were affected by the flow history applied to the debris beds during the time required to change the fluid temperature in the test loop. For cases where an increase in fluid temperature resulted in an increase in pressure drop, the discrepancy was explained by an increase in the relative bulk density of the debris bed.

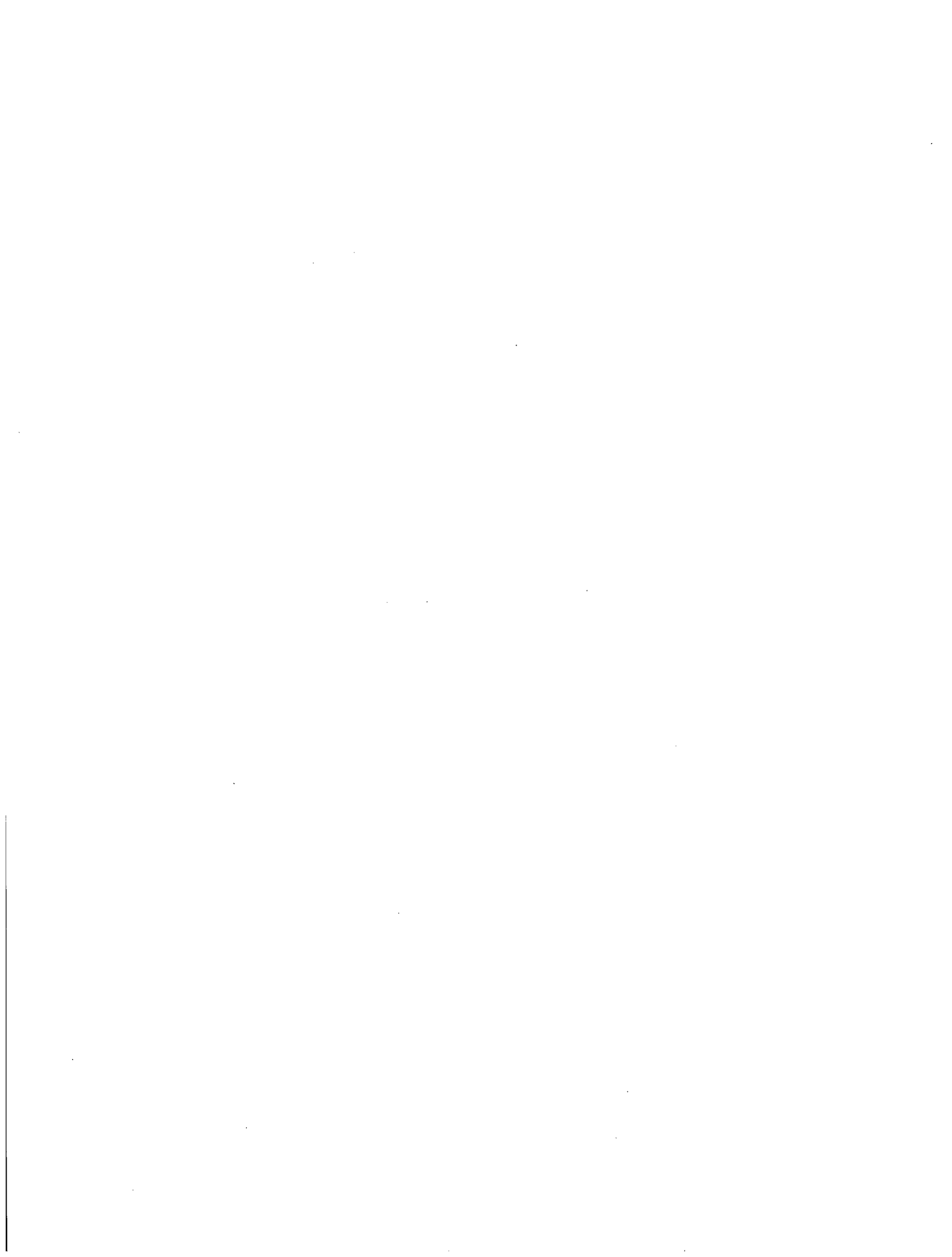
Two NUKON/CalSil debris beds from the benchtop loop that were formed on the 5-mesh woven screen using different debris loading sequences were sectioned and examined using SEM. The SEM analysis identified three distinct layers within the debris beds: a surface CalSil layer, a center porous region, and the bottom wire support region. The uniform surface layer consisted mostly of CalSil particulate supported by NUKON fiber and comprised 6 and 19% of the total post-test debris bed heights for the two cases; however, the compressibility of the individual layers under flow is unknown. The volume percent of CalSil in the surface layer was calculated to be 59 and 64 vol%, and the NUKON fiber concentration was 6.5 and 5.5 vol% for the two beds, respectively.

The center region was very porous and uniform with elevation. The center layer of the two debris beds consisted of NUKON fiber concentrations of 6.1 and 8.3 vol% and CalSil concentrations of 1.4 and 1.9 vol%, respectively. The center porous region comprised approximately 93 and 81% of the total bed heights for the two cases. The cylindrical NUKON fibers ranged in diameter from 5 to 15 microns as determined from the SEM analysis.

The bare perforated plate had a higher flow resistance than the 5-mesh woven wire screen. At a screen approach velocity of 2.0 ft/sec (0.6 m/s), the pressure drop across the perforated plate and 5-mesh screen were 3.7 in. H₂O @ 68°F (9.4 cm H₂O @ 20°C) and 2.3 in. H₂O @ 68°F (5.8 cm H₂O @ 20°C), respectively. No noticeable differences in the head loss measurements were obtained between tests conducted with the perforated plate and 5-mesh screen. However, some differences were observed in how the debris material interacted with the two screen materials. The debris material was more likely to become entangled with the woven wire of the 5-mesh screen so that it was not just resting on the screen but engulfed parts of the wire mesh. Some material was extruded through the holes of the perforated plate, but the degree of entanglement was much less. Removing the debris beds from the perforated plate was easier than removal from the woven wire.

For the limited Coatings test series, the results indicated:

- For the same target mass loadings and debris preparation processes, ALK debris tended to form a more substantial debris bed than ZE material.
- To obtain retrieved mass loadings that are comparable between the ALK and ZE debris, the Coatings tests should be conducted with larger target mass loadings than were used in this test program.
- The structure of the coatings debris resulted in larger retrieved mass loadings being required to obtain pressure drops similar to those obtained in the CalSil and NUKON debris beds.



10.0 References

- Bonaca MV. October 18, 2004. *Safety Evaluation of the Industry Guidelines Related to Pressurized Water Reactor Sump Performance*. ACRSR-2097, U.S. Nuclear Regulatory Commission Advisory Committee on Reactor Safeguards, Washington, D.C.
- Brinkman KW and PW Brady. May 1994. *Results of Hydraulic Tests on ECCS Strainer Blockage and Material Transport in a BWR Suppression Pool*. EC-059-1006 Rev. 0, Pennsylvania Power & Light, Allentown, Pennsylvania.
- European Nuclear Society (ENS). September 18, 1992. 'Swedish N-Utilities Explain BWR Emergency Core Cooling Problem.' No. 358/92, ENS Nuclear News Network, <http://www.nuclearenergynews.com>.
- Kasza K, JH Park, B Fisher, J Oras, K Natesan, and WJ Shack. 2006. *Chemical Effects Head-Loss Research in Support of Generic Safety Issue 191*. NUREG/CR-6913, U.S. Nuclear Regulatory Commission, Washington D.C.
- Konstandopoulos AG. March 2000. *Fundamental Studies of Diesel Particulate Filters: Transient Loading, Regeneration and Aging*. 2000-01-1016. SAE 2000 World Congress, Detroit Michigan, SAE International, Warrendale, Pennsylvania.
- Krotiuk WJ. 2006. *Development of Pressure Drop Calculation Method for Debris-Covered Sump Screens in Support of Generic Safety Issue 191*. NUREG-1862, U.S. Nuclear Regulatory Commission, Washington D.C.
- Merkel GA, WA Cutler, T Tao, A Chiffey, P Phillips, MV Twigg, and A Walker. 2003. "New Cordierite Diesel Particulate Filters for Catalyzed and non-Catalyzed Applications." *Proceedings of the 9th Diesel Engine Emissions Reduction Conference*, Newport, Rhode Island.
- Mizuno T and J Suzuki. 2004. "Development of a New DPNR Catalyst." 2004-01-0578, *SAE 2004 World Congress*, Detroit, Michigan.
- NRC March 2006, *Head Loss Testing*. Office of Nuclear Regulatory Research Division of Engineering Technology Modification to Statement of Work, JCN: N6106.
- Perry Nuclear Power Plant (PNPP). May 1993. "Excessive Strainer Differential Pressure Across the RHR Suction Strainer Could Have Compromised Long-Term Cooling During Post-LOCA Operation." Licensee Event Report 93-011, docket 50-440. Perry Nuclear Power Plant, Cleveland, Ohio.
- Rao DV and F Souto. June 1995. *Experimental Study of Head Loss and Filtration for LOCA Debris*. NUREG/CR-6367 (SEA Report No. 554-06-A.8), Science and Engineering Associates, Inc., Albuquerque, New Mexico.
- Shaffer CJ, MT Leonard, BC Letellier, DV Rao, WA Roesch, JD Madrid, AK Maji, K Howe, A Ghosh, and J Garcia. May 2005. *GSI-191: Experimental Studies of Loss-of Coolant Accident-Generated Debris Accumulation and Head Loss with Emphasis on the Effects of Calcium Silicate Insulation*. NUREG/CR-6874, U.S. Nuclear Regulatory Commission, Washington D.C.

U.S. Nuclear Regulatory Commission (NRC). 1996. *Generic Safety Issue (GSI) 191, Potential Impacts of Debris Blockage on Emergency Recirculation During Design-Basis Accidents at PWRs*. U.S. NRC, Washington, D.C.

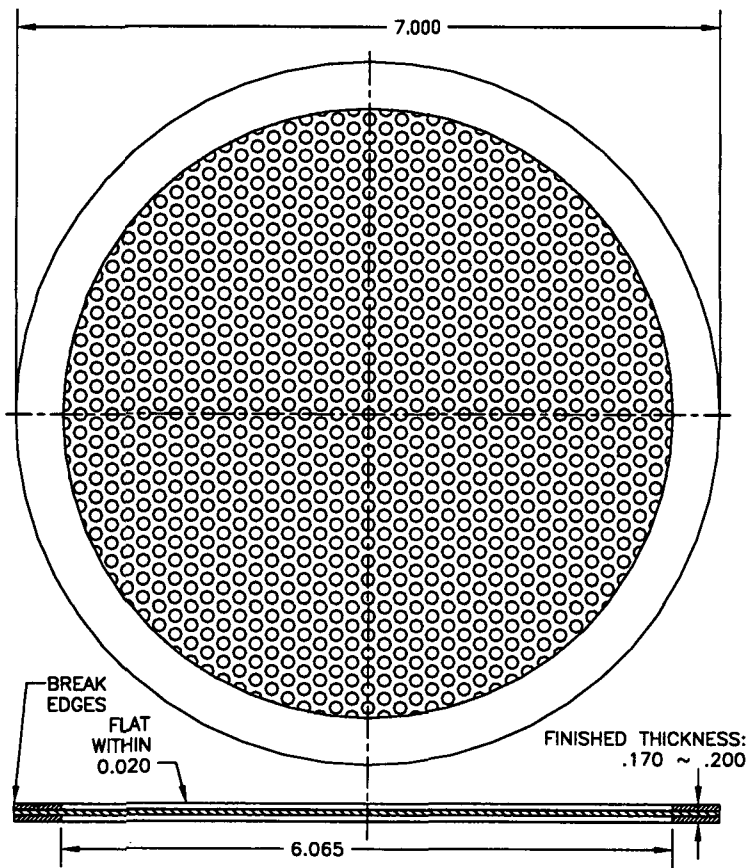
Weast RC (editor). 1975. *Handbook of Chemistry and Physics*. CRC Press. Cleveland, Ohio.

Zigler G, J Brideau, DV Rao, CJ Shaffer, F Souto, and W Thomas. 1995. *Parametric Study of the Potential for BWR ECCS Strainer Blockage Due to LOCA Generated Debris*. NUREG/CR-6224, U.S. Nuclear Regulatory Commission, Washington, D.C.

Appendix A – Test Screens



Appendix A – Test Screens



SCREEN FAB. PROCESS:

1. CUT TWO 304 S.ST. RINGS, 7.00 O.D., 6.025 I.D., .063 T.*
2. CUT A CIRCLE OF PERFORATED METAL, AS PROVIDED, SLIGHTLY LARGER THAN 7.0 O.D.*
3. CLAMP RINGS SNUGLY OVER PERFORATED METAL.
4. SPOT WELD RINGS AND PERFORATED METAL TOGETHER.
5. TRIM EXTRA PERFORATED METAL FROM O.D. OF RINGS.
6. WELD BEAD AROUND RINGS & PERFORATED METAL'S PERIPHERY.
7. TRIM O.D. ON LATHE TO 7.000 +.000 /-.010, CONCENTRIC TO RING I.D.
8. BREAK OUTSIDE EDGES.

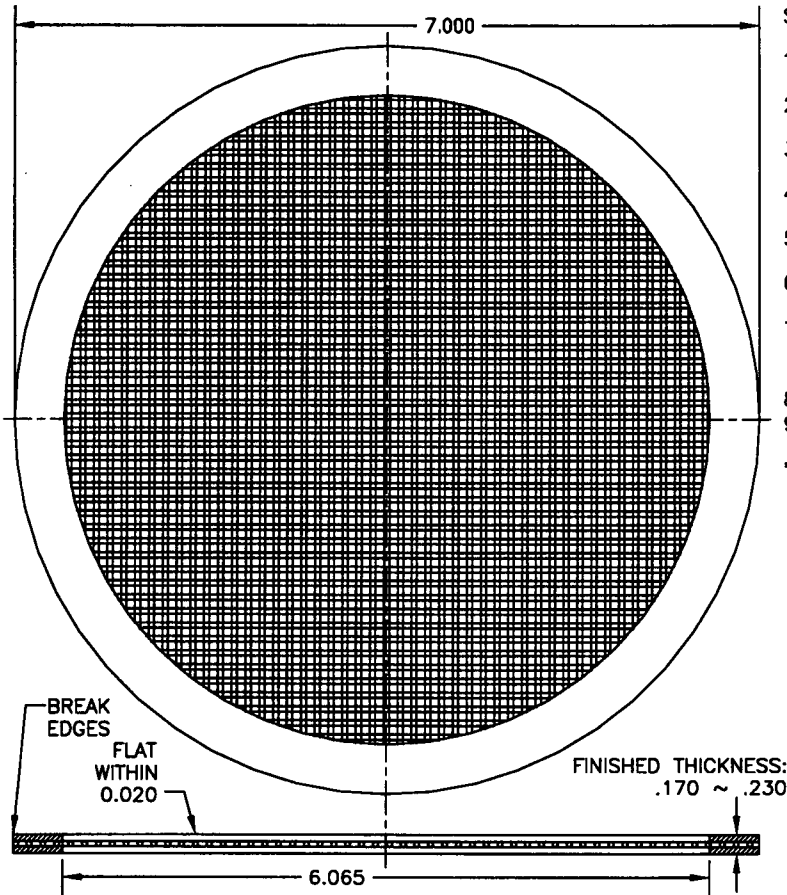
* ABRASIVE WATER JET CUTTING SUGGESTED

TOLERANCES

- 2 PLACE DEC ± .01
- 3 PLACE DEC ± .003
- ANGLES ± 1°
- WITHIN .01 TIR

SCREEN, PERFORATED
METAL VERSION

Figure A.1.1. Perforated Metal Test Screen



SCREEN FAB. PROCESS:

1. CUT TWO 304 S.ST. RINGS, 7.00 O.D., 6.025 I.D., .063 T.*
2. CUT A CIRCLE OF WIRE CLOTH, AS PROVIDED, 7.000 O.D.*
3. CLAMP RINGS LIGHTLY OVER SCREEN.
4. SPOT WELD RINGS AND SCREEN TOGETHER.
5. TRIM EXTRA SCREEN FROM O.D. OF RINGS.
6. WELD BEAD AROUND RINGS & SCREEN'S PERIPHERY.
7. TRIM O.D. ON LATHE TO 7.000, CONCENTRIC TO RING I.D. +.000/- .010.
8. BREAK OUTSIDE EDGES.
9. HEAT/PRESS FLATTEN AS REQUIRED.

* ABRASIVE WATER JET CUTTING SUGGESTED

TOLERANCES

2 PLACE DEC $\pm .01$

3 PLACE DEC $\pm .003$

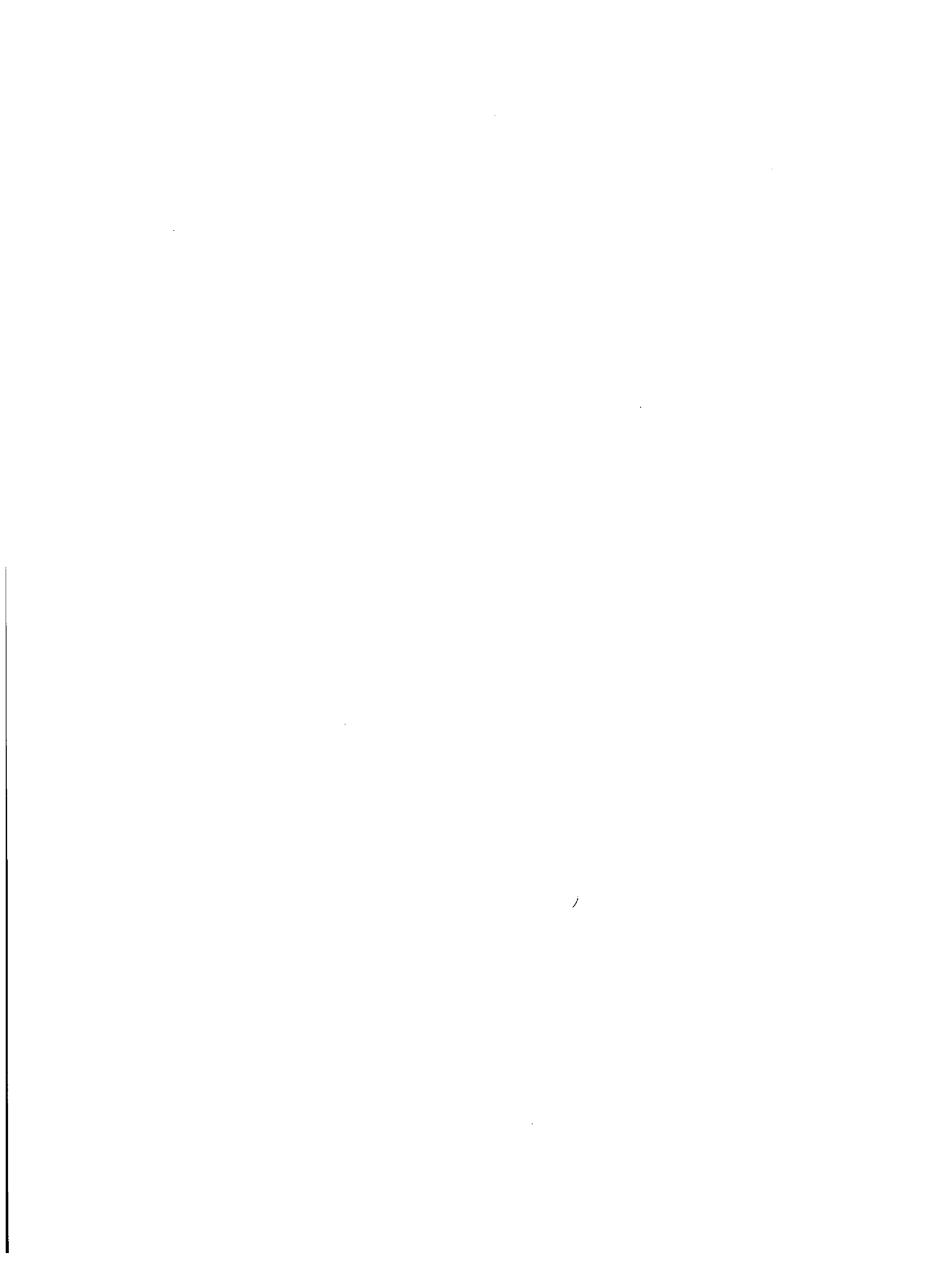
ANGLES $\pm 1^\circ$

○ WITHIN .01 TIR

SCREEN, WIRE CLOTH VERSION

Figure A.1.2. Wire Cloth Test Screen

Appendix B – Drawings



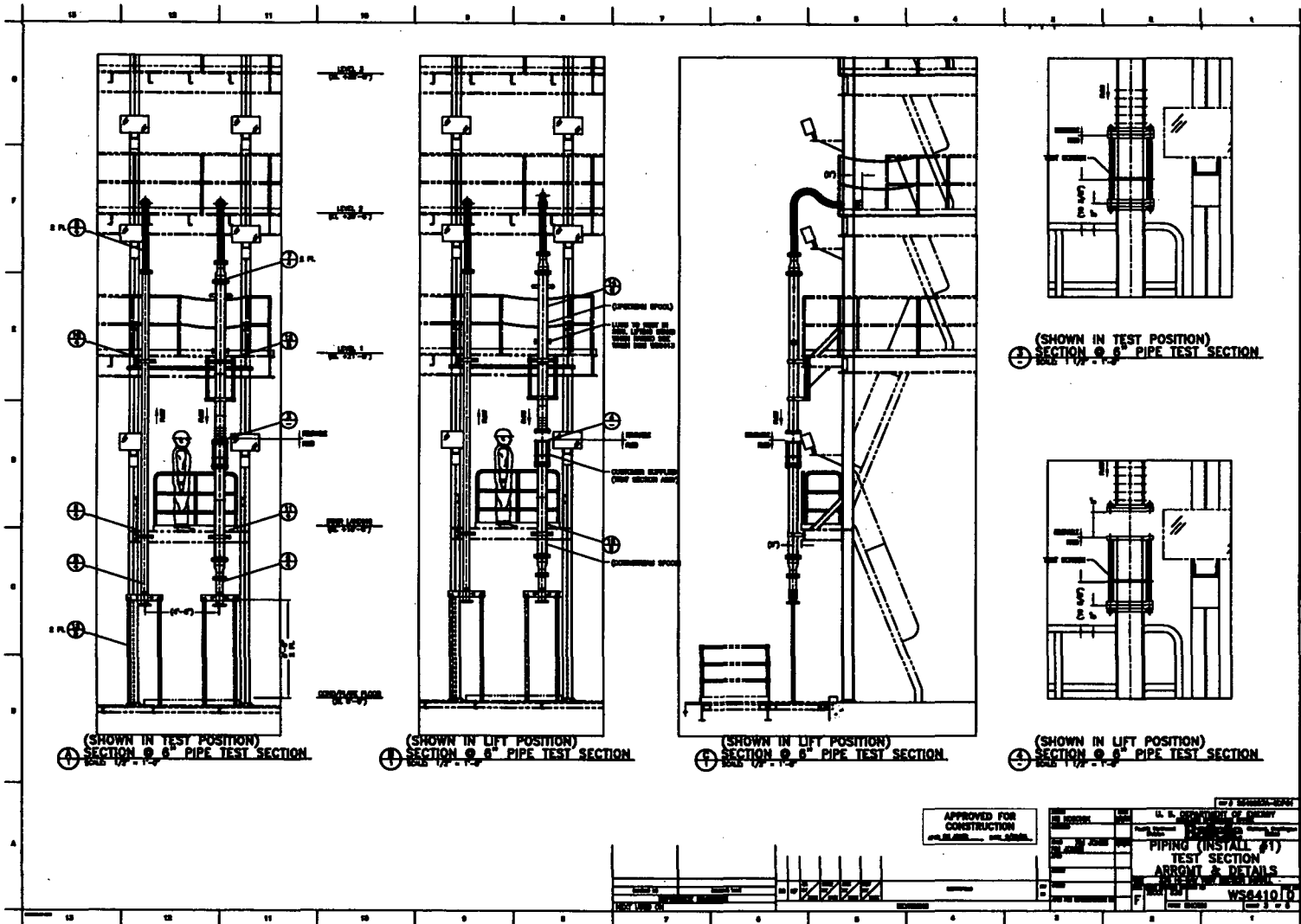


Figure B.1.3. Piping in Test Section

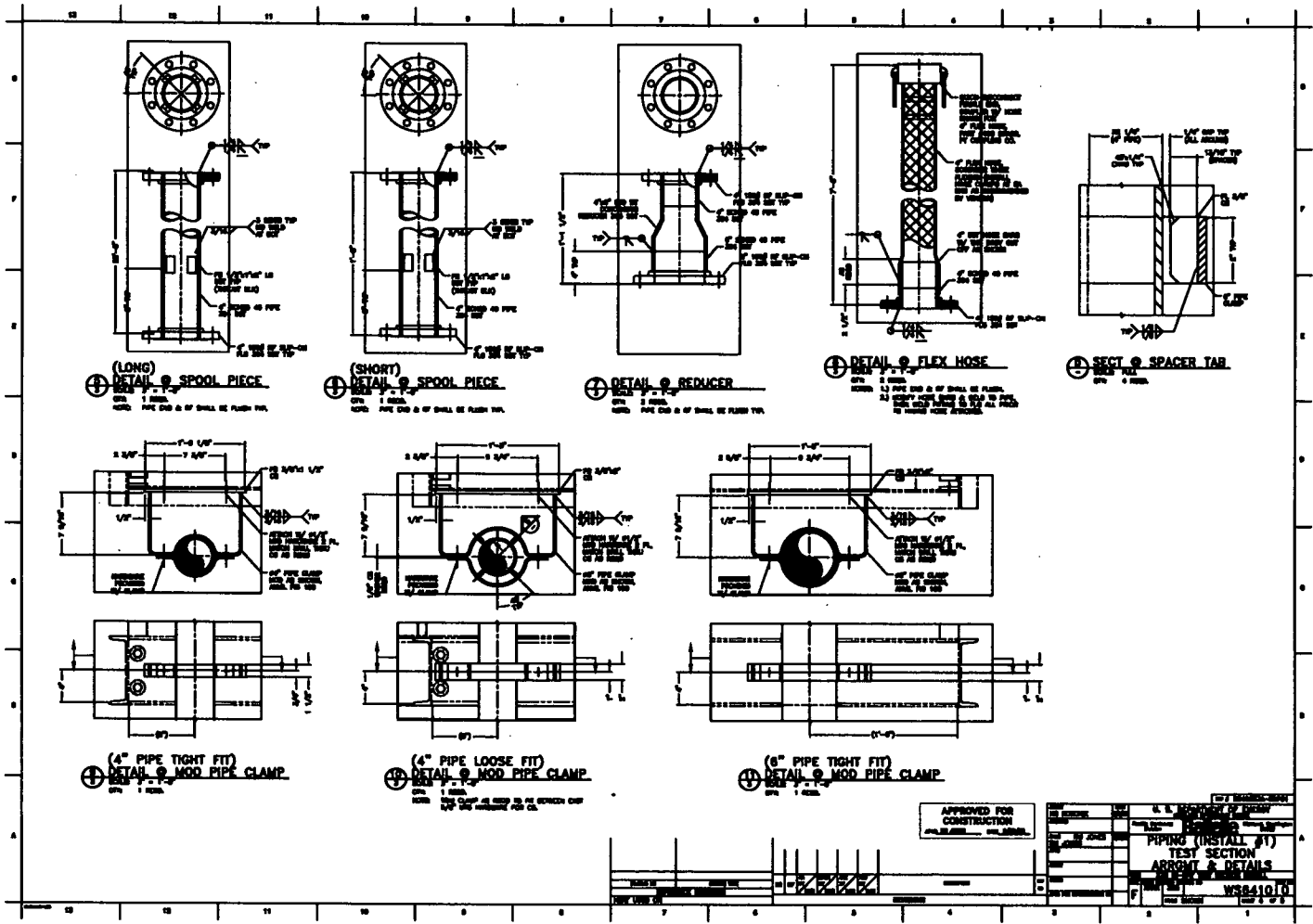


Figure B.1.4. Piping Detail

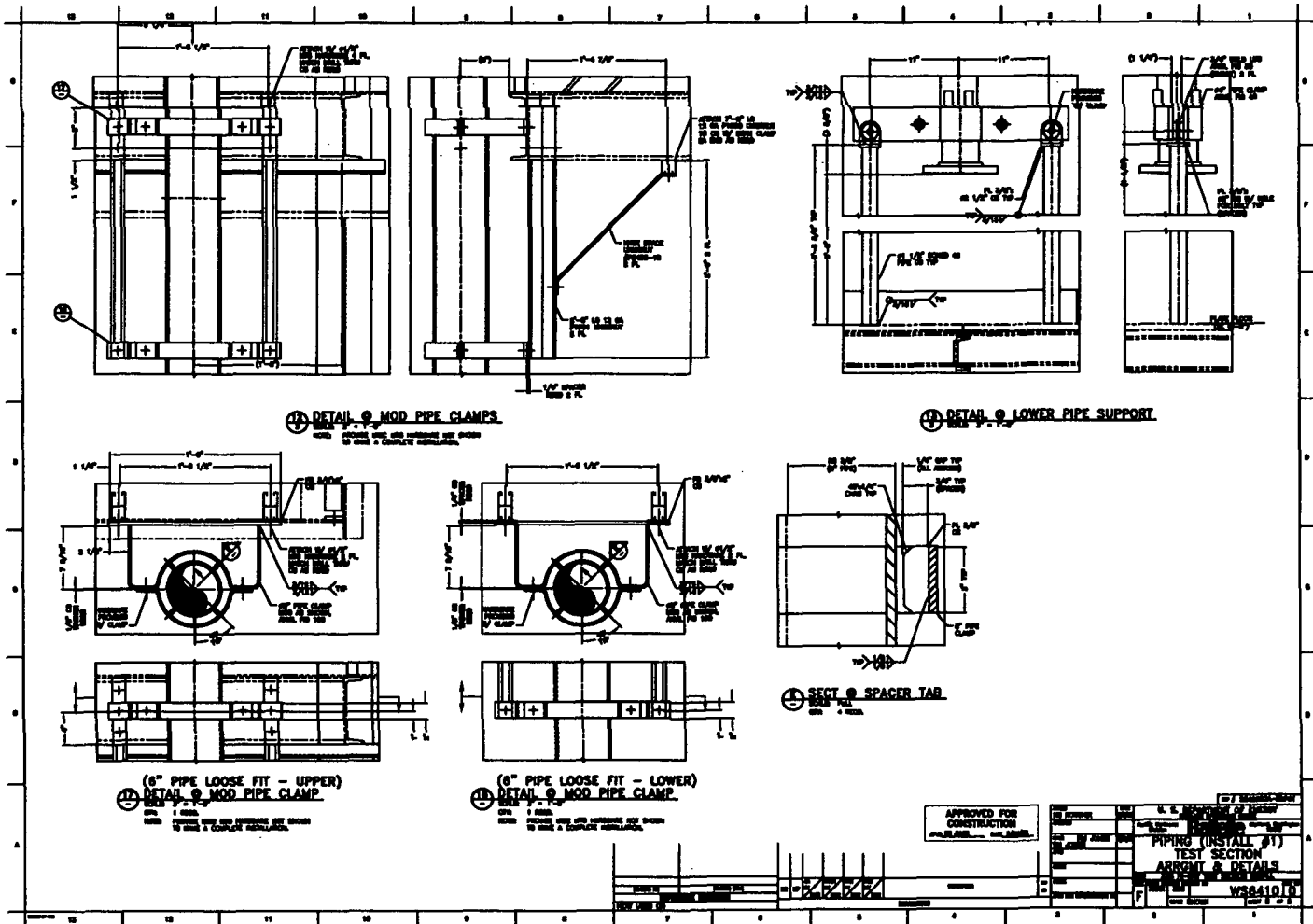


Figure B.1.5. Piping Arrangement and Detail

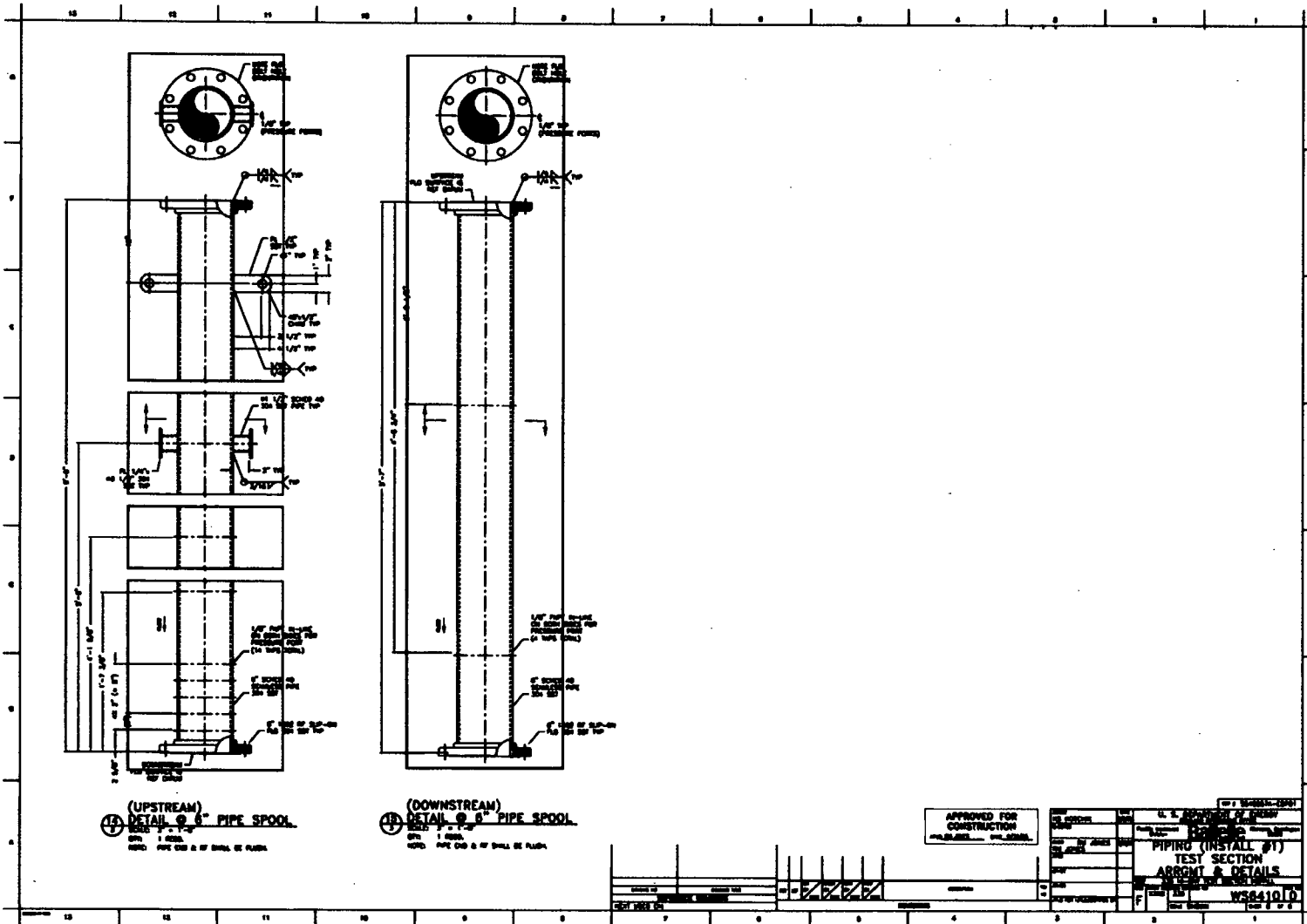


Figure B.1.6. Piping Arrangement and Detail

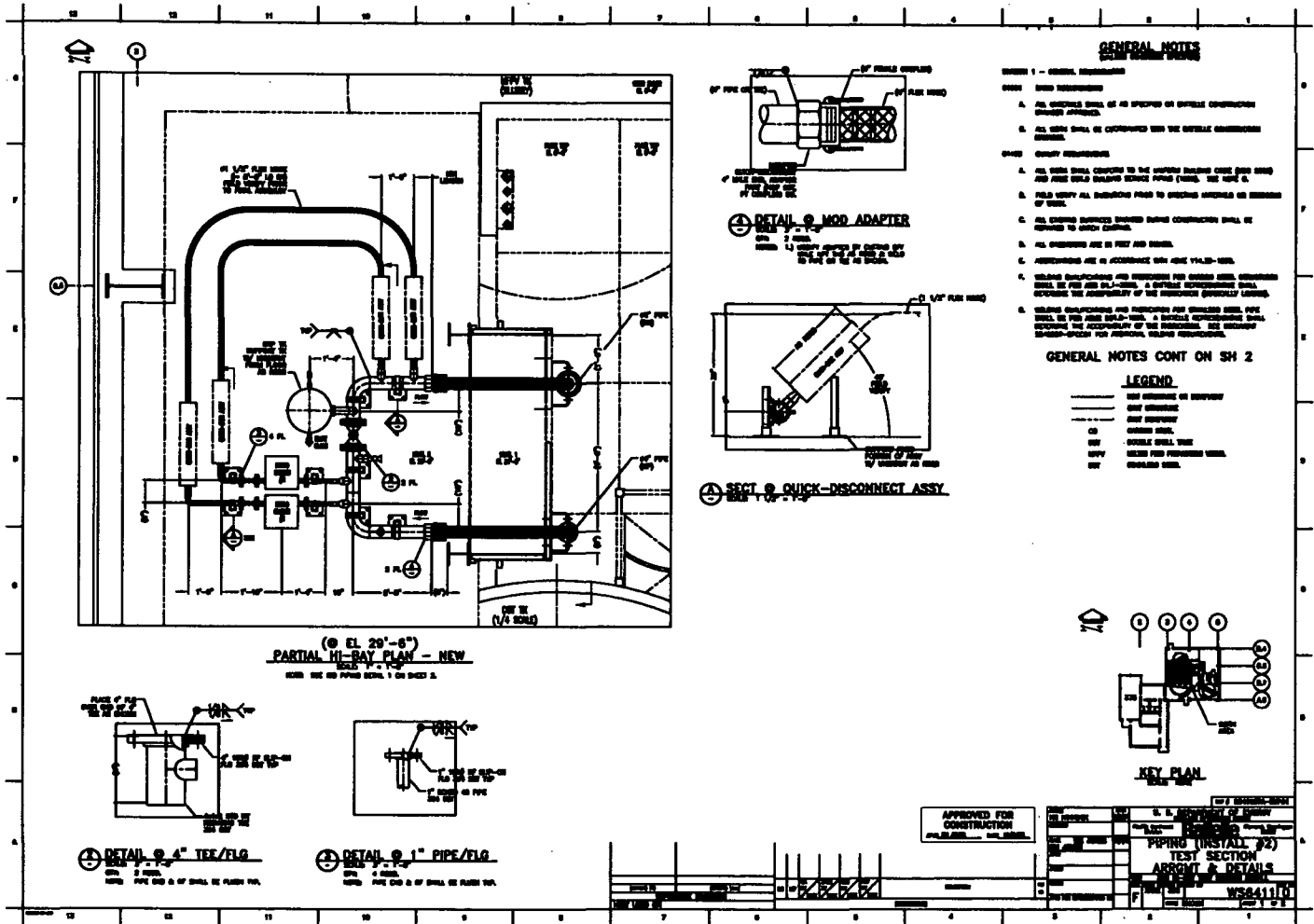


Figure B.1.7. Piping Arrangement and Detail

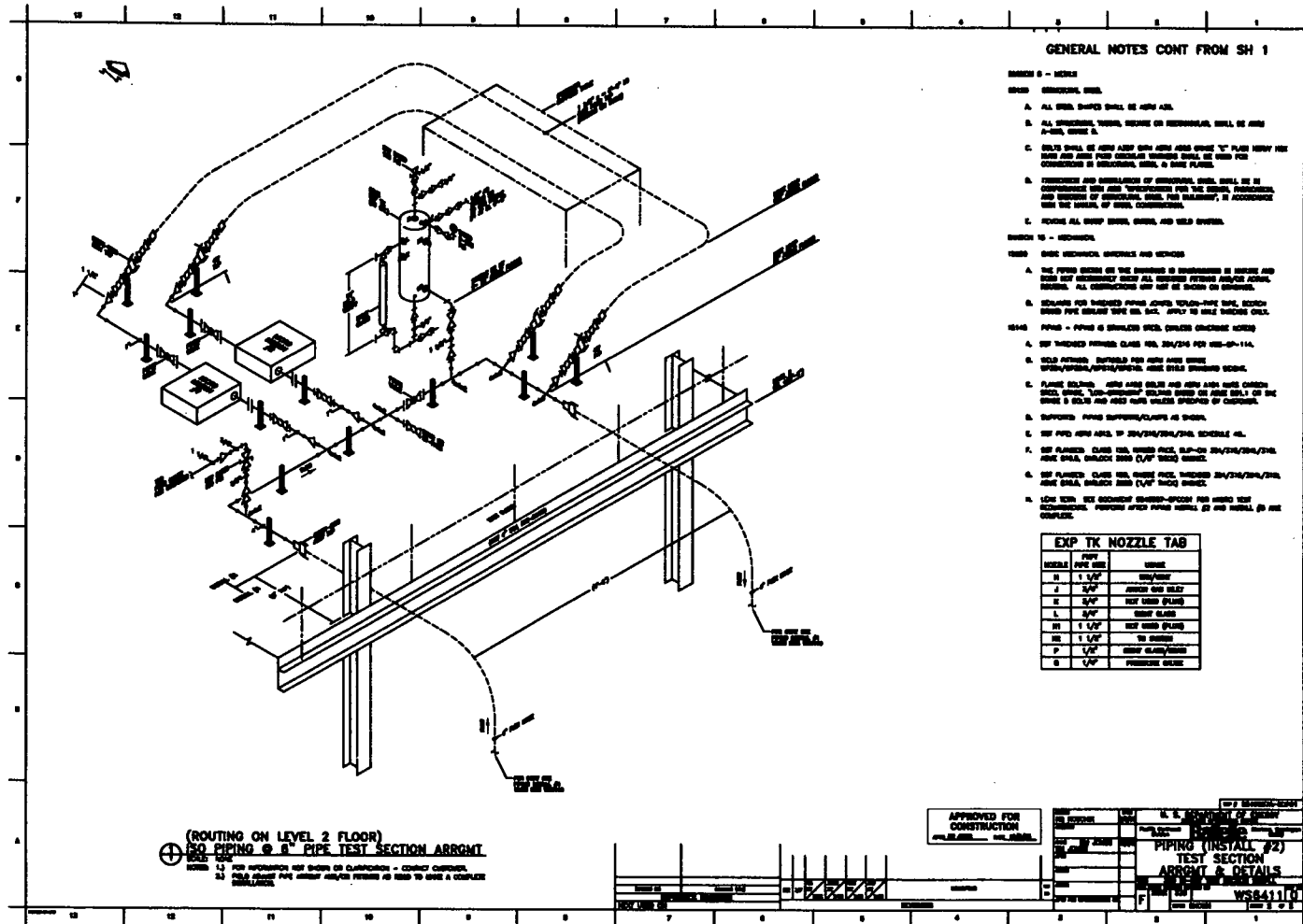


Figure B.1.8. Piping Arrangement and Detail

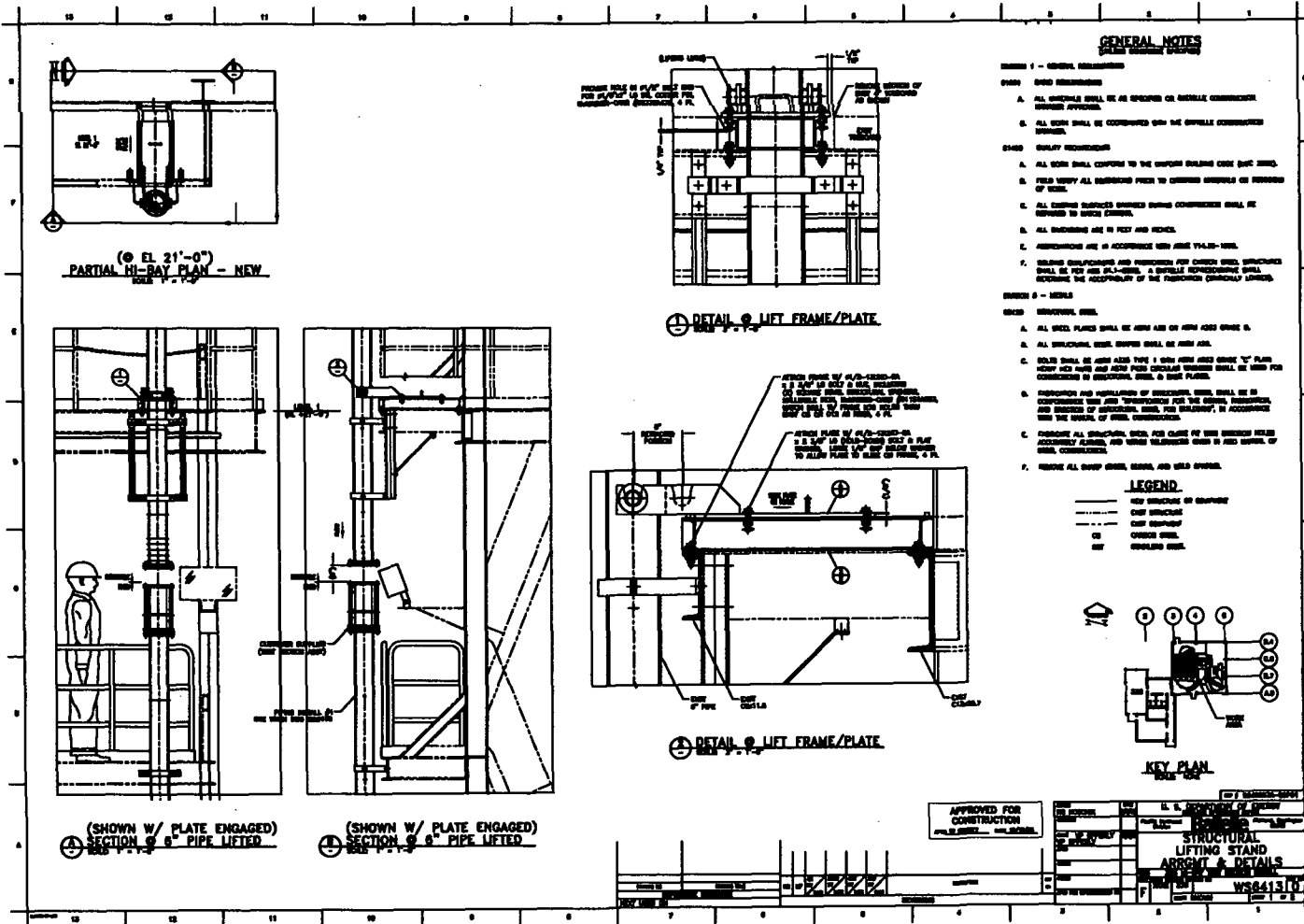


Figure B.1.10. Structural Lifting Stand

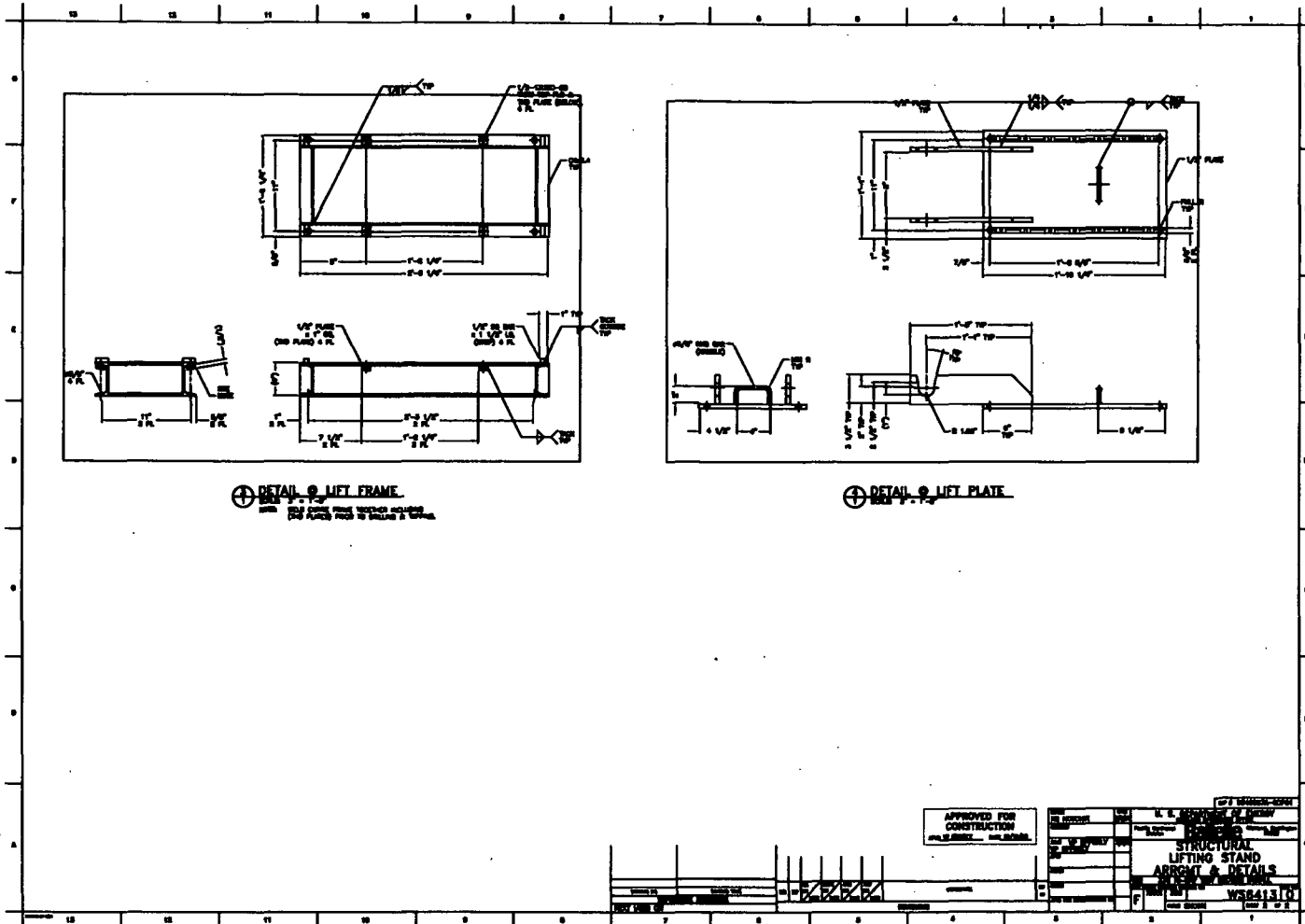
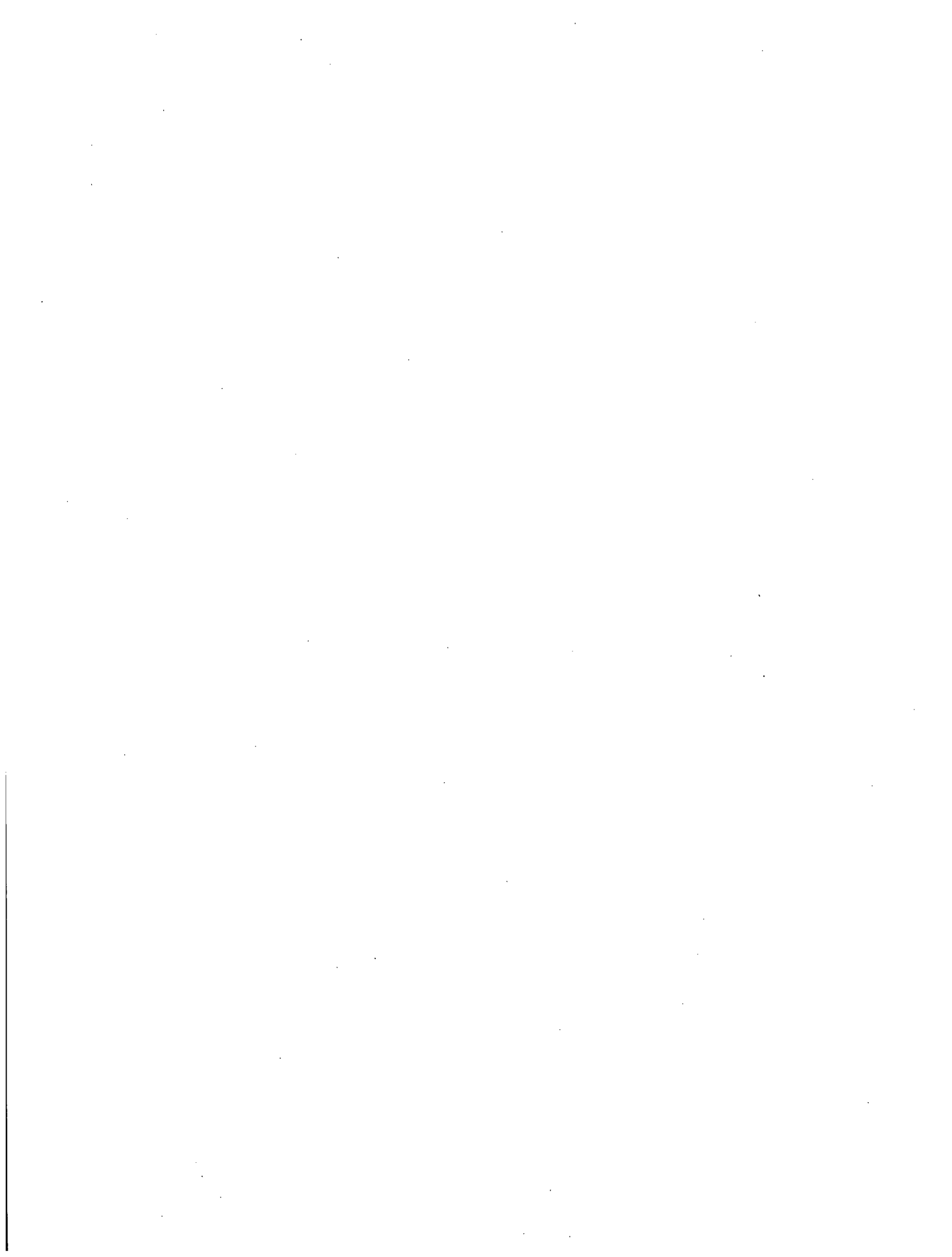


Figure B.1.11. Structural Lifting Stand Detail



Appendix C – Test Loop Measurement and Equipment Listing



Appendix C – Test Loop Measurement and Equipment Listing

Table C.1.1. Large-Scale Test Loop Measurement and Test Equipment Listing

Instruments Connected to Data Acquisition System																	
Parameter	Subsystem	Ch.	Unit	Range	Sensor	Serial No.	Type	Cal. #/ Bar Code	Cal. Due	Transmitter	Serial No.	Signal	5B Module	Series	Par.	Loop Pwr	Transmitter Uncertainty
CMF100 Q	Debris inj. 1	16	kg/s	0-1.5	Micro Motion CMF100 ^(a)	404399	Coriolis	NA	NA	MM 9739	7082246	4-20mA	5B32-02	250	20	Xmtr.	0.1% of rate
CMF100 SG	Debris inj. 1	17	S.G.	0.9-1.5	"	404399	Coriolis	NA	NA	"	7082246	"	5B32-02	NA	20	Xmtr.	0.5% of S.G.
CMF100 Q	Debris inj. 2	19	kg/s	0-1.5	Micro Motion CMF100 ^(a)	404247	Coriolis	NA	NA	"	7091995	4-20mA	5B32-02	250	20	Xmtr.	0.1% of rate
CMF100 SG	Debris inj. 2	20	S.G.	0.9-1.5	"	404247	Coriolis	NA	NA	"	7091995	"	5B32-02	NA	20	Xmtr.	0.5% of S.G.
CMF300 Q	Hi loop flow	22	kg/s	0-15	Micro Motion CMF300 ^(a)	310803	Coriolis	NA	NA	"	?	4-20mA	5B32-02	250	20	Xmtr.	0.1% of rate
CMF300 SG	Hi loop flow	23	SG	0.9-1.5	"	310803	Coriolis	NA	NA	"	?	"	5B32-02	NA	20	Xmtr.	0.5% of S.G.
Line Press.	Lo loop flow	28	PSIG	0-200	Ametek 88F005A2CSSM	40173-1-18	S.G. diaph.	20951	10/27/2006	-	-	4-20mA	5B32-02	NA	20	Loop	0.25% of range
D.P. 1	Test sect.	29	in. H ₂ O	0-5	Rosemount 115-1DR2F120495	1800790	S.G. diaph.	20948	10/27/2006	Integral	1800790	4-20mA	5B32-02	NA	20	Loop	0.5% of range
D.P. 2	Test sect.	30	in. H ₂ O	0-30	Rosemount 115-1DP23E22B2	315882	S.G. diaph.	20950	10/27/2006	Integral	315882	4-20mA	5B32-02	NA	20	Loop	0.25% of range
D.P. 3	Test sect.	31	in. H ₂ O	0-150	Rosemount 115-1DP43E22B2	266332	S.G. diaph.	20947	10/27/2006	Integral	266332	4-20mA	5B32-02	NA	20	Loop	0.25% of range
D.P. 4	Test sect.	32	in. H ₂ O	0-750	Rosemount 115-1DP63E22B3 ^(b)	252749	S.G. diaph.	20949	11/22/2006	Integral	252749	4-20mA	5B32-02	NA	20	Loop	0.25% of range
RTD 1	Loop, upper	33	°C	0-100	Reotemp BX1FAPX1251114X-Q	0443.557012	RTD	21302	Not Calc.	Integral	(same)	4-20mA	5B32-02	NA	20	Loop	0.27°C
T/C 1	Upstairs ambient	35	°C	-100-300	Type J thermocouple	NA	TC	19798	10/4/2005	NA	NA	TC input	5B47J-02	NA	NA	NA	2.2°C
T/C 2	Loop, lower	36	°C	-100-300	Type J thermocouple	NA	TC	NA	10/4/2005	NA	NA	TC input	5B47J-02	NA	NA	NA	2.2°C
T/C 3	D.P. manifold	37	°C	-100-300	Type J thermocouple	NA	TC	19807	10/4/2005	NA	NA	TC input	5B47J-02	NA	NA	NA	2.2°C
Data Acquisition System																	
Hardware:	PC:	Dell Optiplex GX280															
	Board:	Measurement Computing PCI-DAS6402-16															
	Sig. Cond.:	5B modules as tabulated															
Software:	Windows XP Professional																
	DasyLAB 7																
Configuration:	Sample Rate:	100Hz															
	Averaging:	100 samples (1 sec.), arithmetic mean, running, samples															
	Logging:	Controlled by manual log switch, 1 dataset per second logged															
Laboratory Equipment																	
Instrument	Location	Unit	Range	Sensor	S/N/ID#	Cal. #/Bar Code	Cal. Due	Comments				Uncertainty (%)					
Scale	336 Bldg Lab 1	g	0 - 3100	Sartorius BP 3100 S	90707012	N/A	Feb-06					0.000032					
Scale	336 Bldg Lab 1	g	0 - 200	Mettler AE200	1113270529	N/A	Feb-06					0.000015					
Waring blender 1	336 Bldg Lab 1	N/A	N/A	N/A	7011HS Model GB2WTS3	N/A	N/A	120 V, 60 Hz, 5.75 A, 2 spd									
Waring blender 2	336 Bldg Lab 1	N/A	N/A	N/A	7011HS Model GB2WTS3	N/A	N/A	120 V, 60 Hz, 5.75 A, 2 spd									
Kitchen Aid blender	336 Building Lab 1	N/A	N/A	N/A	Model KSB50B4 s/n WS2331476	N/A	N/A	120 V, 60 Hz, 4.8 A, multiple speed settings									
Digital scale	APEL Lab 105	G	0 - 300	Sartorius BP 1202 MP	2810009	N/A	Feb-06										
Digital scale	APEL Lab 105	G	0 - 12100	Mettler Toledo SB 12001	2113046012	N/A	Feb-06										
Digital scale	APEL Lab 105	G	0 - 200	Mettler AE200	182666	N/A	Feb-06										
Digital scale	APEL Lab 105	g	0 - 4400	Mettler AE4400	743886	N/A	Feb-06	No stated range, estimated by applying force up to ~4400 g and from scale model.									
Calcium ISE	APEL Lab 105	ppm	1 to 5x10 ⁻⁴ M	Cole Parmer calcium combination epoxy electrode	Cat No. 27504-06	N/A	N/A	Not calibrated, performance check prior to measurements done to ensure proper operation.									
Ion meter	APEL Lab 105	mV	-500 ~ +500	Oakton Ion 5 A corn	173740	N/A	N/A	Used w/ ISE probe, 3 meters available; performance check of calcium ISE probe.									
Ion meter	APEL Lab 105	mV	-500 ~ +500	Oakton Ion 5 A corn	207075	N/A	N/A	Used w/ ISE probe, 3 meters available; performance check of calcium ISE probe.									
Ion meter	APEL Lab 105	mV	-500 ~ +500	Oakton Ion 5 A corn	173743	N/A	N/A	Used w/ ISE probe, 3 meters available; performance check of calcium ISE probe.									

(a) Requires 250-ohm resistor in series with loop to develop HART FSK signal for configuration via ProLink, primary variable only.
 (b) Was calibrated to 100 psi previous to 11/22/06.

Table C.1.2. Benchtop Test Loop Instrumentation Measurement and Test Equipment Listing

Instruments Connected to Data Acquisition System																		
Parameter	Subsystem	Ch.	Unit	Range	Sensor						Resistor				Sensor/ Transmitter Uncertainty			
					Sensor	Ser. No.	Type	Cal. #/ Bar Code	Cal. Due	Transmitter	Ser. No.	Signal	SB Module	Series		Parallel	Loop Pwr.	
DH038S Q	Debris inj. 1	0	GPM	0-6	Micro Motion D H038S 1199SU ^(a)	188539	Coriolis	NA	NA	RFT 9739	1511637	4-20mA	5B32-02	250	20	Xmtr.	0.1% of rate	
DH038S SG	Debris inj. 1	1	S.G.	0.9-1.5	"	"	Coriolis	NA	NA	"	"	"	5B32-02	N/A	N/A	Xmtr.	0.5% of SG	
D100 Q	Main loop flow	2	GPM	0-60	Micro Motion D 100 ^(a)	233660	Coriolis	NA	NA	RFT 9739	162827	4-20mA	5B32-02	250	20	Xmtr.	0.1% of rate	
D100 SG	Main loop flow	3	S.G.	0.9-1.5	"	"	Coriolis	NA	NA	"	"	"	5B32-02	N/A	N/A	Xmtr.	0.5% of SG	
DP	Test sect.	4	in.H ₂ O	0 ~ 1000	Honeywell Y41104-0011-11-02-07 ^(a)	7637863894003	SG Diaph.	21248	12/8/2006	Integral	(same)	4-20mA	5B32-02	N/A	20	Loop	??	
DH025 SQ	Debris inj. 2	5	GPM	0-3	Micro Motion D H025S 1199SU	188326	Coriolis	NA	NA	RFT 9739	403661	4-20mA	5B32-02	250	20	Xmtr.	0.1% of rate	
DH025S SG	Debris inj. 2	6	S.G.	0.9-1.5	"	"	Coriolis	NA	NA	"	"	"	5B32-02	20	20	Xmtr.	0.5% of SG	
Loop Temp.	Main loop flow	10	°C	-100-+300	Type J thermocouple	N/A	J T/C	19795	4/11/2007	N/A	N/A	J T/C	5B47J-02	N/A	N/A	N/A	2.2°C	
Data Acquisition System																		
Hardware:	PC:	Dell Optiplex GX280																
	Board:	Measurement Computing PCI-DAS6402-16						21623	04/13/07									0.0061%
	Sig. cond.:	5B modules as tabulated																
Software:	Windows XP Professional																	
	DasyLAB 7																	
Configuration:	Sample Rate:	100Hz																
	Averaging:	100 samples (1 sec.), arithmetic mean, running, samples																
	Logging:	Controlled by manual log switch, 1 dataset per second logged																
Laboratory Equipment																		
Instrument	Location	Unit	Range	Sensor	S/N / ID#	Cal. # / Bar Code	Cal. Due	Comments										Uncertainty
Scale	336 Bldg Lab 1	gram	0 ~ 3100	Sartorius BP 3100 S	90707012	N/A	Feb-06											0.00032%
Scale	336 Bldg Lab 1	gram	0 ~ 200	Mettler AE200	1113270529	N/A	Feb-06											0.00015%
Waring blender 1	336 Bldg Lab 1	N/A	N/A	N/A	7011HS Model HGB2WTS3	N/A	N/A	120 V, 60 Hz, 5.75 A, 2 speed										
Waring blender 2	336 Bldg Lab 1	N/A	N/A	N/A	7011HS Model HGB2WTS3	N/A	N/A	120 V, 60 Hz, 5.75 A, 2 speed										
Kitchen Aid blender	336 Bldg Lab 1	N/A	N/A	N/A	Model KSB50B4 s/n WS2331476	N/A	N/A	120 V, 60 Hz, 4.8 A, multiple speed settings										
Digital scale	APEL Lab 105	gram	0 ~ 300	Sartorius BP 1202 MP	2810009	-	Feb-06											
Digital scale	APEL Lab 105	gram	0 ~ 12100	Mettler Toledo SB 12001	2113046012	-	Feb-06											
Digital scale	APEL Lab 105	gram	0 ~ 200	Mettler AE200	L82666	-	Feb-06											
Digital scale	APEL Lab 105	gram	0 ~ 4400	Mettler AE4400	743886	-	Feb-06	No stated range, est. by applying force up to ~4400 gram and from scale model.										
Calcium ISE	APEL Lab 105	ppm	1 to 5 x 10 ⁶ M	Cole Parmer Ca combination epoxy electrode	Cat No. 27504-06	N/A	N/A	Not calibrated, performance check prior to measurements done to ensure proper operation.										
Ion meter	APEL Lab 105	mV	-500 ~ +500	Oakton Ion 5 Acorn	173740	N/A	N/A	Used w/ ISE probe; 3 meters available; performance check of calcium ISE probe.										
Ion meter	APEL Lab 105	mV	-500 ~ +500	Oakton Ion 5 Acorn	207075	N/A	N/A	Used w/ ISE probe; 3 meters available; performance check of calcium ISE probe.										
Ion meter	APEL Lab 105	mV	-500 ~ +500	Oakton Ion 5 Acorn	173743	N/A	N/A	Used w/ ISE probe; 3 ms available; performance check of calcium ISE probe.										
Ion meter	APEL Lab 105	-	mV	-500 to +500	Oakton Ion 5 Acorn series	173743	Ion meter	Meter to be used with the ISE probe; 3 meters available in case one breaks; meter checked with performance check of calcium ISE probe.										

(a) Requires 250-ohm resistor in series with loop to develop HART FSK signal for configuration via ProLink, primary variable only.

Table C.1.3. Benchtop Test Loop Instrumentation Measurement and Test Equipment Listing

Instrument	Location	Unit	Range	Sensor	S/N / ID#	Cal. # / Bar Code	Cal. Due	Comments							Uncertainty
Scale	336 Building Lab 1	gram	0 – 3100	Sartorius BP 3100 S	90707012	N/A	Feb-06								.000032%
Scale	336 Building Lab 1	gram	0 – 200	Mettler AE200	1113270529	N/A	Feb-06								.000015%
Waring blender 1	336 Building Lab 1	N/A	N/A	N/A	7011HS Model HGB2WTS3	N/A	N/A	120 V, 60 Hz, 5.75 amp, 2 speed							
Waring blender 2	336 Building Lab 1	N/A	N/A	N/A	7011HS Model HGB2WTS3	N/A	N/A	120 V, 60 Hz, 5.75 amp, 2 speed							
KitchenAid blender	336 Building Lab 1	N/A	N/A	N/A	Model KSB50B4 s/n WS2331476	N/A	N/A	120 V, 60 Hz, 4.8 amp, multiple speed settings							
Digital scale	APEL Lab 105	gram	0 – 300	Sartorius BP 1202 MP	2810009	-	Feb-06								
Digital scale	APEL Lab 105	gram	0 – 12100	Mettler Toledo SB 12001	2113046012	-	Feb-06								
Digital scale	APEL Lab 105	gram	0 – 200	Mettler AE200	L82666	-	Feb-06								
Digital scale	APEL Lab 105	gram	0 – 4400	Mettler AE4400	743886	-	Feb-06	No stated range, est. by applying force up to ~4400 gram and from scale model.							
Calcium ISE	APEL Lab 105	ppm	1 M to 5×10^{-6} M	Cole Parmer calcium combination epoxy electrode	Cat No. 27504-06	N/A	N/A	Not calibrated, performance check prior to measurements done to ensure proper operation.							
Ion meter	APEL Lab 105	mV	-500 ~ +500	Oakton ion 5 Acorn	173740	N/A	N/A	Used w/ ISE probe, 3 meters available. Performance check of calcium ISE probe.							
Ion meter	APEL Lab 105	mV	-500 ~ +500	Oakton ion 5 Acorn	207075	N/A	N/A	Used w/ ISE probe, 3 meters available. Performance check of calcium ISE probe.							
Ion meter	APEL Lab 105	mV	-500 ~ +500	Oakton ion 5 Acorn	173743	N/A	N/A	Used w/ ISE probe, 3 meters available. Performance check of calcium ISE probe.							
Ion meter	APEL Lab 105	-	mV	-500 to +500	Oakton Ion 5 Acorn Series	173743	Ion meter	Meter to be used with the ISE probe, currently 3 meters available in case one brakes. Meter is checked with performance check of Calcium ISE probe.							

